Clinically Oriented Translational Cancer Multilevel Modelling

Deliverable D4.1

Technical descriptions of cellular/tissue models including information flows

Project Number:	FP7--IST-*223979*
Deliverable id:	D4.1
Deliverable Name:	Technical descriptions of cellular/tissue models including information flows
Submission Date:	15/03/2009

RESTRICTED TO THE ContraCancrum CONSORTIUM AND THE EUROPEAN COMMISSION

Information Society Technologies

COVER AND CONTROL PAGE OF DOCUMENT	
Project Acronym:	CONTRACANCRUM
Project Full Name:	Clinically Oriented Translational Cancer Multilevel Modelling
Document id:	D4.1
Document name:	Technical descriptions of cellular/tissue models including information flows
Document type	RE
Version:	Final
Submission date:	15/03/2009
Editor: Organisation: Email:	Georgios S. Stamatakos ICCS-NTUA gestam@central.ntua.gr

Document type PU = public, INT = internal, RE = restricted

ABSTRACT:

This deliverable provides high level technical descriptions of the cancer modelling modules of the ContraCancrum project pertaining to the cellular and higher levels of biocomplexity. The major functions of the modules along with the fundamental information flows are outlined. A list of the multiscale clinical data to be used for the adapation, optimization and validation of the models is provided. A literature review is also included.

KEYWORD LIST: *in silico* oncology, Oncosimulator, cancer modelling, multiscale biomodeling, glioma, glioblastoma, lung cancer, treatment optimization, tumor growth, Virtual Physiological Human, virtual tumor

MODIFICATION CONTROL			
Version	Date	Status	Author
1.	11/02/2009	Draft	G.Stamatakos
2.	18/02/2009	Revision	D. Dionysiou
3	1/03/2009	Revision	G.Stamatakos
4	11/03/2009	Revision	N.Graf
5	13/03/2009	Final [CC-D4 1.doc]	G.Stamatakos

List of Contributors

G.Stamatakos, ICCS-NTUA
S.Giatili, ICCS-NTUA
A. Roniotis, FORTH-ICS
T.Bily, MFF-CUNI
M.Balek, MFF-CUNI
N.Graf, USAAR
R. Bohle, USAAR
E.Meese, USAAR
E.Kolokotroni, ICCS-NTUA
E.Georgiadi, ICCS-NTUA
D.Dionysiou, ICCS-NTUA
P.Buechler, UBERN
G.Clapworthy, BED
J.Sabcsynski, PFL-H
A.Folarin, UCL
K.Marias, FORTH-ICS

Contents

Publishable Executive Summary

The present document contains high level technical descriptions of the cellular and tissue models of tumour growth and response to treatment that will constitute the ContraCancrum cellular and tissue simulation module. Diagrams depicting information flows enhance and clarify the descriptions. The document begins with an introduction to multiscale cancer modelling and the emerging field of *in silico* oncology focusing on the techniques adopted by the ContraCancrum project. A brief literature review precedes the main technical part of the document. The latter consists of descriptions of models at several spatiotemporal scales. Two cancer types are addressed by the ContraCancrum project: gliomas and lung cancer. Specific agent based models of microscopic mechanisms of tumour growth and response to treatment including i.a. prevascular tumour growth, prevascular tumour response to treatment (chemotherapy, radiotherapy), angiogenesis, invasion and metastasis are delineated. Their main purpose within the project is to enhance our understanding of tumour dynamics related phenomena on the microscopic level so that refinement of the imageable tumour modeling approach could be achieved. Subsequently, the focus is moved onto large (imageable) clinical tumours. Before the modelling part itself a description of the multiscale medical data to be used for the driving, adaptation, optimization and validation of the models is provided. Modelling of such tumours is achieved via two major approaches: a continuum based modelling approach exploiting primarily diffusion theory and a discrete entity/event modelling approach exploiting the potential of cellular automata, the Monte Carlo method, cell clustering into equivalence classes as well as numerous dedicated algorithms. In this way both diffusion phenomena (e.g. tumour invasion) and complex multiscale biological mechanisms of a predominantly discrete character (e.g. symmetric and asymmetric stem cell division) are addressed. High level descriptions of the corresponding simulation strategies along with particuliarities and limitations are provided. A brief description of alternative ways to consider the reponse of normal tissues to treatment is also presented.

1. Introduction [Code: IN]

Understanding and effectively modeling the dynamics of cancer and treatment affected normal tissues at all biocomplexity levels by using any efficient combination of mathematical and computer modeling approaches (discrete, continuous, deterministic, stochastic, analytical, numerical etc.) is a fundamental research challenge in oncology. Obviously this target presupposes success in understanding and modeling numerous critical mechanisms involved in cancer and affected normal tissue development and treatment response, as well as the subsequent integration of all those modeling modules. As the demands of such an endeavour are especially high, a parallelism with the history of Newtonian physics might serve as a source of guidance and inspiration [IN1].

It has been suggested that cancer epitomizes the entire biology. In this context a title like: "Philosophiae Naturalis Principia Mathematica: Pars II, Materia Vivens" (Mathematical Principles of Natural Philosophy: Part II, Living Matter) might to some extent describe the collaborative and heavily multidisciplinary efforts on a worldwide scale to apply the analytical way of thinking on the description of natural phenomena (mechanisms) involving living matter and especially on those related to cancer. Obviously stochasticity is one of the key players in such an approach. A thorough, quantitative, rigorously clinically validated and exploitable understanding of such multi-scale phenomena is expected to dramatically accelerate the achievement of cancer cure on a patient individualized basis through treatment optimization *in silico* (on the computer). In this context the term *In Silico* Oncology has been proposed to denote a new scientific, technological and clinical discipline aiming at both understanding the multiscale cancer and related biological phenomena and optimize treatment in the patient individualized context [IN1].

Within this context the ContraCancrum project aims at advancing *In Silico* Oncology by developing and *clinically* testing *clinically* driven multiscale models of tumour growth and response to various treatment modalities. Two cancer types are adddressed: gliomas and lung cancer. The practical goal of this approach is to provide a clinically trustable support system for the optimization of patient individualized cancer treatment [IN2].

Since a central feature of the ContraCancrum project is the development of an integrated multilevel tumour dynamics simulator, being the main goal of workpackage WP8, a brief delineation of the latter is provided below. This may help in acquiring a broad picture of the entire ContraCancrum project since workpackage WP4 to which this deliverable belongs will also serve as the basis for the integration of several modeling modules into the ContraCancrum Integrated Simulator. The latter will be used for the execution of the simulation tasks as submitted by the end users. Logical and technical validation of the composite simulator (integrator) will be performed before the clinical testing, optimization and validation and will take place in tight interaction with workpackage WP9. It is noted that there will be a strong interaction of WP8 with all the other simulation workpackages throughout most of the project's lifetime in order to optimally orchestrate and harmonize the development of all modules to be finally combined or fused.

The ContraCancrum integrated simulation system will function briefly as follows. Provided that the system has been validated (retrospectively and prospectively) for a specific tumour type, the imaging, histopathological, molecular and clinical data of any given patient following pertinent preprocessing are introduced into the "MULTI-LEVEL CANCER SIMULATOR FOR TUMOUR AND NORMAL TISSUE RESPONSE SIMULATION" module. This module executes the simulation code for a defined candidate treatment scheme (Figure IN1). The prediction is judged by the clinician and if a decision is made to test a further scheme *in silico*

this is done in an analogous way. Alternatively a large number of candidate schemes can be executed concurrently on a cluster or grid platform. Finally the clinician decides on the optimal treatment scheme to be administered to the patient based on his or her formal medical education and knowledge and the predictions of the ContraCancrum integrated simulator. Subsequently comparison of the predictions with the real outcome provides a feedback signal to be exploited for the optimization of the ContraCancrum integrated simulator. The most fundamental processes to be implemented by the ContraCancrum are the following: Processed molecular data is used in order to perturb the radiobiological or pharmacodynamic cell-kill parameters about their population-based mean values. At the heart of the simulation approach lies a prototype system of quantizing cell clusters included within each geometrical cell of a discretizing mesh, covering the anatomic area of interest. Cell-cycle phase durations and imaging-based metabolism distribution define the quantization equivalence classes considered. Several algorithms will be developed so as to simulate various macroscopic mechanisms such as tumour expansion or shrinkage and mechanics, as well as the effects of particular drugs and radiation on the tumorous and normal tissue under consideration.

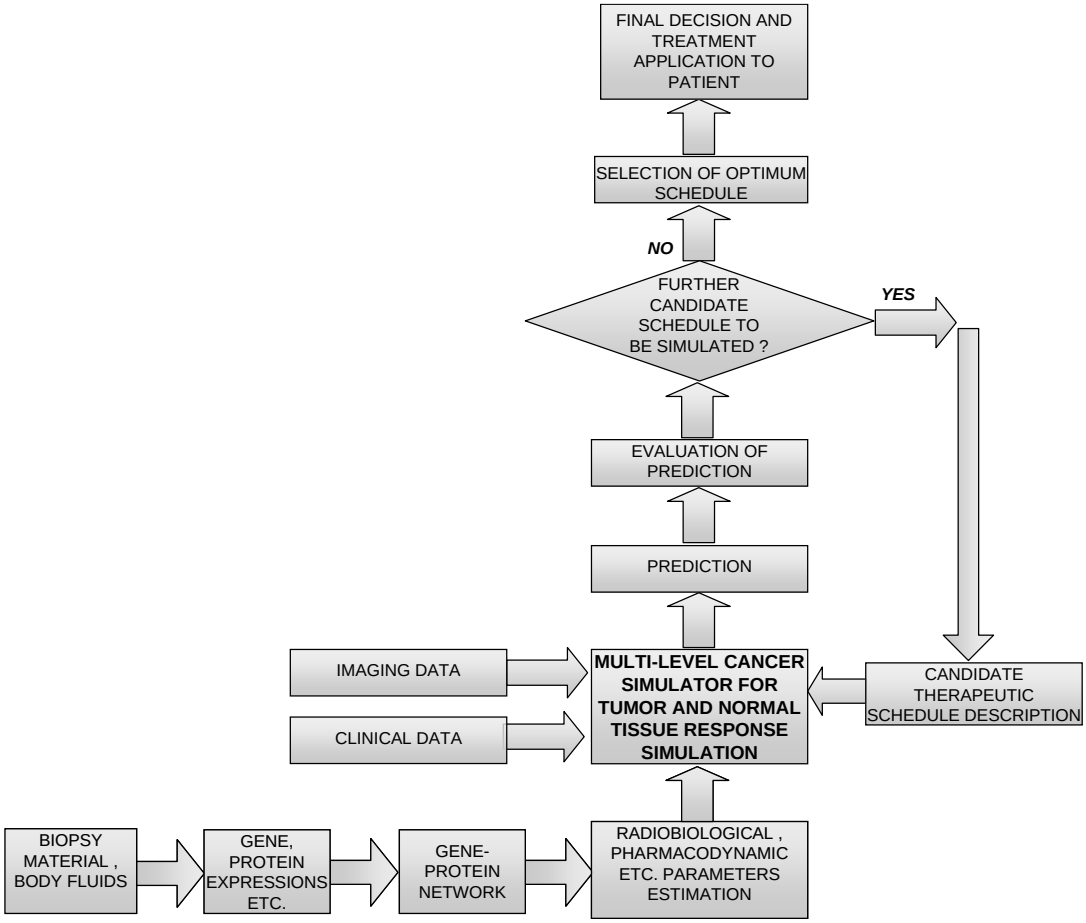

Figure IN1. A generic functional outline of the ContraCancrum integrated simulator

Figure IN2 outlines an example of the “summarize and jump” strategy aiming at a pragmatic biocomplexity “level jumping” and integration. The latter plays a fundamental role in the development of a multiscale simulator. This approach serves as the core philosophy for the multilevel integration of biological data and mechanisms involved in cancer modelling within the framework of ContraCancrum.

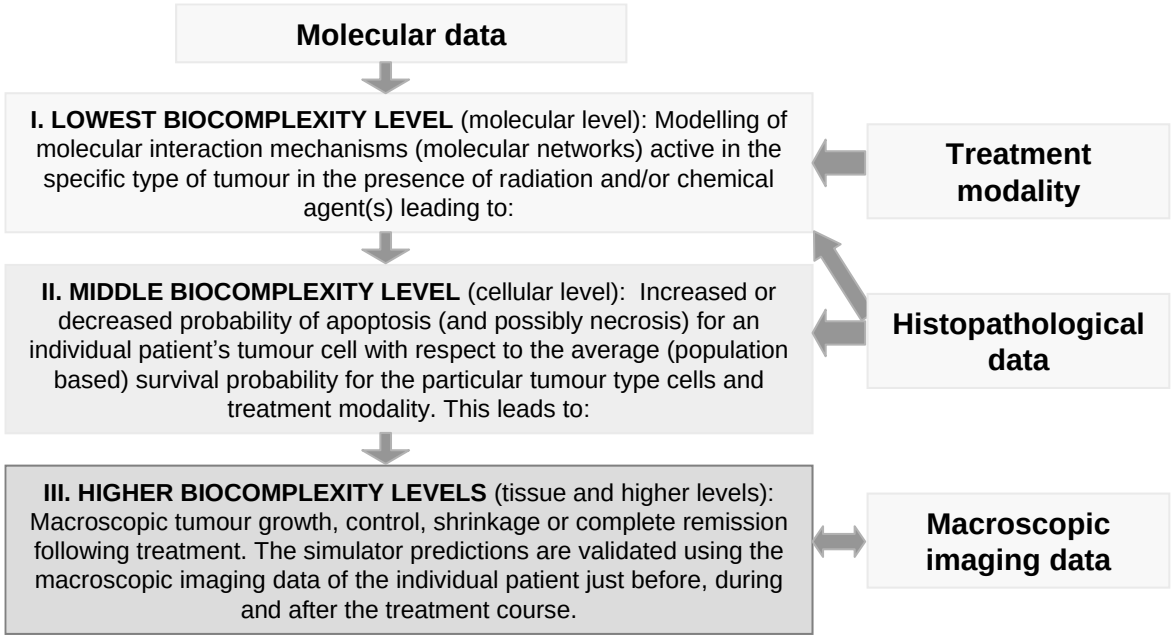

Figure IN2. An example of the "summarize and jump" strategy as applied to the case of tumour response to teatment modlling in the clinical setting. Only three (clusters of) levels are depicted for simplification purposes.

References

IN1. G. Stamatakos, " Spotlight on Cancer Informatics," Cancer Informatics 2006:2 83-86

IN2. N. Graf and A. Hoppe, "What are the expectations of a Clinician from *In Silico* Oncology?," Proc. 2nd International Advanced Research Workshop on In Silico Oncology, Kolympari, Chania, Greece, 25-26 Sept. 2008, Ed. K. Marias and G. Stamatakos, pp. 36-38 (http://www.ics.forth.gr/bmi/2nd-iarwiso/)

IN3. G. Stamatakos 2006, NCI CViT Ask the Expert Forum, password-controlled website https://www.cvit.org/node/128 .

1. Objectives of the Deliverable [Code: OB]

The objectives of the deliverable are the following

1. To provide a brief literature review of models of tumour growth and response to treatment with emphasis on gliomas and lung cancer as well as to provide the goals of workpackage WP4.

2. To outline agent based models of microscopic mechanisms of tumour growth and response to treatment including i.a. prevascular tumour growth, prevascular tumour response to treatment (chemotherapy / radiotherapy), angiogenesis, invasion and metastasis. Their main purpose within the project is to enhance understanding of the tumour dynamics related phenomena in the microscopic level so that refinement of the imageable tumour modeling approach can be achieved.

3. To list the multiscale medical data to be used for the adaptation, optimization and validation of the imageable tumour dynamics models.

4. To provide a high level description of the continuum (diffusion) based models of imageable tumour growth and response to treatment (chemotherapeutic, radiotherapeutic).

5. To provide a high level description of the discrete entity/event based models of imageable tumour growth and response to treatment (chemotherapeutic, radiotherapeutic).

6. To provide a brief description of alternative ways to consider the reponse of normal tissues to treatment.

3. A Brief Overall Literature Review and Workpackage WP4 Tasks [Code: LI]

3.1 Literature Review

Over the past decades considerable progress has been made regarding the development of mathematical and computational models simulating various aspects of cancer behaviour. The majority of the models adopt the "bottom-up" approach i.e. they address biocomplexity by starting from its lower levels (molecular or cellular) and subsequently they try to reach higher and higher levels. Such models refer primarily to the *in vitro* development of tumour spheroids or the non imageable preangiogenetic and further development of tumourlets within the organism by focusing on several mechanisms or combinations of mechanisms [LI1-LI6]. Angiogenesis has been addressed by several investigators [LI7-LI9]. Invasion has also been the subject of a number of theoretical investigations primarily addressing glioma cell diffusion [LI10,LI11,LI13,L14]]. Concerning the modeling of *imageable* large *in vivo* tumours most models tend to focus on the growth aspect by trying to predict the shape of the tumour as a function of time [LI13-LI14]. Nevertheless, a synoptic consideration of treatment response also been included in some of them. Certain models have been developed in order to simulate the response of numbers of non mutually interacting tumour cells or small non imageable tumourlets to therapeutic interventions [LI15-LI31] In the clinical context such models are potentially useful in order to provide a rough estimate of the relative effectiveness of various candidate treatments on non imageable tumourlets. This is the case when only some population based statistical knowledge is available concerning the invasiveness and/or diffusiveness of a specific tumour type instead of exact imaging data (i.e. non imageable glioblastoma micrometastases).

From the clinical point of view, however, it is usually the prediction of the response of an *already grown* clinical tumour to candidate therapeutic schemes (chemotherapeutic, radiotherapeutic, combined etc.) that is of primary importance. This is also the context where tumour models can in principle be validated in a *quantitative* manner (based on multiscale medical data). Theefore, clinical validation is best achieved within the *clinical environment* and preferrably in conjunction with clinical trials. Within this framework the *In Silico* Oncology Group, Institute of Communication and Computer Systems, National Technical University of Athens [LI50] has developed the "top-down" discrete event/entity treatment simulation approach which starts from the macroscopic imaging data of the patient and subsequently integrates information stemming from lower and lower biocomplexity levels (histological, molecular etc.). In collaboration with experimentalists, radiobiologists and clinicians it has produced a number of treatment simulation models addressing both tumour and treatment affected normal tissue behaviour that are based on the individual data of the patient [LI29- LI49].

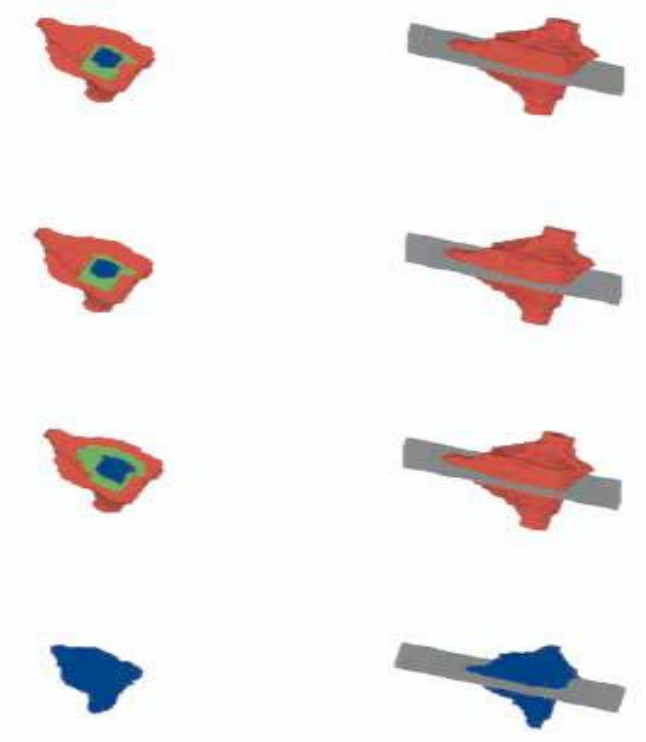

Figure LI1. Irradiation response simulation of an imageable glioblastoma tumour according to the standard fractionation scheme (2 Gy once a day, 5 days per week, 60 Gy in total). Left panel: 3-D sections of the tumor shown in the right panel. Top row: before the beginning of irradiation. Second row: one fictitious day after the beginning of irradiation. Third row: two fictitious days after the beginning of irradiation. Bottom row: three fictitious days after the beginning of irradiation. Color code red: proliferating cell layer; green: dormant cell layer (G); blue: dead cell layer. The colouring criterion "99.8%" used to visualize the predictions has been defined as follows. "For a geometrical cell of the discretizing mesh, if the percentage of dead cells is lower than 99.8% then f if percentage of proliferating cells > percentage of G cells, then paint the geometrical cell red (proliferating cell layer), else paint the geometrical cell green (G cell layer)g else paint the geometrical cell blue (dead cell layer)." The values of certain parameters (e.g., cell loss) have been deliberately exaggerated in order to facilitate the demonstration of the ability of the model to simulate the shrinkage effect. Adapted from [G.S.Stamatakos, D.D.Dionysiou, E.I.Zacharaki, N.A.Mouravliansky, K.Nikita, N.Uzunoglu, "In silico radiation oncology: combining novel simulation algorithms with current visualization techniques", Proceedings of the IEEE, vol. 90, No 11, pp.1764-1777, Nov. 2002.]

Figure LI1 shows a typical three-dimensional rendering of these models' predictions. An initial clinical trial based retrospective validation of some models has already been achieved [LI35,LI45] whereas within the EC funded ACGT project new *in silico* oncology "top-down" models have been developed and tested by exploiting actual running clinicogenomic trials [LI46-LI49]. The primary target of this approach is to provide the clinician or the researcher with a system of *simulators* in order to perform *in silico* experiments regarding the likely outcome of several candidate therapeutic schemes/schedules for any given individual patient. The experiments refer to both tumour behaviour and to a lesser degree of detail to normal tissue treatment response. The simulators will act as dynamic integrators of the multilevel data and mechanisms corresponding to the spatiotemporal *natural phenomenon of cancer* as is manifest in the individual patient. Subsequently, following a rigorous clinical

optimization and validation, the clinician is expected to be able to decide on the optimal treatment scheme and/or schedule to be administered to the particular patient based on the predictions of the simulators and his or her own formal medical education, experience and logic.

3.2 Tasks of workpackage WP4

The cell and higer biocomplexity level simulators of the project will be primarily based on the "top-down" simulation approach described above which will be applied for the first time to the simulation of treatment response of lung cancer. The same approach will also be considerably refined and adapted for the case of gliomas. Special emphasis will be put on stem and limited mitotic potential tumour cells. In this way multilevel information will be being extracted and used in a realistic level of detail by always taking into account that the whole endeavour is to be confined within the clinical setting. However, the "bottom-up"approach will also be adopted in simulating non-imageable tumour growth, especially the process of glioblastoma local invasion. It is noted that in parallel with the tumour response models, rather simple experimentally and clinically based toxicology models potentially in combination with discrete simulation of the replenishment of normal tissue stem, transit and differentiated cells will provide safety limits beyond which any candidate treatment scheme would be clinically unacceptable regardless of its tumour control predicted outcome. The multilevel clinical testing, optimization and validation processes to be performed mainly within the framework of workpackages WP8 and WP9 will constitute per se another novelty of the project in the context of gliomas and lung cancer.

3.3 Mathematical Notation Convention

The following mathematical notation convention has been adopted throughout the document *unless otherwise stated or clearly implied*:

A bare letter denotes a *scalar* quantity (e.g. "*c*" stands for tumour cell concentration)

A letter with a right arrow on top of it denotes a *vector* quantity (e.g. "$\vec{J}$" stands for the diffusion flux of tumour cells)

A letter with a left-right arrow on top of it denotes a *tensor* or *matrix* (e.g. "$\vec{\vec{D}}$" stands for the tumour cell diffusion tensor)

References

LI1. Duechting, W., Ulmer, W., Lehrig, R., Ginsberg, T., Dedeleit, E., 1992. Computer simulation and modelling of tumour spheroid growth and their relevance for optimization of fractionated radiotherapy. Strahlenther. Onkol. 168, 354-360.

LI2. G.Stamatakos, N.Uzunoglu, K.Delibasis, M.Makropoulou, N.Mouravliansky, A.Marsh, "A simplified simulation model and virtual reality visualization of tumor growth in vitro," Future Generation Computer Systems, vol. 14, pp.79-89, 1998.

LI3. Byrne, H., Matthews, P., 2002. Assymetric growth of avascular solid tumours: exploiting symmetries. IMA J Mathematics Applied in Medicine and Biology 19, 1–29.

LI4. E. I.Zacharaki, G. S.Stamatakos, K.S. Nikita, N. K.Uzunoglu, "Simulating growth dynamics and radiation response of avascular tumour spheroid model validation in the case of an EMT6/Ro multicellular spheroid," Computer Methods and Programs in Biomedicine (2004) 76, 193—206.

LI5. Alarcon, T., Byrne, H.M., Maini, P.K., 2004b. A mathematical model of the effects of hypoxia on the cell-cycle of normal and cancer cells. J. Theor. Biol. 229, 395–411.

LI6. Kansal, A.R., Torquato, S., Harsh, I.V., Chiocca, E.A., Deisboeck, T.S.,2000b. Cellular automaton of idealized brain tumour growth dynamics. BioSystems 55,119–127.

LI7. Michelson, J. T. Leith, "Positive feedback and angiogenesis in tumor growth control", Bull. Math. Biol,. vol. 59, no. 2, pp. 233-254, 1997

LI8. S. K. Hobbs, W. L. Monsky, F. Yuan, W. G. Roberts, L. Griffith, V. P. Torchilin, R. K. Jain, "Regulation of transport pathways in tumor vessels: role of tumor type and microenvironment", Proc. Natl. Acad. Sci. USA, vol. 95, pp. 4607–4612, 1998

LI9. P. Carmeliet, R. K. Jain, "Angiogenesis in cancer and other diseases", Nature, vol. 407 pp. 249-259, 2002

LI10. Kansal, A.R., Torquato, S., Harsh, G.R., Chiocca, E.A., Deisboeck, T.S., 2000a. Simulated brain tumour growth dynamics using a three-dimensional cellular automaton. J Theor Biol 203, 367–382.

LI11. Cristini, V., Frieboes, H.B., Gatenby, R., Caserta, S., Ferrari, M., Sinek, J.P.,2005. Morphological instability and cancer invasion. Clin. Cancer Res. 11, 6772–6779.

LI12. G. Stamatakos, D. Dionysiou, N. Mouravliansky, K. Nikita, G. Pissakas, P. Georgolopoulou and N. Uuznoglu, "Algorithmic Description of the Biological Activity of a Solid Tumor in Vivo", in Proc. EUROSIM 2001 Congress, Delft, The Netherlands, June 26-29, 2001 (CD-ROM Edition)

LI13. K.Swanson, E.C.Alvord Jr., J.D.Murray, "Dynamics of a model for brain tumors reveals a small window for the therapeutic intervention," Discrete and Continuous Dynamical Systems-Series B, vol. 4, no 1, pp.289-295, 2004.

LI14. Olivier Glatz, Maxime Sermesant, Pierre-Yves Bondiau, Hervé Delingette, Simon K. Warfield, Grégoire Malandain, and Nicholas Ayache. Realistic Simulation of the 3D Growth of Brain Tumors in MR Images Coupling Diffusion with Mass Effect. IEEE Transactions on Medical Imaging, 24(10):1334-1346, October 2005.

LI15. Fowler, J.F., 1989. The linear-quadratic formula and progress in fractionated radiotherapy. Br. J. Radiol. 62, 679–694.

LI16. Haas-Kogan, D.A., Yount G., Haas M., Levi D., Kogan S.S., Hu L., Vidair C., Deen D.F., Dewey W.C., Israel M.A., 1996. p53-dependent G_1 arrest and p53 independent apoptosis influence the radiobiologic response of glioblastoma, Int. J. Radiat. Oncol. Biol. Phys. 36, 95-103.

LI17. Steel, G., 2002. Basic Clinical Radiobiology. Arnold, London, UK.

LI18. E. I.Zacharaki, G. S.Stamatakos, K.S. Nikita, N. K.Uzunoglu, "Simulating growth dynamics and radiation response of avascular tumour spheroid model validation in the case of an EMT6/Ro multicellular spheroid," Computer Methods and Programs in Biomedicine (2004) 76, 193—206.

LI19. S. Chuang, "Mathematic models for cancer chemotherapy: pharmacokinetic and cell kinetic considerations", Cancer Chemother. Rep., vol. 59, ,no. 4, pp. 827-42, 1975

LI20. V.A.Levin, C.S. Patlak, H.D.Landahl, "Heuristic modeling of drug delivery to malignant brain tumors", J. Pharmacokinet. Biopharm., pp. 257-2968, 1980

LI21. S.Ozawa, Y.Sugiyama, J.Mitsuhashi, and M. Inaba, "Kinetic analysis of cell killing effect induced by cytosine arabinoside and cisplatin in relation to cell cycle phase specificity in human colon cancer and chinese hamster cells", Cancer Res., vol. 49, pp. 3823-3828, 1989

LI22. Y.Jean, J. De Traversay, P.Lemieux, "Teaching cancer chemotherapy by means of a computer simulation", Int. J. Biomed. Comput., vol. 36, pp. 273-280, 1994

LI23. F.K.Nani, M.N.Oguztereli, "Modelling and simulation of chemotherapy of haematological and gynaecological cancers", IMA J. Math. Appl. Med. Biol,. vol. 16, pp. 39-91, 1999

LI24. A.Iliadis and D. Barbolosi, "Optimizing drug resistance in cancer chemotherapy by an efficacy-toxicity mathematical model", Comput. Biomed. Res,. vol. 33, pp. 211-226, 2000

LI25. D.Barbolosi, A. Iliadis, "Optimizing drug regimens in cancer chemotherapy: a simulation study using a PK-PD model", Comput. Biol. Med., vol. 31, pp. 157-172, 2001

LI26. J. Davis and I. F. Tannock, "Repopulation of tumour cells between cycles of chemotherapy: a neglected factor", The Lancet Oncol, vol. 1, pp. 86-93, 2000

LI27. S.N.Gardner, "Modeling multi-drug chemotherapy: tailoring treatment to individuals", J. theor. Biol.,, vol. 214, pp. 181-207, 2002

LI28. J.P.Ward, J.R.King, "Mathematical modeling of drug transport in tumour multicell spheroids and monolayer cultures", Mat. Biosci., vol. 181, pp. 177-207, 2003

LI29. G. Stamatakos, E. I. Zacharaki, N. K. Uzunoglu, K. S. Nikita, "Tumor growth and response to irradiation in vitro: a technologically advanced simulation model", Int. J. Radiat. Oncol. Biol. Phys., vol. 51 ,no. 1, pp. 240-241, 2001

LI30. G.Stamatakos, E.Zacharaki, M.Makropoulou, N.Mouravliansky, K.Nikita, and N.Uzunoglu, "Tumour growth in vitro and tumour response to irradiation schemes: a simulation model and virtual reality visualization," Radiother. Oncol, vol. 56, Suppl.1, pp.179-180, 2000.

LI31. G.Stamatakos, E.Zacharaki, M.Makropoulou, N.Mouravliansky, A.Marsh, K.Nikita, and N.Uzunoglu, "Modeling tumor growth and irradiation response in vitro - a combination of high-performance computing and web based technologies including VRML visualization," IEEE Trans. Inform. Technology Biomedicine, vol. 5, No 4, 279-289, 2001.

LI32. G.S.Stamatakos, D.D.Dionysiou, E.I.Zacharaki, N.A.Mouravliansky, K.Nikita, N.Uzunoglu, "In silico radiation oncology: combining novel simulation algorithms with current visualization techniques", Proceedings of the IEEE, vol. 90, No 11, pp.1764-1777, Nov. 2002.

LI33. Stamatakos, G. S., P.Antipas, V., Uzunoglu, N. K., 2006c. A spatiotemporal, patient individualized simulation model of solid tumor response to chemotherapy in vivo: the paradigm of glioblastoma multiforme treated by temozolomide. IEEE Trans Biomed. Engineering 53, No 8, 1467-1477.

LI34. D. D. Dionysiou, G. S. Stamatakos, N.K. Uzunoglu, K. S. Nikita, A. Marioli, "A four-dimensional simulation model of tumour response to radiotherapy in vivo: parametric validation considering radiosensitivity, genetic profile and fractionation," Journal of Theoretical Biology 230 (2004) 1–20

LI35. G. S. Stamatakos, V.P. Antipas, N. K. Uzunoglu, R. G. Dale, "A four dimensional computer simulation model of the in vivo response to radiotherapy of glioblastoma multiforme: studies on the effect of clonogenic cell density." British Journal of Radiology, 2006, vol. 79, 389-400

LI36. V. P Antipas, G. S Stamatakos, N. K Uzunoglu, D. D Dionysiou, R. G Dale, " A spatio-temporal simulation model of the response of solid tumours to radiotherapy in vivo: parametric validation concerning oxygen enhancement ratio and cell cycle duration," Phys. Med. Biol. 49 (2004) 1485–1504

LI37. G.S.Stamatakos, V.P. Antipas, N.K. Uzunoglu, "Simulating chemotherapeutic schemes in the individualized treatment context: The paradigm of glioblastoma multiforme treated by temozolomide in vivo." Comput Biol Med. Comput Biol Med. 36, 1216–1234, 2006.

LI38. G. Stamatakos, " Spotlight on Cancer Informatics," Cancer Informatics No 2, pp.99-102, 2006.

LI39. D. Dionysiou, G. Stamatakos and K. Marias, "Simulating cancer radiotherapy on a multi-level basis: biology, oncology and image processing," Lecture Notes in Computer Science, Special Issue on Digital Human Modeling, Vol. 4561, pp.569-575, 2007.

LI40. Antipas, V.P., Stamatakos, G.S., Uzunoglu, N.K., 2007. A patient-specific in vivo tumor and normal tissue model for prediction of the response to radiotherapy: a computer simulation approach. Methods Inf. Med. 46, 367-375.

LI41. Dionysiou,D.D., Stamatakos, G.S., Uzunoglu,N.K., Nikita,K.S, 2006. A computer simulation of *in vivo* tumour growth and response to radiotherapy: New algorithms and parametric results. Computers in Biology and Medicine 36 448–464

LI42. Stamatakos, G., Dionysiou, D., Nikita, K., Zamboglou, N., Baltas, D., Pissakas, G., et al., 2001. *In vivo* tumour growth and response to radiation therapy: a novel algorithmic description. Int. J. Radiat. Oncol. Biol. Phys.,51 Suppl. 1, 240.

LI43. Stamatakos, G.S., 2006d. Towards a collaborative formulation of the Mathematical Principles of Natural Philosophy: Living Matter. The paradigm of *In Silico* Oncology. DIMACS Workshop on Computational Tumor Modeling, DIMACS Center, Rutgers University, Piscataway, NJ, USA. http://dimacs.rutgers.edu/Workshops/TumorModeling/abstracts.html

LI44. Stamatakos, G. S. and Uzunoglu, N., 2006. Computer Simulation of Tumour Response to Therapy. Cancer Bioinformatics: from therapy design to treatment. Edited by Sylvia Nagl. John Wiley & Sons, Ltd., Chichester,UK.

LI45. Dionysiou, D.D. and Stamatakos, G.S., 2006. Applying a 4D multiscale in vivo tumor growth model to the exploration of radiotherapy scheduling: the effects of weekend treatment gaps and p53 gene status on the response of fast growing solid tumors. Cancer Informatics 2, 113-121.

LI46. Stamatakos GS, Dionysiou DD, Graf N, et al. "The "Oncosimulator": a multilevel, clinically oriented simulation system of tumor growth and response to therapeutic schemes. Towards clinical evaluation of in silico oncology." 29th Annual International Conference of the IEEE Engineering in Medicine and Biology Society in conjunction with the biennial Conference of the French Society of Biological and Medical Engineering (SFGBM), August 23-26, 2007, Conf Proc IEEE Eng Med Biol Soc

LI47. N.Graf, C.Desmedt, A. Hoppe, M.Tsiknakis, D.Dionysiou, G. Stamatakos, "Clinical requirements of "In Silico Oncology" as part of the integrated project ACGT (Advancing Clinico-Genomic Trials on Cancer)," European Journal of Cancer, Vol. 5, No 4, Supl. ECCO 14 Abstract Book, p83,2007.

LI48. E. A. Kolokotroni, G. S. Stamatakos, D. D. Dionysiou, E. Ch. Georgiadi, Ch. Desmedt, N. M. Graf, "Translating Multiscale Cancer Models into Clinical Trials: Simulating Breast Cancer Tumor Dynamics within the

Framework of the “Trial of Principle” Clinical Trial and the ACGT Project.,” Proc. 8th IEEE International Conference on Bioinformatics and Bioengineering (BIBE 2008), Athens, Greece, 8-10 Oct. 2008. IEEE Catalog Number: CFP08266, ISBN: 978-1-4244-2845-8, Library of Congress: 2008907441, Paper No. BE-2.1.1, length: 8 pages (in electronic format). *In press*

LI49. E. Ch. Georgiadi, G. S. Stamatakos, N. M. Graf, E. A. Kolokotroni, D. D. Dionysiou, A. Hoppe, N. K. Uzunoglu, "Multilevel Cancer Modeling in the Clinical Environment: Simulating the Behavior of Wilms Tumor in the Context of the SIOP 2001/GPOH Clinical Trial and the ACGT Project," Proc. 8th IEEE International Conference on Bioinformatics and Bioengineering (BIBE 2008), Athens, Greece, 8-10 Oct. 2008. IEEE Catalog Number: CFP08266, ISBN: 978-1-4244-2845-8, Library of Congress: 2008907441, Paper No. BE-2.1.2, length: 8 pages (in electronic format). *In press*

LI50. http://www.in-silico-oncology.iccs.ntua.gr

4. Modelling Basic Mechanisms of Microscopic Tumour Growth and Response to Treatment [Code: MI]

This chapter begins with a specialized literature review of models pertaining to microscopic mechanisms of tumour growth and response to treatment including i.a. prevascular tumour growth, non imageable tumour response to treatment (chemotherapy / radiotherapy), angiogenesis, invasion and metastasis. Subsequently an agent based unified approach to treat these mechanisms is delineated. The main purpose of the development of these microscopic models within the ContraCancrum framework is to enhance our understanding of the tumour dynamics related phenomena on the microscopic level so that refinement of the imageable tumour models (Chapters 6 and 7) can be achieved. Figure MI1 depicts the basic branches of the microscopic model.

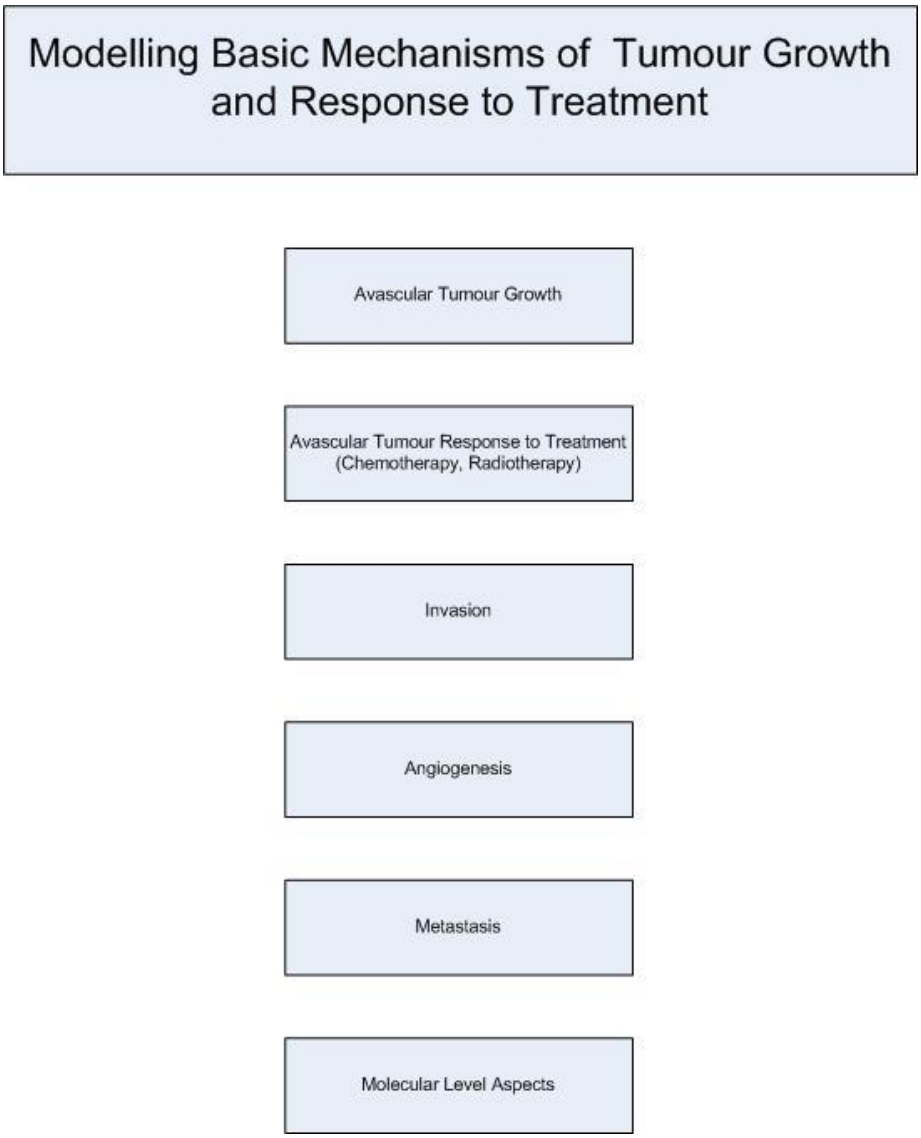

Figure MI1. The basic branches of the microscopic model

4.1 A Brief Overview

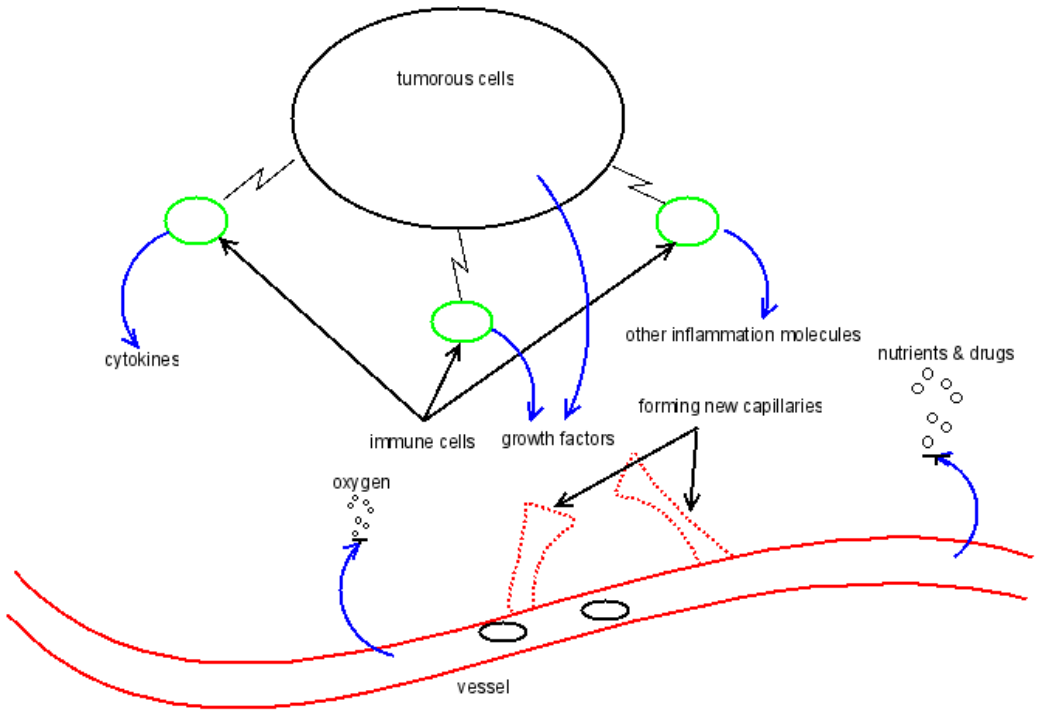

Figure MI2 The microscopic tumour growth scene

The mathematical models of tumour growth and tumour induced interactions with other cells (Figure MI2) fall into four major categories:

i. Continuum models that treat cell density and chemical species like continuous variables that evolve according to the reaction-diffusion system
ii. Discrete, cell-based models in which cells are treated as units and where the cells move, grow and divide according to the prescribed rules
iii. Hybrid or multilevel/multiscale models that uses discrete models at certain levels of complexity, and continuous models at another levels of complexity and integrate solutions together
iv. Agent based models where every entity is an “intelligent” agent with some prescribed (not necessarily same) rules and where these entities interact with each other
v. Discrete event/entity models in which cells are clustered into dynamic equivalence classes, each one characterized by its own fate and rules of interaction with the other classes. This is an efficient approach to simulate the response of large imageable tumours to treatment in a discrete way and therefore to retain the potential of a detailed multiscale biological simulation able to address i.a. different cell categories (stem, progenitor, differentiated, dead cells), different cell cycle phases, different cell phase dependent treatment sensitivities etc. Chapter 7 deals with this approach.

All basic features of cancer biology demonstrate that tumour growth is a multiscale natural phenomenon. The complexity of cancer progression manifests itself at least in the following three scales that can be readily distinguished and described by mathematical models: molecular/sub-cellular, cellular and tissue scale. More specifically

- The molecular and sub-cellular scale refers to phenomena that take place within the cell or at its plasma membrane. Examples of such phenomena include gene mutations or changes in gene expression patterns, alterations of signaling cascades and/or metabolic pathways, cytoskeleton rearrangement and altered membrane activity, progression through and control of the cell cycle, etc.
- The cellular scale refers to cellular interactions between tumour and host cells such as endothelial cells, macrophages, lymphocytes, and even the local components of the extracellular matrix (ECM). This pathological communication between tumour and stroma is mediated through the synthesis and secretion of stimulatory growth factors and cytokines by neoplastic and host cells [MI49]. In addition, this level includes cell-cell and cellmatrix adhesion mechanisms that determine cell aggregation properties, remodeling of the adjacent ECM that seems to be a necessary step in the microinvasion of cancer cells, etc.
- The tissue scale is concerned with processes occurring at the tissue level such as cell migration, convection and diffusion of nutrients and chemical factors, mechanical stress, rupture of capsules or basement membranes and invasion of nearby tissues, etc.

Several combinations of these scales have been addressed by cancer modellers. Some examples related to ContraCancrum can be found in [MI64, MI215-MI233].

4.1.1 Avascular tumour growth

Mathematical models of avascular tumour growth are usually based on the biological model of multicellular tumour spheroids [MI215], [MI14],[MI16]. Spheroids are aggregates of tumour cells that can be grown in precisely externaly controlled nutrient conditions. The spheroids nutrient supply is provided through diffusion from their surface. Spheroids develop many features identical with characteristics of avascular tumours such as altered metabolism, proliferation arrest, necrotic death and therapy resistance. Data from experiments with multicellular tumour spheroids can be used to determine model parameters and to validate simulation results.

Models of avascular tumour growth take into account many processes such as cell proliferation and growth, nutrient consumption and diffusion, waste material production and diffusion, effects of growth promoting and inhibitory factors, intracellular adhesion, cell-environment interactions as well as the geometry of the tumour and the individual cells.

Continuum models describe cells and chemicals density using continuous variables according to a reaction-diffusion system [MI1]. Several possible growth laws including exponential, Gompertz and logistic growth have been utilized. Some models take also into account the interaction of the tumour with immune cells [MI2]. The interaction between immune and tumour cells can be described in a predator-prey way where the role of the predator is played by immune cells whereas the role of the prey by tumour cells.

Discrete, hybrid and agent based models take the cell cycle state into account. Cells behave differently depending on the cell cycle state in which they are found. It is also important to efficiently describe tumour growth and its interaction with the local microenvironment.

On the cellular level certain hybrid models make use of discrete lattice/graphs with some deterministic [19] or stochastic rules regarding cell growth, proliferation, death and/or intercellular adhesion (e.g. some Monte Carlo models, the extended large-Q Potts model etc.). On the subcellular level a simplified expression regulatory network (Boolean protein expression regulatory network [MI16]) may control the cell cycle state [MI19]. On the tissue level a system of differential equations usually describes the diffusion, consumption and production of nutrients, metabolites, growth promoters and inhibitors [MI16], [MI19].

4.1.2 Tumour induced angiogenesis

A typical continuum model consists of a balance number of endothelial cells (EC) which is coupled nonlinearly with a set of mass balances describing selected factors in the EC environment [MI18]. The models assume that endothelial cells migrate through random motility, chemotaxis (i.e. a directed migratory response of cells to soluble, diffusible growth factors) in response to tumour angiogenic factors released by the tumour, and haptotaxis (i.e. a directed migration response of cells to insoluble, nondiffusible molecules) in response to fibronectin gradients in an extracellular matrix [MI8].

Blood rheological properties (viscosity, hematocrit, etc.) and microvascular network remodeling represent interrelated issues as blood flow creates stress on the vascular wall (shear stress) that leads to an adaptation of the vascular diameter via vasodilatation or constriction. This in turn leads to adaptation and relaxation of the microvascular network architecture. The flow of blood, a non-Newtonian fluid, can be approximated by a Poiseuille-like expression. This leads to a dynamic adaptive tumour induced angiogenesis [MI9].

On the tissue level certain hybrid models of angiogenesis (e.g. [MI17]) describe the diffusion, uptake and decay of the tumour-secreted pro-angiogenic factor by means of differential equations. On the cellular level the cellular Potts model which is based on the system-energy reduction has been used in order to describe endothelial cell migration, growth, division, and cellular adhesion.

4.1.3 Response to Treatment

Models of tumour response to treatment take into account several factors and treatment modalities (e.g. chemotherapy, irradiation). Immune response may also play some role in the treatment outcome [MI1], [MI2]. One way to model tumour response to chemotherapy is by adding a specific drug killing function [MI217],[MI221], [MI2], [MI12] for each type of cells and by changing the cell cycle state to necrosis or apoptosis depending on the current cell cycle state and its treatment sensitivity. Other supporting drugs such as anti-angiogenic drugs [MI12] can also be taken into account as inhibitory factors.

Irradiation can be modeled by a linear quadratic model [MI20] or extended by a multiscale model that takes into account the key regulation signals (e.g. hypoxia) influencing tumour growth by a Boolean genetic network ([MI3]) or by discrete models of cell cycle [MI216], [MI218], [MI219], [MI3], [MI15] that lead to apoptosis/necrosis depending on the previous cycle state. A crucial phenomenon in understanding tumour response to treatment is that drug and nutrients delivery/diffusion is non homogeneous throughout the tumour. Besides there is a clear dependence of radiosensitivity and chemosensitivity on the cell cycle phase [MI216-MI221], [MI223-MI229], [MI5], [MI13], [MI4], [MI6], [MI7], [MI10], [MI11].

Several methods have been used in order to model drug delivery and drug-tumour interactions such as ordinary differential equations, stochastic differential equations, S-system formalism, power law equations, partial differential equations, molecular dynamics,

variants of the Petri nets, discrete cellular automata, agent based methods, Pi Calculus, discrete event/entity formalism etc. [MI21], MI6], [MI217],[MI221].

4.2 Prevascular Tumour Growth Models

In general, there are two main approaches to model avascular tumour growth. The first one is usually termed *continuous* since it is based on modelling physical and chemical processes through partial differential equations. The second one is usually termed *discrete* and focuses on modelling the behaviour of single cells and their mutual communication. The mathematical apparatus for the latter is usually based on the cellular automata theory. Multiscale approaches are also possible. In a multiscale approach, each level is described in terms of distinct models and all of them are coupled in a single model, [MI215], [MI70-MI72].

In mathematical terms, the tumour and its host environment can be described by a macroscopic state vector $\vec{u}(\vec{x},t)$ whose components can include cell population densities, concentrations of the nutrients and chemical factors, mechanical quantities, such as pressure, describing the response of the tissue to external forces. Cell populations are characterized by the internal functional state of each of their cells specified by a discrete or continuous variable.

In the following a short presentation of the main ideas applied on most approaches will be made and subsequently the approaches to be adopted for the development of the microscopic models of the ContraCancrum project will be commented on.

All computations involved in the continuous approach make use of statistical data i.e. they deal with average densities of both cell numbers and chemical concentrations in the environment. Basically these processes are focused on three different areas: reaction kinetics, diffusion of chemicals and convection. Each area is described by a set of suitable equations. Quite extensive research has also been taking place in the field of the mechanical aspects of the interaction between tumour cells and their surrounding cells.

A usual assumption is that diffusion in conjunction with nutrient consumption limits tumour growth. This approach was firstly proposed by Burton [MI149]. There has been published a wide range of papers using similar approaches [MI147],[MI148-MI205]. The following excerpt from [MI24] outlines this fundamental basis of most models dealing with tumour nutrition:

"Tumour cells consume nutrients. Nutrients diffuse into the tumour tissue from the surrounding tissue. Therefore, if the tumour is very large, the nutrients cannot reach all parts of the tumour tissue. This leads to a decrease in tumour cell proliferation and eventual cell death in regions lacking nutrients. The steady size of the tumour spheroid is reached when the cell proliferation in regions rich in nutrients balances cell death in regions poor in nutrients."

A way to formulate the above mentioned statement in the language of partial differential equations is given below by summariazing the paper by Casciari, Sotirchos and Sutherland [MI148]. In this context the tumour is assumed to be a spheroid and therefore all calculations have been done within this framework.

On the **molecular/sub-cellular level** interacting molecules within sub-cellular compartments (e.g. nucleus, cytosol and plasma membrane) are usually modelled through stoichiometric and reaction kinetics approaches.

In the continuous approach ordinary differential equations (ODEs) are derived on the basis of kinetic principles. This can be applied on reactions involving molecular interactions and flows between adjacent subcompartments or extracellular microenvironment.

Subcellular models can supply parameters to the cellular and tissue models. Synthesized molecules and their derivatives determine the cell phenotype (state). These products may be put on the cell surface or may be excreted or diffused through the whole tissue. A typical continuous formulation [MI73] can be expressed as

Reaction equation

$$\frac{dC_i}{dt} = self\left(C_1,...,C_n\right) + interact\left(C_1,...,C_n\right)$$

$$self\left(C_1,...,C_n\right) = \sum_j k_j C_j$$

$$interact\left(C_1,...,C_n\right) = \sum_{i,j} k_{ij} C_i C_j$$

Compartment flow equations

$$\frac{dC_m^{(j)}}{dt} = diff\left(C_m^{(0)},...,C_m^{(n)}, j\right)$$

$$diff\left(C_m^{(0)},...,C_m^{(n)}, j\right) = \sum_i k_i C_m^{(i)}$$

The cell state is determined on the basis of the concentration of chemicals.

The conservation equations for the chemical species are

$$\frac{\partial C_i}{\partial t} + \nabla \cdot \vec{N}_i = P_i,$$

where C_i are concentrations of the chemical species (oxygen, glucose, lactate ion, carbon dioxide, bicarbonate ion, chloride ion and hydrogen ion concentration are considered); $\vec{N}_i$ is the flux inside the tumour spheroid and P_i is the net rate of consumption/production of the chemical species (including mutual reactions of chemical species as well as tumour cells consumption/production).

The flux is calculated according to Fick's law of diffusion but since some of the chemicals are ionic electric field driven charge migration has also to be considered. The resulting equations can thus take the following form

$$\vec{N}_i = -z_i u_i F C_i \nabla \Phi - D_i \nabla C_i$$

where D_i are (positive) constant diffusion coefficients; z_i is the ionic charge of species, u_i is the mobility, F is the Faraday constant, and Φ is the electrical potential (the first term vanishes in the case of uncharged chemicals i.e. glucose, oxygen, and carbon dioxide).

Casciari, Sotirchos, and Sutherland [MI148] have choosen u_i to be given by the Nernst–Einstein equation

$$u_i = D_i / R_g T$$

where R_g is the gas constant and T is the absolute temperature. By applying the assumption that there is zero net electrical current so that $\sum_k z_k \vec{N}_k = 0,$ the equation for the flux of the ionic species can be rewritten in the form

$$\vec{N}_i = -D_i \left(\nabla C_i - z_i C_i \frac{\sum_k z_k D_k \nabla C_k}{\sum_k z_k^2 D_k C_k} \right).$$

In this way all ionic species are entangled and their flow is dependent on the concentrations of other ionic chemicals.

Moreover, from the part dealing with chemical reactions the authors of [MI148] consider breakdown of glucose through glycolysis and the Krebs cycle and include the detailed metabolic pathway for pH regulation. An overview of these equations can be found in [MI24] or [MI148].

The **cellular level** is usually described in terms of ordinary differential equations [MI75,MI76] or cellular automata evolution rules [MI66],[MI67] for the size N_i (i = 1, 2, . . . , n) of each cell population and the functional state of every cell . The dynamics is determined by intra- and intercellular interactions that can modify the state of the interacting cells and generate cell replication and death. $N_i(s,t)$- the number of cells of type i being in the state s at time t - evolves as

$$\frac{\delta N_i(s,t)}{\delta t} = -I_i(\vec{u},s,t) + J_i(\vec{u},s,t) + P_i(\vec{u},s,t) - D_i(\vec{u},s,t) + S_i(\vec{u},s,t)$$

where $\vec{u}(\vec{x},t)$ is a macroscopic state vector whose components can include cell population densities, concentrations of the nutrients and chemical factors, mechanical quantities, such as pressure, describing the response of the tissue to external forces. The internal evolution I_i takes into account all those intracellular phenomena such as phenotypic transitions triggered by mutations that change the functional state of a cell. The conservative interactions J_i represent cell-cell interactions which change the functional state of one or both interacting cells, but do not lead to cell replication or death. Proliferation is accounted for by the term P_i whereas cell destruction by the term D_i. The term S_i associated with external sources or sinks refers to processes such as the production of immune cells, the destruction of tumour cells by medical treatments or the injection of cells. The simplest expression of the conservative interactions J_i is provided by the following quadratic form

$$J_i(\vec{u},s,t) = \sum_j \sum_{s_1} \sum_{s_2} T_{ij}(s_1,s_2,s) N_i(s_1,t) N_j(s_2,t) - N_i(s,t) \sum_j \sum_{s_1} T_{ij}(s,s_1,s_2) N_j(s_2,t)$$

where $T_{ij}(s_1, s_2, s)$ is the transition rate of the *i th*-cell type to the state s. The initial state is s_1 and the state of the interacting cells belonging to the *j th*-population is s_2. The first term of J_i takes into account those cells that end up with a state s. The second one is a loss term related to those cells that transit from the state s into another state following pair interactions with other cells.

An alternative approach at the cellular level is based on cellular automata models [MI79,MI80]. In the cellular automata framework a set of evolution rules for the discrete state variables inspired by generic features of the system dynamics is suggested. These rules (deterministic or stochastic) are local in space and in time. They replace a set of ODEs used in continuous models to describe the evolution in time of the system at the cellular level. All the components of the system have their states updated in parallel.

The Q-state Potts model

A discrete lattice is used in this model [MI23]. Each lattice site has a state $\sigma \in \{1,2,...,Q\}$. The domains of the lattice sites with the same index describe cells while the links between lattice sites with different indices correspond to cell surfaces. The free energy of the system is described by the Potts Hamiltonian H. A lattice site is chosen at random and a new trial index is also chosen at random from one of the other $Q - 1$ states. The probability of changing the index at the chosen lattice site to the new index is:

$$P = \begin{cases} 1 & \Delta H \le H_{diss} \\ e^{-\frac{\Delta H}{T}} & \Delta H > H_{diss} \end{cases}$$

where $\Delta H = H_{after} - H_{before}$ denotes the difference between the total energy before and after the index reassignment, and T is temperature. H_{diss} represents the dissipation costs involved in deforming a boundary. A Potts model simulation measures time in Monte Carlo Steps (MCS): one MCS is defined as as many trial substitutions as the number of lattice sites.

$$H_1 = \sum_{neighbor\{\vec{i},\vec{j}} J_{\tau(\sigma(\vec{i})),\tau(\sigma(\vec{j}))} \left(1 - \delta_{\sigma(\vec{i}),\sigma(\vec{j})}\right)$$

$$H_2 = \sum_{\vec{i}} \mu C_{\vec{i}}$$

$$H_3 = \sum_{\sigma} \Gamma(\tau(\sigma)) \left[v(\sigma) - V(\tau(\sigma), t) \right]^2$$

$$H = H_1 + H_2 + H_3$$

where $\sigma(\vec{i})$ represents the state of site $\vec{i}$, $\tau(\sigma)$ represents the type of cell σ, J_{τ_1,τ_2} stands for the coupling between cell type τ_1 and cell type τ_2 with respect to the cell surface adhesive energy, $\delta_{i,j}$ is the Kronecker delta, μ stands for the chemical potential, $C_{\vec{i}}$ stands for the chemical concentration at site $\vec{i}$, Γ stands for the cell type rigidity , v is the current volume

and V is the type dependent target volume. The latter depends on the cell cycle since the cell may be growing.

The first term of the energy represents the cell type dependent adhesion energy. The second term represents all bulk properties of the cell such as membrane elasticity, cytoskeletal properties and osmotic pressure. The third term represents chemotaxis where the chemical potential determines if cells move towards or away from higher chemical concentrations.

At the **tissue level**, a continuous approach is based on the assumption that there is a sufficiently large number of cells and relevant molecules in order to define average continuous values for the macroscopic variables. Continuum models are mathematically formulated in terms of PDEs in the area of fluid and continuum mechanics. The majority of them establish an evolution equation for the field $\vec{u}(\vec{x},t)$. For those components of $\vec{u}$ representing cells and chemical substances, the derivation of the corresponding evolution equations follow from the mass balance principle applied to each element volume:

$$\frac{\partial u_j}{\partial t} = -\nabla \cdot (\vec{v} u_j) - \nabla(D \nabla u_j) + \Gamma(u_j) - \delta u_j$$

where $\vec{v}$ is the convective velocity, D is the diffusion coefficient, $\Gamma(u_j)$ is the proliferation term per unit volume, and δ is the death coefficient of the $j\,th$ - cell type population density or concentration. The evolution equation depends on sinks, sources and appropriate boundary conditions determined by the distribution of cells and blood vessels, leading generally to the so-called moving boundary problems [MI81]. For the complete specification of the macroscopic model, it is necessary to introduce constitutive laws to characterize for instance the mechanical properties of the tumour [MI82-MI84].

Tumour growth is modelled using the mass conservation law and thus the velocity of cell movement $\vec{v}$ is given by

$$\nabla \cdot \vec{v} = \lambda F(C_i)$$

where λ is the maximum rate of cell proliferation and $F(C_i)$ is the scaling function for the nutrient/chemical species dependent proliferation. The function $F(C_i)$ is obtained empirically from several experiments. In [MI148] the rate of cell proliferation is represented by

$$F(C_i) = G_1 \left(\frac{C_a}{G_a + C_a} \right) \left(\frac{C_b}{G_b + C_b} \right) \left(\frac{1}{C_g} \right)^n$$

where G_i's are fitting parameters for the measured data (subscript a stands for oxygen, b for glucose, and g for hydrogen ion concentration). The weakness of function F is that it is always positive and hence is not able to describe any necrotic cores in the tumour.

Solving the equations for spherical symmetry leads to the following equation for the radial cell velocity v_r at a point inside the spheroid and the rate of growth of the tumour boundary R:

$$v_r(r) = \lambda \frac{1}{r^2} \int_0^r F(C_i)\, d\bar{r}$$

$$\frac{dR}{dt} = v_r(R) = \lambda \frac{1}{R^2} \int_0^R F(C_i)\, d\bar{r}$$

The above mentioned model of proliferation constitutes the basic version which can be generalized in several ways. It can be enriched by describing the tumour as a conglomerate of several phases of the cellular "material". A separate description of cell movements (by random diffusive movement) and cell deaths can also be taken into account. The general formulation in this case is as follows:

$$\frac{\partial \Phi_i}{\partial t} + \nabla \cdot (\vec{v}_i \Phi_i) = \nabla \cdot (D_i \nabla \Phi_i) + \lambda_i (\Phi_i, C_i) - \mu_i (\Phi_i, C_i),$$

where for each phase/type i which occupies the volume Φ_i (all Φ_i sum up to the total volume 1) the velocity v_i is determined by diffusion with coefficient D_i. The terms λ_i and μ_i represent production and degradation respectively.

In this general form the model seems to be too complicated since there are too many parameters to be experimentally determined for validation purposes. The simplest case addressing only two phases i.e. living and dead cells has been treated in [MI190,MI191]. If n is the living cell density and m the dead cell density the following relation is obtained

$$\frac{\partial n}{\partial t} + \nabla \cdot (\overrightarrow{v_n} n) = \nabla \cdot (D \nabla n) + \lambda (n, C_i) - \mu (n, C_i)$$

$$\frac{\partial m}{\partial t} + \nabla \cdot (\overrightarrow{v_m} m) = \mu (n, C_i)$$

If the average volumes of living cells (V_L) and dead cells (V_D) are given, by assuming constant volume $nV_L + mV_D = 1$ and the same velocities for the dead and living cells the following equation can be obtained

$$\nabla \cdot \vec{v} = \nabla \cdot (D \nabla n) V_L + \lambda (n, C_i) V_L - \mu (n, C_i)(V_L - V_D)$$

This equation can be solved in a way similar to the one applied to the radial symmetry case. This can be done mainly because of the force balance which allows to take into account momentum changes between the particular phases.

There are several other possible modifications aiming at a qualitative description of the possible evolution of the nutrient-limited tumour spheroid. For example use of time delays could explain oscillations in tumour spheroids growth as were studied by Burkowski [MI206] and Byrne [MI207].

Until now consideration of any mechanical aspects of tumour growth have been avoided by assuming radial symmetry. Although this facilitates understanding of the chemical processes involved, biomechanics cannot be ignored in the clinical context.

Some simple initial models calculated the tumour cell interaction with normal tissue by computing the internal pressure within the tumour. This has been done by Greenspan [MI174] and Byrne and Chaplain [MI208]. By omitting technical details in general such models correlate cell velocity with pressure by using Darcy's law of fluid dynamics which can be expressed by the following equation

$$\vec{v} = -\mu \nabla p$$

where μ is a positive constant accounting for the viscosity properties of tumour cells. Combining this equation with the above mentioned equation for velocity and using proliferation parameters the following equation for the internal pressure within a spheroid is obtained

$$-\mu \nabla^2 p = \lambda F\left(C_i\right)$$

The movement of the tumour boundary along an outwards pointing normal unit vector $\vec{n}$ is then given by

$$\vec{n} \cdot \frac{d\vec{r}}{dt} = \vec{v} \cdot \vec{n} = -\mu \nabla p \cdot \vec{n}$$

Furthermore, two boundary conditions are given. The first one states that the pressure on the tumour boundary is in equilibrium with the pressure of the outer environment. The second one proposed in [MI208] connects nutrient concentration with boundary curvature by assuming that nutrient is the source of energy of cell adhesion. It is described by the Gibbs-Thompson relation $c = c_\infty\left(1 - 2\gamma\kappa\right)$, where γ is the surface tension and κ is the mean curvature.

Regarding experimental measurements there is still much to be done. Direct measurement of the pressures in tumour tissue is almost technically impossible. However, a method proposed by Helmlinger et al. [MI212] has been widely discussed. Instead of measuring pressure directly the influence of the outer pressure on tumour growth is calculated by cultivating tumours in differing stiffness agarose gels. Both the experimental and theoretical aspects of this approach have been addressed in many other publications [MI209, MI210,MI211].

The notion of internal cell pressure, inspired by models of fluids does not reflect the internal structure of a cell. Threfore, it could be partly replaced in the future by more informative notions which would take into account the subcellular micro skeleton structures. Theoretical work presented in [MI214] and [213] has pointed towards that direction.

Mathematically, the link between the molecular/sub-cellular, cellular and tissue levels has to be referred to the parameters (growth, death, uptake or absorption, degradation rates, threshold densities, diffusion coefficients, drift velocities, etc.) characterizing the model.

4.3 Models of Prevascular Tumour Response to Chemotherapy and Radiotherapy

In order to describe drug flow in the organism the concept of compartments has been proposed. Common pharmacokinetics models [MI25] make use of diffusion and compartmental modeling to investigate cellular drug uptake and intracellular drug interactions as well as to provide insight into the cellular mechanisms contributing to drug resistance. The flux between compartments is commonly described by the equation

$$\frac{dC^{(j)}}{dt} = \sum_i \left(k_{ij} C^{(i)} - k_{ji} C^{(j)}\right)$$

where $C^{(i)}$ is concentration of drug in the compartment i and k_{ij} represents the rate of transfer between compartments.

Drug cytotoxicity is described by pharmacodynamics [MI27]. The mechanisms contributing to the drug effects are still not completely known. Several phenomenological models adequately describe the fractional cell survival S as a function of concentration and time exposure history. The Hill type model is frequently used

$$S = \frac{1}{\left(1 + Ax^m\right)}$$

where A,m are constants, x is a measure of the cellular damage proportional to extra- or intracellular area under (the) curve (AUC) of the concentration of drug as a function of time.

$$AUC = \int C\,dt$$

Another possibility is an exponential kill model.

$$S = e^{-kx}$$

where x is a suitable measure of damage and k is a constant.

The linear-quadratic model is often used in order to quantify the biological response to radiation. The surviving fraction is expressed as

$$S = e^{\alpha D + \beta D^2}$$

where D is the dose in Gy. The α and β parameters depend on the cell type and the cell cycle phase.

4.4 Modeling Angiogenesis, Invasion and Metastasis

4.4.1 "Hollow" Capillary Networks

This model has been inspired by the tumour-induced angiogenesis model proposed by Anderson & Chaplain [MI8]. It is assumed that endothelial cells migrate through random motility, chemotaxis in response to TAF (tumour angiogenic factor) released by the tumour and haptotaxis in response to fibronectin (FN) gradients in the extracellular matrix. Let n be the endothelial cell density per unit area. The equation describing endothelial cell conservation is as follows

$$\frac{\partial n}{\partial t} = D\nabla^2 n - \nabla(\chi(c)n\nabla c) - \rho\nabla(n\nabla f)$$

The chemotactic migration is representd by the function $\chi(c) = \chi/(1+\delta c)$ which reflects the decrease in chemotactic sensitivity with increased TAF concentration c. The coefficients *D,*

χ, ρ characterize the random, chemotactic, and haptotactic cell migration respectively. f stands for fibronectin concentration.

TAF and the extracellular matrix-macromolecule FN bind to specific membrane receptors on endothelial cells and subsequently trigger molecular cascades inside the ECs, activating cell migratory machinery. One consequence of this activation process is the production of matrix degrading enzymes (MDEs). The endothelial cells become able to exert the traction forces required to propel themselves during migration. In the initial model [MI8] endothelial cell densities and their global influence on TAF and FN concentrations were considered in a continuous formulation. In the model under development the focus will be on local effects and the influence of each individual cell on its local environment will be considered. The model can then be formulated through the following set of equations:

$$\frac{\partial c}{\partial t} = -\eta n_i c$$

$$\frac{\partial f}{\partial t} = \beta n_i - \gamma m f$$

$$\frac{\partial m}{\partial t} = \alpha n_i + \varepsilon \nabla^2 m - \nu m$$

where c represents the TAF concentration, f represents the FN concentration, m represents the MDE concentration and n_i is a Boolean parameter (1 or 0) indicating the presence or absence of an endothelial cell at a given position. The parameters β and α characterize the production rate of FN and MDE by an individual endothelial cell respectively and η its TAF consumption rate. The MDE, once produced, diffuses locally with diffusion coefficient ε, and is spontaneously degraded at a rate ν .

The displacement of each individual endothelial cell located at the tips of each growing sprout is given by the discretized form of the endothelial cell mass conservation equation. The migration of each cell is consequently determined by a set of coefficients emerging from this equation. They are related to the likelihood of the cell remaining stationary, moving left, moving right, moving up, or moving down (in 2 dimensions for simplicity). These coefficients incorporate the effects of random, chemotactic and haptotactic movement and depend on the local chemical environment (FN and TAF concentrations). Proliferation of the endothelial cells at the capillary tips and branching at capillary tips are implemented in the model at the discrete level. Tip branching depends on the TAF concentration at a given spatial location .

4.4.2 Blood Flow

Blood is a very complex biphasic medium, composed of many different constituents, including red blood cells (erythrocytes), white blood cells (leukocytes), and platelets involved in clotting cascades.Because of its biphasic nature, blood does not behave as a continuum and the relative viscosity μ_{rel} measured while flowing at different rates in microvessels is not constant.

$$\mu_{rel}(R, H_D) = \left[1 + (\mu_{0.45} - 1) f(H_D) \left(\frac{2\mathrm{R}}{2\mathrm{R} - 1.1}\right)^2\right] \left(\frac{2\mathrm{R}}{2\mathrm{R} - 1.1}\right)^2$$

where $\mu_{0.45}$ is the viscosity corresponding to the normal average value of the discharge hematocrit (H_D = 0.45), R is the vessel radius, and $f(H_D)$ is a function of the hematocrit.

In the case of a non-Newtonian fluid the local relationship between pressure gradient ΔP and flow Q at the scale of a single capillary element of length L and radius R can be approximated by the following Poiseuille- like expression:

$$Q = \frac{\pi R^4 \Delta P}{8\mu_{app}(R, H_D)L}$$

where $\mu_{app}(R, H_D) = \mu_{rel}\,\mu_{plasma}$ is the product of relative and plasma viscosities. When considering flow calculations through a network of interconnected capillary elements having distributed radii simple conservation of mass or flow (if the fluid is incompressible) at each junction where the capillary elements meet has to be applied.

4.4.3 Adaptation and remodelling

Blood rheological properties and microvascular network remodelling are interrelated issues as blood flow creates stresses on the vascular wall (shear stress, pressure, tensile stress) that lead to the adaptation of the vascular diameters via either vasodilation or vasoconstriction.

The wall shear stress is given by

$$S_{wss} = \log(\tau_w + \tau_{ref})$$

where

$$\tau_w = \frac{4\mu(R, H_D)}{\pi R^3}(Q)$$

and τ_{ref} is a constant included to avoid singular behaviour at low shear rates.

The intravascular pressure is given by

$$S_p = k_P \log(\tau_e(P))$$

where k_P is a constant that dictates the relative intensity of the stimulus, P is the local intravascular pressure and accounts for the dependence of wall shear stress on pressure.

The metabolic hematocrit-related stimulus is given by

$$S_m = k_m \log\left(\frac{Q_{ref}}{QH_D} + 1\right)$$

where Q_{ref} is a reference flow, Q_{ref} corresponds to the flow in the parent vessel, H_D represents the discharge hematocrit in the vessels, Q stands for the flow in the vessel under

consideration and k_m is a constant characterizing the relative intensity of the metabolic stimulus.

The vessel adaptation ΔR is provided by the following equation

$$\Delta R = \left(S_{wss} + S_p + S_m - k_s \right) R \, \Delta t$$

The additional term k_s represents the shrinking tendency of a vessel.

The vessel branching probability $P_{branching}$ is given by

$$P_{branching} = P_{normalize} \frac{\tau_{wss}}{\tau_{max}} \frac{C_{TAF}}{C_{TAF_{max}}}$$

where C_{TAF} stands for the TAF concentration.

4.4.4 Invasion

A tumour experiences unstable growth due to a diffusional instability caused by the competition of the growth of tumour mass and the surface tension (cell adhesive forces) that tends to oppose this growth [MI28]. The instability is enhanced by the development of a necrotic core and its associated volume sink. The presence of the inhomogeneous nutrient field due to angiogenesis tends to further destabilize the tumour because the tumour tends to co-opt the complexly shaped neovasculature in order to maximize nutrient transfer [MI29]. Gatenby et al. [MI30] have addressed in their modeling work the change of extra cellular *pH* that helps tumour invasion. Malignant cells exhibit characteristically altered metabolic patterns when compared with normal mammalian cells with increased reliance on anaerobic metabolism of glucose to lactic acid even in the presence of abundant oxygen. This leads to normal cell death via *p53*-dependent apoptosis pathways, as well as degradation of the interstitial matrix, loss of intercellular gap junctions, enhanced angiogenesis, and inhibition of the host immune response to tumour antigens. Transformed cells maintain their proliferative capacity in acidic extracellular *pH* because of mutations in *p53* or some other component in the apoptotic pathways**.**

4.4.5 Metastasis

Metastasis is characterized by a complex series of events in which cancer cells leave the original tumour site and migrate to other parts of the body via the bloodstream or the lymphatic system. To do so malignant cells break away from the primary tumour and attach to and degrade proteins that make up the surrounding extracellular matrix (ECM) which separates the tumour from the adjacent tissue. By degrading these proteins cancer cells are able to breach the ECM and escape. The body resists metastasis by a variety of mechanisms through the actions of a class of proteins known as metastasis suppressors of which about a dozen are known. One of the critical events required is the growth of a new network of blood vessels called tumour angiogenesis. It has been found that angiogenesis inhibitors would therefore prevent the growth of metastases.

4.5 Particuliarities of Glioblastoma and Lung Cancer

4.5.1 Glioblastoma

Glioblastoma multiforme is characterized by the presence of small areas of necrotic tissue that is surrounded by anaplastic cells (pseudopalisading necrosis). This characteristic in conjunction with the presence of hyperplastic blood vessels differentiates the tumour from grade 3 astrocytomas which do not exhibit these features. Although glioblastoma multiforme can be formed from lower-grade astrocytomas post-mortem autopsies have revealed that most glioblastomas multiforme are not caused by previous lesions in the brain.

Glioblastomas multiforme (GBM) can form in either the gray matter or the white matter of the brain. Most GBM however arise from the deep white matter and quickly infiltrate the brain often becoming very large before producing symptoms. The tumour may extend to the meningeal or ventricular wall leading to a high protein content of cerebrospinal fluid(CSF) (> 100 mg/dL) as well as an occasional pleocytosis of 10 to 100 cells, mostly lymphocytes. Malignant cells carried in the CSF may spread to the spinal cord or cause meningeal gliomatosis. However, metastasis of GBM beyond the central nervous system is extremely rare. About 50% of GBM occupy more than one lobe of a hemisphere or are bilateral. Tumours of this type usually arise from the cerebrum and may exhibit the classic infiltration across the corpus callosum producing a butterfly (bilateral) glioma. The tumour may take on a variety of appearances depending on the amount of hemorrhage,necrosis or its age. A CT scan usually shows a nonhomogeneous mass with a hypodense center and a variable ring of enhancement surrounded by edema. The mass effect from the tumour and edema may compress the ventricles and cause hydrocephalus.

Some recent models incorporate anatomical features to help model tumour growth in a more realistic way based on the characteristics of heterogeneous brain tissue. Some of these models extend the conventional modeling approach of gliomas at the macroscopic scale to explain tumour invasion at the microscopic cellular level. Certain models take into account the fact that glioma diffusion through white and gray matter is different. Differential motility is estimated using the Fisher's approximation [MI32].

4.5.2 Lung cancer

The vast majority of lung cancers are carcinomas i.e. malignancies that arise from epithelial cells. There are two main types of lung carcinoma categorized by the size and appearance of the malignant cells as seen by a histopathologist under the microscope: non small cell (80.4%) and small cell (16.8%) lung carcinoma. This classification based on histological criteria has important implications for clinical management and prognosis of the disease.

The non small cell lung carcinomas are grouped together because their prognosis and management are similar. There are three main subtypes of non small cell carcinoma: squamous cell lung carcinoma, adenocarcinoma, and large cell lung carcinoma. Accounting for 31.2% of lung cancers, squamous cell lung carcinoma usually starts near a central bronchus. Cavitation and necrosis within the center of the tumour is a common finding. Well differentiated squamous cell lung cancers often grow more slowly than other cancer types. Adenocarcinoma accounts for 29.4% of lung cancers. It usually originates in peripheral lung tissue. Most cases of adenocarcinoma are associated with smoking; however, among people who have never smoked ("never-smokers"), adenocarcinoma is the most common form of lung cancer. A subtype of adenocarcinoma, the bronchioloalveolar carcinoma, is more common in female never-smokers and may have different responses to treatment. Small cell lung carcinoma (SCLC, also called "oat cell carcinoma") is less common. It tends to arise in the larger airways (primary and secondary bronchi) and grows rapidly becoming quite large.

The “oat” cell contains dense neurosecretory granules (vesicles containing neuroendocrine hormones) which are responsible for an endocrine/paraneoplastic syndrome association. While initially more sensitive to chemotherapy it ultimately carries a worse prognosis and is often metastatic at presentation. Small cell lung cancers are divided into limited stage and extensive stage disease. This type of lung cancer is strongly associated with smoking.The lung is also a common place for metastasis from tumours in other parts of the body. These cancers are identified by the site of origin; thus, a breast cancer metastasis to the lung is still known as breast cancer. They often have a characteristic round appearance on chest x-ray. Primary lung cancers themselves most commonly metastasize to the adrenal glands, liver, brain, and bone.

4.6 The Digital Biological Cell (DBC) Approach

In this section some representative high level features of the Digital Biological Cell (DBC or dbc) approach are briefly outlined. DBC is a generic microscopic biomodeling method that has been adopted for the development of the microscopic tumour models within the framework of the ContraCancrum project. A central mathematical feature of the approach is the extensive use of the diffusion equation. A detailed mathematical formalism of the basics of the method has also been developed [MI19].

4.6.1 The Environment Model

The environment of the biological system under consideration is modeled at two different levels. At the local level it posseses a lattice structure to allow relatively precise calculations. Its global structure is handled by an oriented graph which is suitable for the description of the topological structure of the domain. All relevent pieces of information are integrated into a *graph of locations* characterized by the following features

1. *nodes* (local environments). Each node (environment) is represented by a discrete lattice. A lattice site contains a homogeneous concentration of vaxes [*entities that can interact*] and dbcs. A lattice can be dynamically subdivided into sublattices. The ratio of the volumes of two neighborhood sites can take values up to 1:6.
2. *edges* (connections between local environments over a long distance). They describe the transfer of vaxes and dbcs. An edge represents the connection of a set of sites in a source node and a set of sites in a destination node as well as the temporal transfer function of vaxes and dbcs.

4.6.2 Vaxes

In order to simulate chemical reactions and signaling the *vax* notion denoting an entity that can interact is utilized [MI1, MI19, MI31]. The complementary notions of *provax* (a vax in the environment that is not bound to a dbc) and *revax* (a vax bound to a membrane) are also used.

4.6.3 Digital Biological Cells (dbcs)

Cells are represented by dbcs [MI19] [MI31]. Some representative dbc features (Figure MI3) are listed below

- Membrane system (a dbc membrane) [MI26].
- Membrane enclosed part of the environment. It defines the dbc shape and divides a lattice into inner and outer lattice cells.
- Membrane elements which correspond to the boundaries of two lattice cells. They

contain revaxes. A revax can be oriented into the inner or the outer part of a lattice cell.

- External membrane. An external membrane determines the boundaries of a dbc.
- Revax reaction functions. They define reactions among provaxes/revaxes and revaxes. [MI1,MI31,MI34].
- Seasonal/cumulative vax sets. Such sets determine the most influencing revaxes during some period e.g. those that maximize the revax reaction function. A seasonal vax set determines the state of a dbc.
- Vax gradient
- Cost resources
- Zygotic graphs (ZG). Their nodes represent vaxes. Oriented edges determine actions (Figure MI4) [MI31] . Basic features of the zygotic graphs are the following
    - *nodes* representing vaxes
    - *edges* representing actions (producing provaxes, adding revaxes, moving, dividing, death as well as their parameters and costs)
    - an action is not performed if there are not enough resources
    - provaxes and revaxes can be distributed homogeneously or inhomogeneously
    - A zygotic graph can have the following main subgraphs:
        - *production (sub)graph.* It determines how many and which vaxes will be spilled into the environment (for each membrane)
        - *revax (sub)graph*. It determines how many and which vaxes will be added to the membranes
        - *motion/growth (sub)graph*. It determines a dbc movement or a change of shape.
- The number of non used revaxes decreases with time
- dbc membrane division
    - a dividing action is determined from the ZG
    - the number of revaxes on a membrane reaches the maximum revax number
    - division transformation
        - a membrane is divided into two membranes and its resources are distributed to each one of the new membranes (homogeneously or non-homogeneously)
        - a direction of division is selected
        - a time of division is determined
        - abnormalities during division are determined and performed
- dbc membrane death
    - the number of revaxes on a membrane reaches the minimum revax number. The dbc membrane disappears (model of apoptosis)
    - resources are not enough or the number of internal provaxes of the membrane reaches its maximum . The dbc membrane cracks and spills its resources into the environment (model of necrosis)
- Membrane transfer function. It determines a transfer of provaxes through a

membrane

- Each action has a time range within which it can be performed. For example interactions of chemicals take ms whereas cell cycling can take hours
- The state of a dbc is determined by the number of revaxes and by the number of provaxes in the inner and the outer environment and their reactions
- The state of a dbc is changing with time depending on changes in the inner and the outer environment.

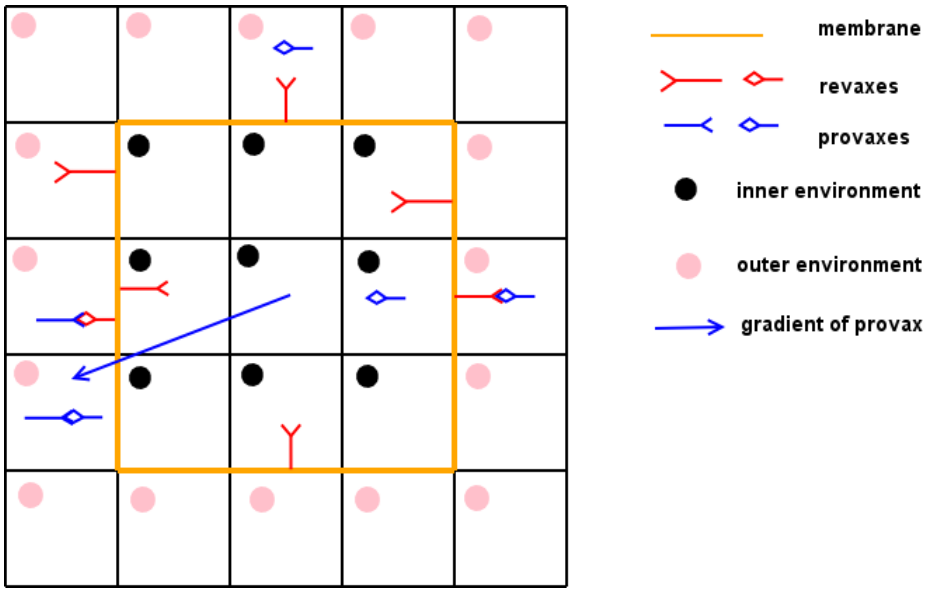

Figure MI3. A digital biological cell (DBC or dbc) on the two dimensional domain

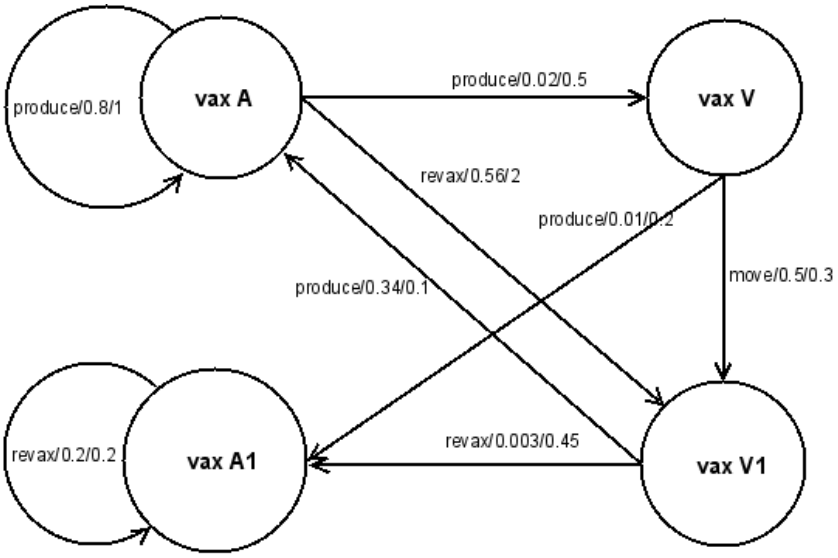

Figure MI4. An example of zygotic graph

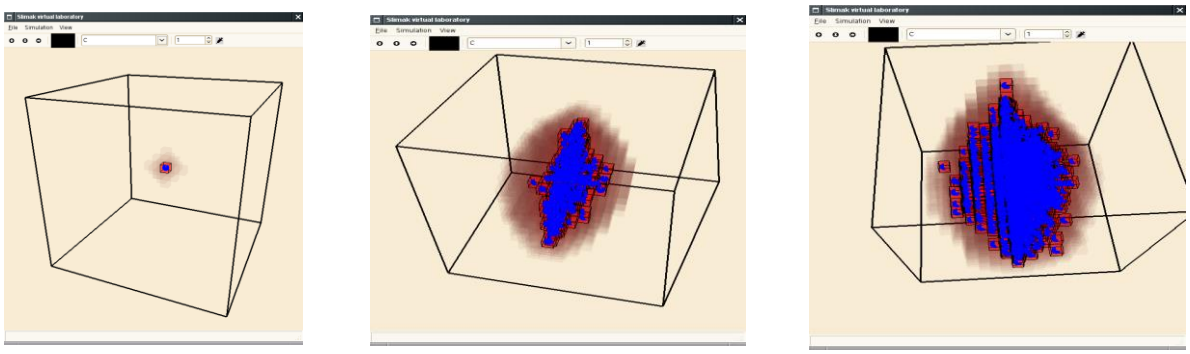

Figure MI5. dbc model of avascular tumor growth with small adhesion and diffusion

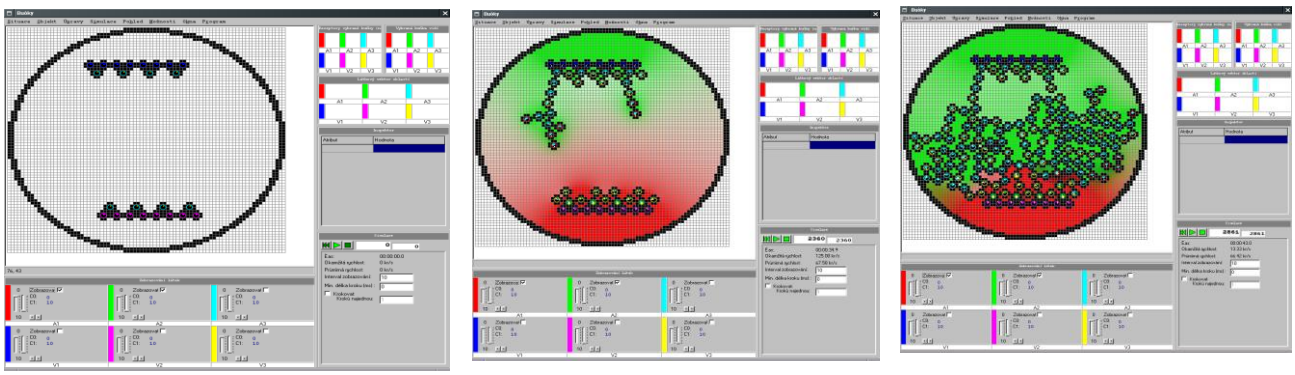

Figure MI6. dbc model of vasculogenesis with chemotaxis and haptotaxis

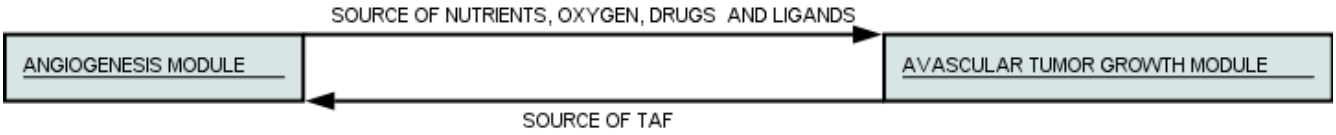

Figure MI7. Cooperation of angiogenesis module and avascular tumour growth module as source sink cooperation

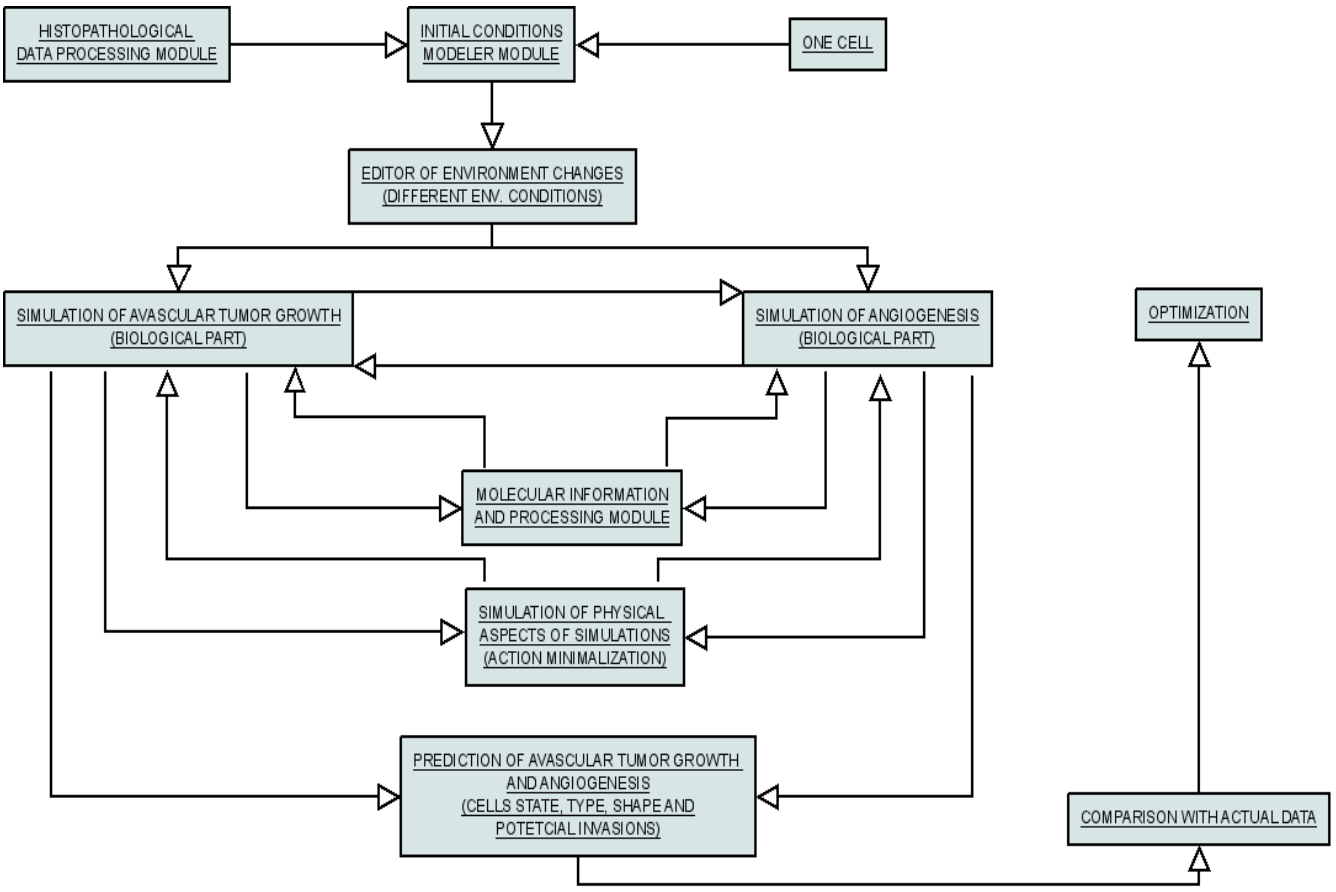

Figure MI8. Workflow diagram

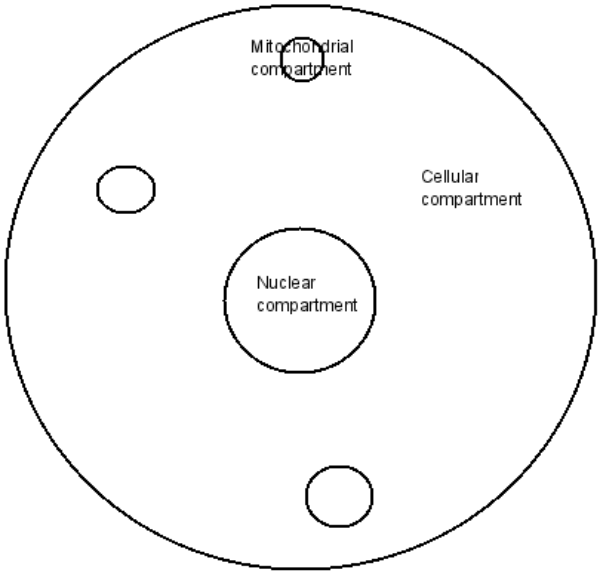

Figure MI9. Compartmental model

4.7 Digital Biological Cell (DBC) Models of Avascular Tumour Growth, Invasion, Angiogenesis and Treatment Response

An adaptive discrete and discretized continuous approach (Figure MI3) has been adopted in order to model avascular tumour growth, invasion, angiogenesis and drug interactions (Figure MI5, Figure MI6, Figure MI7, Figure MI8). The tumour is considered a spatiotemporal distribution of discrete cells and chemicals/ligands (e.g. oxygen, nutrients, drugs) regions.

The envisaged main features and functioning of the corresponding microscopic cancer modeling module in the research setting will be as follows (Figure MI8)

i. The microscopic imaging data of the tumour (e.g. microphotographs of histopathological sections) are provided.
ii. The data is processed so that certain characteristics of tumour cells and the cell system (including shapes and states) are quantified.
iii. The pre-treatment spatial distribution of non imageable tumour cells within the patient from whom the tissue has been excised is estimated.
iv. An editor of microenviromental changes provides the utility to change the micro-environment parametrers.
v. Molecular data (e.g. diffusion, stoicheiometry, status, amplification and expressions of critical genes which have been shown to drastically affect the response of the tumour under consideration to the treatment addressed, receptors present etc.) are provided. Estimates (even semi-qualitative) of their production and state changes are made.
vi. The compartmental model of Figure MI9 is used as a reference for the study of cell shape, cell-drug interactions, energetic conditions and other tumour dynamics aspects.

vii. The model parameters are estimated based on the previously mentioned data as well as literature based information.

viii. Appropriate rules are applied at every time scale considered. These refer to state changes, cell proliferation, cell death, cell-drug/chemical interaction, cell movement, cell shape changes etc. The outcome is an update of the spatiotemporal cell states of the tumour cells over the tumour.

ix. An avascular tumour growth submodule (TM) provides sources of TAF to the angiogenesis module (AM). AM in turn provides sources of chemicals to TM (Figure MI7).

In parallel with the solution of the biological problem a physical refinement concerning shapes,convective movement etc. will take place based on minimazition of action (e.g. according to the cellular Q-Potts models). Any physical data available (primarily through literature) will be utilized to this end.

Acceleration of the simulation code will be addressed in order to significantly lower the computing time demands. Execution of the code on fast computing systems (eventually including clusters and/or grid) have been planned.

The prediction of the spatiotemporal cell state and shape of a non macroscopically imageable tumour will be made for both the free growth and the rsponse to treatment (chemotherapy, radiotherapy) cases. Several visualization forms of the predictions (graphs, 3D and 4D rendering etc.) will be offered.

The simulated treatment outcome will be compared with any relevant data following treatment (e.g. microphotographs of histology slides after surgery) and an optimization loop of the parameters estimation (and if necessary of the model algorithm) will be implemented.

4.8 Testing of the Microscopic Models

The quantitative connection of mathematical models with biological observations is represented by the mathematical model parameters. Each parameter of the model under consideration refers to a particular phenomenon and has a particular effect on a specific cell population or a chemical substance or a sub-cellular process within a given cell type. Certain parameters can be evaluated from biological assays, obtained from generic databases or derived from mathematical models which justify the increasing effort to develop a quantitative and structural information infrastructure suitable to support physiological modeling [MI85].

Up to now only very few experimentally validated models considering cell population and nutrient interactions have appeared. The link between the microscopic and the macroscopic description remains an open problem [MI75]. The reason is that subcellular and cellular models involve a more detailed dynamics dependent on the state of the cells whereas this kind of information is largely lost in macroscopic models. A plausible approach to tackle this problem is the ‘summarise and jump’ strategy outlined in Chapter 1. Section 4.7 contains i.a. a high level consideration of the microscopic model testing approach to be adopted.

Each modeling approach be it discrete or continuous assumes a time and space scale and a specific nature of the physical or biological interactions involved. Indeed the continuous evolution equation for the cell population densities essentially describes mean field like cellular interactions. Cellular automata or agent-based models rely on local or short-range interactions. Generally both types of interactions can occur. In addition, the balance between

determinism and stochasticity depends on the time and length scale on which the questions are posed. At the molecular level protein-protein and protein-DNA interactions are stochastic but at the cellular level and for a long time span average concentrations can be statistically defined so that their evolutions can be described by deterministic equations. Moreover, unknown or incompletely understood biological mechanisms that play a role in the phenomena considered can lead to stochastic model descriptions.

It is noted that the main role of the development of microscopic models within ContraCancrum is to provide insight into and better understanding of the biological mechanisms of cancer so that i.a. refinement of the imageable tumour models (Chapters 6 and 7) can be achieved. Therefore, the clinical validation focus within ContraCancrum (Chapter 5) is on the latter rather on the microscopic models themselves.

References

[MI1] Lisette G. de Pillis, Ami E. Radunskaya and Charles L. Wiseman: A Validated Mathematical Model of Cell-Mediated Immune Response to Tumor Growth, Cancer Research 65 (2005), 7950-7958

[MI2] L.G. De Pillis, A. Radunskaya: A mathematical tumor model with immune resistance and drug therapy: an optimal control approach. Journal of Theoretical Medicine 2001;3:79-100.

[MI3] Benjamin Ribba, Thierry Colin and Santiago Schnell: A multiscale mathematical model of cancer, and its use in analyzing irradiation therapies ,Theoretical Biology and Medical Modelling 2006, 3:7

[MI4] Pabitra N. Sen and Peter J. Basser: A Model for Diffusion in White Matter in the Brain,Biophysical Journal 89:2927-2938 (2005)

[MI5] Chao-Wei Hwang, Elazer R. Edelman: Arterial Ultrastructure Influences Transport of Locally Delivered Drugs, Circulation Research. 2002;90:826

[MI6] Sean H.J. Kim, Sunwoo Park, Amina A. Qutub, and C. Anthony Hunt: In Silico Modeling of Blood-Brain Barrier:Agent-Based Simulation of Cerebral Glucose Transport, 2005 Spring Simulation Multiconference, San Diego, California

[MI7] S. Kalyanasundaram, V. D. Calhoun, and K. W. Leong: A finite element model for predicting the distribution of drugs delivered intracranially to the brain, Am. J. Physiol. Regul. Integr. Comp. Physiol. 273: R1810-R1821, 1997;

[MI8] Anderson, Chaplian: Continous and discrete mathematical models of tumor-induced angiogenesis, Bull. Math. Biol. 63: 801-63, 1998

[MI9] Chaplain, McDougall, Anderson: Mathematical Modeling of Tumor-Induced Angiogenesis, Annu. Rev. Biomed. Eng. 8: 233-57, 2006

[MI10] Charles Nicholsonh: Diffusion and related transport mechanisms in brain tissue, Rep.Prog.Phys. 64 (2001) 815-884

[MI11] R. Venkatasubramanian, M. A. Henson, N. S. Forbes: Incorporating energy metabolism into a growth model of multicellular tumor spheroids, J. of Theor. Biology 242 (2006) 440-453

[MI12] R.K.Sachs, L.R.Hlatky and P.Hahnfeld: Simple ODE Models of Tumor Growth and Anti-Angiogenic or Radiation Treatment, Math. And Computer Modeling 33 (2001) 1297-1305

[MI13] John P. Ward, John R. King: Mathematical modelling of drug transport in tumour multicell spheroids and monolayer cultures, Mathematical Biosciences 181 (2003) 177-207

[MI14] G.J.Pettet, C.P.Please, M.J.Tindall, D.L.A.McElwain: The Migration of cells in Multicell Tumor Spheroids, Bull. Of Math. Biology 63 (2001), 231-257

[MI15] T.M.Pawlik, K.Keyomarsi: Role of Cell Cycle in Mediating Sensitivity To Radiotherapy, Int.J.Rad.Onco.Bios.Phys. Vol 19. No 4. 928-942, 2004

[MI16] Yi Jiang, Jelena Pjesivac-Grbovic, Charles Cantrell and James P. Freyer: A Multiscale Model for Avascular Tumor Growth, Biophysical Journal 89:3884-3894 (2005)

[MI17] Amy L. Bauer , Trachette L. Jackson and Yi Jiang: A Cell-Based Model Exhibiting Branching and Anastomosis during Tumor-Induced Angiogenesis, Biophysical Journal 92:3105-3121 (2007)

[MI18] Nikos Mantzaris, Steve Webb, & Hans G. Othmer: Mathematical Modeling of Tumor-induced Angiogenesis, J.Math.Biol. 41,111,2004

[MI19] Michal Karasek: Computer simulations of biological cells in non-standard states, Diploma thesis, Charles University in Prague Faculty of Math and Physics, 2005

[MI20] Thames HD. Hendry JH: Fractionation in Radiotherapy, Londo: Taylor and Francis, 1987

[MI21] Wayne Materi, David S. Wishart: Computational systems biology in drug discovery and development: methods and applications, Drug Discovery Today, Vol 12, Num 7/B, 2007

[MI22] M.L. Martins, S.C. Ferreira Jr., M.J. Vilela: Multiscale models for the growth of avascular tumors, Physics of Life Rev. 4 (2007) 128-156

[MI23]Mark Alber, Maria Kiskowski, James Glazier and Yi Jiang, "On Cellular Automaton Approaches to Modeling Biological Cells", in IMA 134: Mathematical systems theory in biology, communication, and finance. Springer-Verleg, New York. , pp. 12, 2002

[MI24] T. Roose, S. J. Chapman, P. K. Maini: Mathematical Models of Avascular Tumor Growth, SIAM REVIEW 2007, Vol. 49,No. 2,pp. 179–208

[MI25] Ardith W El-Kareh and Timothy W Secomb: A Mathematical Model for Cisplatin Cellular Pharmacodynamics. Neoplasia. 2003 March; 5(2): 161–169.

[MI26] J.Macia and R.V.Sole: Synthetic Turing protocells: vesicle self-reproduction through symmetry-breaking instabilities, arXiv:q-bio/0607035v1

[MI27] Sanga, Sinek, Frieboes, Ferrari, Fruehauf, Cristini: Mathematical modeling of cancer progression and response to chemotherapy. Expert Rev. Anticancer Ther. 6(10), 1361-1376 (2006)

[MI28] Byrne, H., Chaplain, M., 1997. Free boundary value problems associated with the growth and development of multicellular spheroids. Eur. J. Appl. Math. 8, 639.

[MI29] X. Zheng, S.M. Wise, V. Cristini:Nonlinear simulation of tumor necrosis, neo-vascularization and tissue invasion via an adaptive finite-element/level-set method. Bulletin of Mathematical Biology 67 (2005) 211259

[MI30] Robert A. Gatenby and Edward T. Gawlinski: The Glycolytic Phenotype in Carcinogenesis and Tumor Invasion: Insights through Mathematical Models. CANCER RESEARCH 63, 38473854, July 15, 2003

[MI31] Alberts, Bray, Johnson, Lewis, Raff, Roberts, Walter: Essential cell biology, Garland Publishing, 1998

[MI32] K. R. Swanson, E. C. Alvord, Jr. and J. D. Murray. A quantitative model for differential motility of gliomas in grey and white matter. *Cell Prolif.*, 33:317329, 2000.

[MI33] P.W.Zandstra, D.A.Lauffenburger, C.J.Eaves: A ligand-receptor signaling threshold model of stem cell differentiation control: a biological conserved mechanism applicable to hematopoesis. Blood. 2000;96:1215-1222

[MI34] Kumar V, Abbas AK, Fausto N. Robbins and Cotran pathologic basis of disease. 7th ed. W.B. Saunders Co.; 2004.

[MI35] McGee JO'D, Isaacson PG, Wright NA, editors. Oxford textbook of pathology. Oxford: Oxford University Press; 1992.

[MI36] Murray CJL, Lopez AD. Alternative projections of mortality and disability by cause 19902020: Global burden of disease study. Lancet 1997;349:1448504.

[MI37] Peto J. Cancer epidemiology in the last century and the next decade. Nature 2001;411:3905

.[MI38] Clark WH. Tumour progression and the nature of cancer. Br J Cancer 1991;64:63144.

[MI39] Badii R, Politi A. Complexity: Hierarchical structures and scaling in physics. Cambridge: Cambridge University Press; 1997.

[MI40] Gibbs JB. Mechanism-based target identification and drug discovery in cancer research. Science 2000;287:196973.

[MI41] Lindahl T. Instability and decay of the primary structure of DNA. Nature 1993;362:70915.

[MI42] Alberts B, Johnson A, Lewis J, Raff M, Roberts K, Walter P. Molecular biology of the cell. 4th ed. New York: Garland Science; 2002.

[MI43] Lodish H, Berk A, Zipurski SL, Matsudaira P, Baltimore D, Darnell J. Molecular cell biology. 4th ed. New York: W.H. Freeman and Company; 2000.

[MI44] Lilley J. Nuclear physics: Principles and applications. Chichester: Willey; 2001.

[MI45] Hoeijmakers JH. Genome maintenance mechanisms for preventing cancer. Nature 2001;411:36674.

[MI46] Weinberg RA. One renegate cell. New York: Basic Books; 1998.

[MI47] Vogelstein B, Kinzler KW. Cancer genes and the pathways they control. Nature Medicine 2004;10(8):789-99.

[MI48] Evan GI, Vousden KH. Proliferation, cell cycle and apoptosis in cancer. Nature 2001;411:3428.

[MI49] Liotta LA, Kohn EC. The microenvironment of the tumour-host interface. Nature 2001;411:3759.

[MI50] Khavari PA. Modelling cancer in human skin tissue. Nature Rev Cancer 2006;6:27080.

[MI51] Weinberg RA. How cancer arises. Sci Am 1996;275(3):3240.

[MI52] Ruoslahti E. How cancer spreads. Sci Am 1996;275(3):427

[MI53] Hanahan D, Weinberg RA. The hallmarks of cancer. Cell 2000;100:5770

[MI54] Loeb LA. Mutator phenotype may be required for multistage carcinogenesis. Cancer Res 1991;51:30759.

[MI55] Sieber OM, Heinimann K, Tomlinson IPM. Genomic instability—the engine of tumorigenesis? Nature Rev Cancer 2003;3:7018.

[MI56] Rubin H. Degrees and kinds of selection in spontaneous neoplastic transformation: An operational analysis. Proc Natl Acad Sci USA 2005;102(26):927681.

[MI57] Rubin H. Selected cell and selective microenvironment in neoplasic development. Cancer Res 2001;61:799807.

[MI58] Chow M, Rubin H. Clonal selection versus genetic instability as the driving force in neoplastic transformation. Cancer Res 2000;60:65108.

[MI59] Clarke MF, Fuller M. Stem cells and cancer: two faces of Eve. Cell 2006;124:11115.

[MI60] Huntly BJP, Gilliland DG. Leukaemia stem cells and the evolution of cancer-stem-cell research. Nature Rev Cancer 2005;5:31121.

[MI61] Jones PA, Baylin SB. The fundamental role of epigenetic events in cancer. Nature Rev Genet 2002;3:415-28.

[MI62] Laken SJ, Petersen GM, Gruber SB, Oddoux C, Oster H, Giardiello FM, Hamilton SR, Hampel H, Markowitz A, Klimstra D, Jhanwar S, Winawer S, Offit K, Luce MC, Kinzler KW, Vogelstein B. Familial colorectal cancer in Ashkenazim due to a hypermutable tract in APC. Nature Gen 1997;17:7983.

[MI63] Weinberg RA. The biology of cancer. New York: Garland Science; 2007.

[MI64] Preziosi L. Cancer modelling and simulation. London: Chapman& Hall/CRC Press; 2003.

[MI65] Byrne HM, Alarcon T, Owen MR, Webb SD, Maini PK. Modelling aspects of cancer dynamics: a review. Phil Trans R Soc A 2006;364:1563 78.

[MI66] Moreira J, Deutsch A. Cellular automaton models of tumor development: A critical review. Adv Compl Syst 2002;5(23):24767.

[MI67] Araujo RP, McElwain LS. A history of the study of solid tumor growth: The contribution of mathematical modelling. Bull Math Biol 2004;66:103991.

[MI68] Gatenby RA, Gillies RJ. Why do cancers have high aerobic glycolysis? Nature Rev Cancer 2004;4(11):8919.

[MI69] Gatenby RA, Gawlinski ET. The glycolytic phenotype in carcinogenesis and tumor invasion: insights through mathematical models. Cancer Res 2003;63:384754.

[MI70] Glimm J, Sharp DH. Multiscale science. A challenge for the twenty-first century. SIAM News 1997:30,4,17,19.

[MI71] Krumhansl JA. Multiscale science: Materials in the 21st century. Materials Science Forum 2000;3278:18.

[MI72] Li J, Kwank M. Exploring complex systems in chemical engineering—the multi-scale methodology. Chem Eng Sci 2003;58:52135.

[MI73] Athale A, Mansury Y, Deisboeck TS. Simulating the impact of a molecular `decision-process' on cellular phenotype and multicellular patterns in brain tumors. J Theor Biol 2005;233(4):46981.

[MI74] Odor G. Universality classes in nonequilibrium lattice systems. Rev Mod Phys 2004;76(3):663724.

[MI75] Bellomo N, Preziosi L. Modelling and mathematical problems related to tumour evolution and its interaction with the immune system. Math Comp Model 2000;32:41352.

[MI76] Bellomo N, De Angelis E. Strategies of applied mathematics towards an immuno mathematical theory on tumour and immune system interactions. Math Models Meth Appl Sci 1998;8:140329.

[MI77] Patel AA, Gawlinski ET, Lemieux S, Gatenby RA. A cellular automaton model of early tumor growth and invasion: The effects of native tissue vascularity and increased anaerobic tumor metabolism. J Teor Biol 2001;213:31531.

[MI78] May RM. Models for two interacting populations. In: May RM, editor. Theoretical ecology: Principles and applications. Philadelphia: W.B. Saunders Company; 1976. p. 4970.

[MI79] Wolfram S. Theory and application of cellular automata. Singapore: World Scientific; 1986.

[MI80] Ermentrout GB, Edelstein-Keshet L. Cellular automata approaches to biological modeling. J Theor Biol 1993;160:97133.

[MI81] Alarcon T, Byrne HM, Maini PK. A cellular automata model for tumour growth in inhomogeneous environment. J Theor Biol 2003;255:257 74.

[MI82] Chen CY, Byrne HM, King JR. The influence of growth-induced stress from the surrounding medium on the development of multicell spheroids. J Math Biol 2001;43:191220.

[MI83] Jackson TL, Byrn HM. A mathematical model of tumour encapsulation. Math Biosci 2002;180:30728.

[MI84] Byrne HM, King JR, McElwain DLSC, Preziosi L. A two-phase model of solid tumour growth. Appl Math Lett 2003;16:56773.

[MI85] Ribba B, Tracqui P, Boix J, Boissel J, Randall Thomas S. QxDB: a generic database to support mathematical modeling in biology. Phil Trans R Soc A 2006;364:151732.

[MI86] Ferreira Jr. SC, Martins ML, Vilela MJ. Reaction-diffusion model for the growth of avascular tumor. Phys Rev E 2002;65:021907.

[MI87] Nowell PC. The clonal evolution of tumor cell populations. Science 1976;194:238.

[MI88] Scalerandi M, Romano A, Pescarmona GF, Delsanto PP, Condat CA. Nutrient competition as a determinant for cancer growth. Phys Rev E 1999;59:220617.

[MI89] Scalerandi M, Pescarmona GP, Delsanto PP, Capogrosso Sansone B. Local interaction simulation approach for the response of the vascular system to metabolic changes of cell behavior. Phys Rev E 2000;63:011901.

[MI90] Alarcon T, Byrne HM, Maini PK. Towards whole-organ modelling of tumour growth. Prog Bio Mol Biol 2004;85:45172.

[MI91] Thiery JP. Epithelial-mesenchymal transitions in tumour progression. Nature Rev Cancer 2002;2:44254.

[MI92] Friedl PF, Wolf K. Tumour-cell invasion and migration: diversity and escape mechanisms. Nature Rev Cancer 2003;3:36274.

[MI93] Folkman J, Hochberg M. Self-regulation of growth in three-dimensions. J Exp Med 1973;138:74553.

[MI94] Sutherland RM. Cell and environment interactions in tumour microregions: the multicell spheroid model. Science 1988;240:17784.

[MI95] Eden M. A two dimensional growth process. In: Neyman J, editor. Biology and problems of health. Proceedings of the fourth Berkeley symposium on mathematical statistics and probability, vol. IV. Berkeley: University of California Press; 1961.

[MI96] Ward JP, King JR. Mathematical modelling of avascular tumour growth. IMA J Math Appl Med Biol 1997;14:3669.

[MI97] Ward JP, King JR. Mathematical modelling of avascular tumour growth, II. Modelling growth saturation. IMA J Math Appl Med Biol 1999;16:171211.

[MI98] Ward JP, King JR. Mathematical modelling of the effects of mitotic inhibitors on avascular tumour growth. J Theor Med 1999;1:287311.

[MI99] Kerr JFR, Searle J, Harmon BV, Bishop CJ. Apoptosis. In: Potten CS, editor. Perspectives in mammalian cell death. Oxford: Oxford University Press; 1987.

[MI100] Byrne HM. The effect of time delays on the dynamics of avascular tumour growth. Math Biosci 1997;144:83117.

[MI101] Sherratt JA, Chaplain MAJ. A new mathematical model for avascular tumour growth. J Math Biol 2001;43:291312.

[MI102] Jiang Y, Pjesivac-Grbovic J, Cantrell C, Freyer JP. A multiscale model for avascular tumor growth. Biophys J 2005;89:388494.

[MI103] Smolle J, Stettner H. Computer simulation of tumor cell invasion by a stochastic growth model. J Theor Biol 1993;160:6372.

[MI104] Ferreira Junior SC, Martins ML, Vilela MJ. A growth model for primary cancer. Phys A 1998;261:56980.

[MI105] Ferreira Jr. SC, Martins ML, Vilela MJ. A growth model for primary cancer (II). New rules, progress curves and morphology transitions. Phys A 1999;272:24556.

[MI106] Meakin P. Fractals, scaling and growth far from equilibrium. Cambridge: Cambridge University Press; 1998.

[MI107] Barabási A-L, Stanley HE. Fractal concepts in surface growth. Cambridge: Cambridge University Press; 1995.

[MI108] Vicsek T. Fractal growth phenomena. 2nd ed. Singapore: World Scientific; 1992.

[MI109] Dormann S, Deutsch A. Modelling of self-organized tumour growth with a hybrid cellular automaton. Silico Biol 2002;2:0035.

[MI110] Gatenby RA, Gawlinsky ET. A reaction-diffusion model of cancer invasion. Cancer Res 1996;56:574553.

[MI111] Chaplain MAJ. A vascular growth, angiogenesis and vascular growth in solid tumours: the mathematical modelling of the stages of tumour development. Math Comput Modelling 1996;23:4787.

[MI112] Xu Y. A free boundary problem model of ductal carcinoma *in situ*. Discrete Cont Dyn Syst 2004;4:33748.

[MI113] Franks SJ, Byrne HM, King JR, Lewis CE. Modelling the early growth of ductal carcinoma *in situ*. J Math Biol 2003;47:42452.

[MI114] Franks SJ, Byrne HM, Mudar HS, Underwood JCE, Lewis CE. Mathematical modelling of comedo ductal carcinoma *in situ* of the breast. Math Med Biol 2004;20:277308.

[MI115] Franks SJ, Byrne HM, Underwood JCE, Lewis CE. Biological inferences from a mathematical model of comedo duct carcinoma *in situ* of the breast. J Theor Biol 2005;232:52343.

[MI116] Mullins WW, Sekerka RF. Morphological stability of a particle growing by diffusion or heart flow. J Appl Phys 1963;34:3239.

[MI117] Hatzikirou H, Deutsch A, Schaller C, Simon M, Swanson K. Mathematical modelling of glioblastoma tumour development: a review. Math Mod Meth Appl Sci 2005;15:177994.

[MI118] Sander LM, Deisboeck TS. Growth patterns of microscopic brain tumors. Phys Rev E 2002;66:051901.

[MI119] Kansal AR, Torquato S, Harsh IV GR, Chiocca EA, Deisboeck TS. Simulated brain tumor growth dynamics using a three-dimensional cellular automaton. J Theor Biol 2000;203:36782.

[MI120] Swanson KR, Alvord Jr. EC, Murray JD. A quantitative model for differential motility of gliomas in gray and white matter. Cell Prolif 2000;33:31730.

[MI121] Wurzel M, Schaller C, Simon M, Deutsch A. Cancer cell invasion of normal brain tissue: Guided by prepattern? J Theor Med 2005;6:2131.

[MI122] Stein AM, Demuth T, Mobley D, Berens M, Sander LM. A mathematical model of glioblastoma tumor spheroid invasion in a three- dimensional in vitro experiment. Biophys J 2007;92:35665.

[MI123] Ferreira Jr. SC, Martins ML, Vilela MJ. Morphology transitions induced by chemotherapy in carcinomas in situ. Phys Rev E 2003;67:051914.

[MI124] Swanson KR, Alvord Jr. EC, Murray JD. Quantifying efficacy of chemotherapy of brain tumours (gliomas) with homogeneous and hetero- geneous drug delivery. Acta Biotheor 2002;50:22337.

[MI125] Kozusko F, Chen P-H, Day BW, Panetta JC. A mathematical model of in vitro cancer cell growth and treatment with antimitotic agent curacin A. Math Biosci 2001;170:116.

[MI126] Scalerandi M, Capogrosso Sansone B. Inhibition of vascularization in tumor growth. Phys Rev Lett 2002;89:218101.

[MI127] Levine HA, Pamuk S, Sleeman BD, Nilsen-Hamilton M. A mathematical model of capillary formation and development in tumor angiogen- esis: penetration into the stroma. Bull Math Biol 2001;63:80163.

[MI128] Jackson TL. Vascular tumour growth and treatment: consequences of polyclonality, competition and dynamic vascular support. J Math Biol 2002;44:20126.

[MI129] Plank MJ, Sleeman BD. A reinforced random walk model of tumour angiogenesis and anti-angiogenic strategies. IMA J Math Med Biol 2003;20:13581.

[MI130] Owen MR, Byrne HM, Lewis CE. Mathematical modelling of the use of macrophages as vehicles for drug delivery to hypoxic tumour sites. J Theor Biol 2004;226:37791.

[MI131] Raj K, Ogston P, Beard P. Virus-mediated killing of cells that lack p53 activity. Nature 2001;412:9147.

[MI132] Bischoff JR, Kirn DH, Williams A, Heise C, Horn S, Muna M, Ng L, Nye JA, Sampson-Johannes A, Fattaey A, McCormick F. An adenovirus mutant that replicates selectively in p53-deficient human tumor cells. Science 1996;274:3736.

[MI133] Coffey MC, Strong JE, Forsyth PA, Lee PWK. Reovirus therapy of tumors with activated Ras pathways. Science 1998;282:13324.

[MI134] Lorence RM, Katubig BB, Reichard KW, Reyes HM, Phuangsab A, Sassetti MD, Walter RJ, Peeples ME. Complete regression of human fibrosarcoma xenografts after local newcastle disease virus therapy. Cancer Res 1994;54:601721.

[MI135] Chase RM, Chung YE, Chiocca EA. An oncolytic viral mutant that delivers the CYP2B1 transgene and augments cyclophosphamide chemotherapy. Nature Biotechnol 1998;16:4448.

[MI136] Parato KA, Senger D, Forsyth PAJ, Bell JC. Recent progress in the battle between oncolytic viruses and tumours. Nature Rev Cancer 2005;5:96576.

[MI137] Ferreira Jr. SC, Martins ML, Vilela MJ. Fighting cancer with viruses. Phys A 2005;345:591602. [138] Wu JT, Byrne HM, Kirn DH, Wein LM. Modeling and analysis of a virus that replicates selectively in tumor cells. Bull Math Biol 2001;63:73168.

[MI139] Heise CC, Williams AM, Xue S, Propst M, Kirn DH. Intravenous administration of ONYX-015, a selectively replicating adenovirus, induces antitumoral efficacy. Cancer Res 1999;59:26238.

[MI140] Wein LM, Wu JT, Kirn DH. Validation and analysis of a mathematical model of a replication-competent oncolytic virus for cancer treatment: implications for virus design and delivery. Cancer Res 2003;63:131724.

[MI141] Louzoun Y, Solomon S, Atlan H, Cohen IR. Proliferation and competition in discrete biological systems. Bull Math Biol 2003;65(3):37596.

[MI142] Solé R, Valls J, Bascompte J. Spiral waves, chaos and multiple attractors in lattice models of interacting populations. Phys Lett A 1992;166(2):1238.

[MI143] Dixit NM, Perelson AS. Complex patterns of viral load decay under antiretroviral therapy: influence of pharmacokinetics and intracellular delay. J Theor Biol 2004;226:95109.

[MI144] Lewin SR, Ribeiro RM, Walters T, Lau GK, Bowden S, Locarnini S, Perelson AS. Analysis of hepatitis B viral load decline under potenty therapy: Complex decay profiles observed. Hepatology 2001;34(5):101220.

[MI145] Hermann E, Lee J-H, Marinos G, Modi M, Zeuzem S. Effect of ribavirin on hepatitis C viral kinetics in patients treated with pegylated interferon. Hepatology 2003;37:13518.

[MI146] Glimm J, Sharp DH. Prediction and the quantification of uncertainty. Phys D 1999;133:15270.

[MI147] J.A. Adam, Mathematical models of perivascular spheroid development and catastrophe theoretic description of rapid metastatic growth/tumor remission, Invastion and Metastasis, 16 (1996), pp. 247–267.

[MI148] J.J. Casciari, S.V. Sotirchos, and R.M. Sutherland, Mathematical modelling of microenvironment and growth in EMT6/Ro multicellular tumour spheroids, Cell Proliferation, 25 (1992), pp. 1–22.

[MI149] A.C. Burton, Rate of growth of solid tumours as a problem of diffusion, Growth, 30 (1966), pp. 157–176.

[MI150] J.A. Adam, A simplified mathematical model of tumor growth, Math. Biosci., 81 (1986), pp. 229–244.

[MI151] J.A. Adam, A mathematical model of tumor growth. II. Effects of geometry and spatial uniformity on stability, Math. Biosci., 86 (1987), pp. 183–211.

[MI152] J.A. Adam, A mathematical model of tumor growth. III. Comparison with experiments, Math. Biosci., 86 (1987), pp. 213–227.

[MI153] J.A. Adam and S.A. Maggelakis, Mathematical models of tumor growth. IV. Effects of a necrotic core, Math. Biosci., 97 (1989), pp. 121–136.

[MI154] J.A. Adam and S.A. Maggelakis, Diffusion regulated characteristics of a spherical perivascular carcinoma, Bull. Math. Biol., 52 (1990), pp. 549–582.

[MI155] A.R.A. Anderson, M.A.J. Chaplain, E.L. Newman, R.J.C. Steele, and A.M. Thompson, Mathematical modelling of tumour invasion and metastasis, J. Theoret. Medicine, 2 (2000), pp. 129–154.

[MI156] B.H. Arve and A.I. Liapis, Oxygen tension in tumors predicted by diffusion with absorption model involving a moving free boundary, Math. Comput. Modelling, 10 (1988), pp. 159–174.

[MI157] H.M. Byrne and M.A.J. Chaplain, Growth of nonnecrotic tumours in the presence and absence of inhibitors, Math. Biosci., 130 (1995), pp. 151–181.

[MI158] H.M. Byrne and M.A.J. Chaplain, Growth of necrotic tumours in the presence and absence of inhibitors, Math. Biosci., 135 (1996), pp. 187–216.

[MI159] H.M. Byrne and S.A. Gourley, The role of growth factors in avascular tumour growth, Math. Comput. Modelling, 26 (1997), pp. 35–55.

[MI160] H.M. Byrne, The importance of intercellular adhesion in the development of carcinomas, IMA J. Math. Appl. Medicine Biol., 14 (1997), pp. 305–323.

[MI161] H.M. Byrne and M.A.J. Chaplain, Free boundary value problems associated with the growth and development of multicellular spheroids, European J. Appl. Math., 8 (1997), pp. 639–658.

[MI162] H.M. Byrne and M.A.J. Chaplain, Necrosis and apoptosis: Distinct cell loss mechanisms in a mathematical model of avascular tumour growth, J. Theoret. Medicine, 1 (1998), pp. 223–235.

[MI163] H.M. Byrne, A weakly nonlinear analysis of a model of avascular solid tumour growth,J. Math. Biol., 39 (1999), pp. 59–89.

[MI164] H.M. Byrne and P. Matthews, Asymmetric growth of models of avascular solid tumours: Exploiting symmetries, IMA J. Math. Appl. Medicine Biol., 19 (2002), pp. 1–29.

[165] M.A.J. Chaplain and N.F. Britton, On the concentration profile of a growth inhibitory factor in multicell spheroids, Math. Biosci., 115 (1993), pp. 233–245.

[166] M.A.J. Chaplain, D.L. Benson, and P.K. Maini, Nonlinear diffusion of a growth inhibitory factor in multicell spheroids, Math. Biosci., 121 (1994), pp. 1–13.

[MI167] V. Cristini, J. Lowengrub, and Q. Nie, Nonlinear simulation of tumor growth, J. Math. Biol., 46 (2003), pp. 191–224.

[MI168] A.S. Deakin, Model for the growth of a solid in vitro tumor, Growth, 39 (1975), pp. 159–165.

[MI169] S.B. Cui and A. Friedman, A free boundary problem for a singular system of differential equations: An application to a model of tumor growth, Trans. Amer. Math. Soc., 355 (2003), pp. 3537–3590.

[MI170] F.L. Degner and R.M. Sutherland, Mathematical modelling of oxygen supply and oxygenation in tumor tissues: Prognostic, therapeutic and experimental implications, Internat. J. Radiation Oncology Biol. Phys., 15 (1988), pp. 391–397.

[MI171] S.J. Franks and J.R. King, Interactions between a uniformly proliferating tumour and its surroundings: Uniform material properties, Math. Medicine Biol., 20 (2003), pp. 47–89.

[MI172] J.P. Freyer and R.M. Sutherland, Regulation of growth saturation and development of necrosis in EMT6/Ro multicellular spheroids by glucose and oxygen supply, Cancer Res., 46 (1986), pp. 3504–3512.

[MI173] H.P. Greenspan, Models for the growth of a solid tumor by diffusion, Stud. Appl. Math., 52 (1972), pp. 317–340.

[MI174] H.P. Greenspan, On the growth and stability of cell cultures and solid tumors, J. Theoret. Biol., 56 (1975), pp. 229–242.

[MI175] U. Grossmann, Profiles of oxygen partial pressure and oxygen consumption inside multicellular spheroids, Recent Results in Cancer Res., 95 (1984), pp. 150–159.

[MI176] K.A. Landman and C.P. Please, Tumour dynamics and necrosis: Surface tension and stability, IMA J. Math. Appl. Medicine Biol., 18 (2001), pp. 131–158.

[MI177] J. Landry, J.P. Freyer, and R.M. Sutherland, A model for the growth of multicellular spheroids, Cell and Tissue Kinetics, 15 (1982), pp. 585–594.

[MI178] J. Landry and J.P. Freyer, Regulatory mechanisms in spheroid aggregates of normal and cancerous cells, Recent Results in Cancer Res., 95 (1984), pp. 50–66.

[MI179] B.P. Marchant, J. Norbury, and A.J. Perumpanani, Traveling shock waves arising in a model of malignant invasion, SIAM J. Appl. Math., 60 (2000), pp. 463–476.

[MI180] B.P. Marchant, J. Norbury, and J.A. Sherratt, Travelling wave solutions to a haptotaxis-dominated model of malignant invasion, Nonlinearity, 14 (2001), pp. 1653–1671.

[MI181] M. Marusic, Z. Bajzer, J.P. Freyer, and S. Vuk-Pavlovic, Modeling autostimulation of growth in multicellular tumor spheroids, Internat. J. Biomedical Comput., 29 (1991), pp. 149–158.

[MI182] D.L.S. McElwain and P.J. Ponzo, A model for the growth of a solid tumor with non-uniform oxygen consumption, Math. Biosci., 35 (1977), pp. 267–279.

[MI183] D.L.S. McElwain, A reexamination of oxygen diffusion in a spheroid cell with Michaelis-Menten oxygen uptake kinetics, J. Theoret. Biol., 71 (1978), pp. 255–267.

[MI184] W. Mueller-Klieser, Method for the determination of oxygen consumption rates and diffusion coefficients in multicellular spheroids, Biophys. J., 46 (1984), pp. 343–348.

[MI185] G.J. Pettet, C.P. Please, M.J. Tindall, and D.L. McElwain, The migration of cells in multicell tumor spheroids, Bull. Math. Biol., 63(2001), pp. 231–257.

[MI186] C.P. Please, G.J. Pettet, and D.L.S. McElwain, A new approach to modelling the formation of necrotic regions in tumours, Appl. Math. Lett., 11 (1998), pp. 89–94.

[MI187] C.P. Please, G.J. Pettet, and D.L.S. McElwain, Avascular tumour dynamics and necrosis, Math. Models Methods Appl. Sci., 9 (1999), pp. 569–579.

[MI188] J.A. Sherratt, Traveling wave solutions of a mathematical model for tumor encapsulation, SIAM J. Appl. Math., 60 (1999), pp. 392–407.

[MI189] R.M. Shymko and L. Glass, Cellular and geometric control of tissue growth and mitotic instability, J. Theoret. Biol., 63 (1976), pp. 355–374.

[MI190] J.P. Ward and J.R. King, Mathematical modelling of avascular tumour growth,IMAJ. Math. Appl. Medicine Biol., 14 (1997), pp. 36–69.

[MI191] J.P.Ward and J.R. King, Mathematical modelling of avascular tumour growth. II. Modelling growth saturation, IMA J. Math. Appl. Medicine Biol., 16 (1999), pp. 171–211.

[MI192] J.P. Ward and J.R. King, Mathematical modelling of the effects of mitotic inhibitors on avascular tumour growth, J. Theoret. Medicine, 1 (1999), pp. 287–311.

[MI193] S.A. Maggelakis and J.A. Adam, Mathematical model of perivascular growth of a spherical carcinoma, Math. Comput. Modelling, 13 (1990), pp. 23–38.

[MI194] J.A. Sherratt, Cellular growth control and travelling waves of cancer, SIAM J. Appl. Math., 53 (1993), pp. 1713–1730.

[MI195] D.L.S. McElwain and L.E. Morris, Apoptosis as a volume loss mechanism in mathematical models of solid tumor growth, Math. Biosci., 39 (1978), pp. 147–157.

[MI196] L.M. Sander and T.S. Deisboeck, Growth patterns of microscopic brain tumors, Phys. Rev. E, 66 (2002), pp. 66–73.

[MI197] M.A.J. Chaplain, Avascular growth, angiogenesis and vascular growth in solid tumours: The mathematical modelling of the stages of tumour development, Math. Comput. Modelling, 23(1996), pp. 47–87.

[MI198] J.A. Sherratt and M.A.J. Chaplain, A new mathematical model for avascular tumour growth, J. Math. Biol., 43(2001), pp. 291–312.

[MI199] K.E. Thompson and H.M. Byrne, Modelling the internalisation of labelled cells in tumour spheroids, Bull. Math. Biol., 61 (1999), pp. 601–623.

[MI200] S. Tohya, A. Mochizuki, S. Imayama, and Y. Iwasa, On rugged shape of skin tumor (basal cell carcinoma), J. Theoret. Biol., 194 (1998), pp. 65–78.

[MI201] S. Habib, C. Molina-Paris, and T.S. Deisboeck, Complexdynamics of tumors: Modeling an emerging brain tumor system with coupled reaction-diffusion equations, Phys. A, 327 (2003), pp. 501–524.

[MI202] J.P. Ward and J.R. King, Mathematical modelling of drug transport in tumour multicell spheroids and monolayer cultures, Math. Biosci., 181 (2003), pp. 177–207.

[MI203] M.A.J. Chaplain, M. Ganesh, and I.G. Graham, Spatio-temporal pattern formation on spherical surfaces: Numerical simulation and application to solid tumor growth, J. Math. Biol., 42 (2001), pp. 387–423.

[MI204] K. Maseide and E. Rofstad, Mathematical modeling of chronical hypoxia in tumors considering potential doubling time and hypoxic cell lifetime, Radiotherapy and Oncology, 54 (2000), pp. 171–177.

[MI205] L.M. Wein, J.T. Wu, A.G. Ianculescu, and R.K. Puri, A mathematical model of the impact of infused targeted cytotoxic agents on brain tumours: Implications for detection, design and delivery, Cell Proliferation, 35 (2002), pp. 343–361.

[MI206] F.J. Burkowski, A computer simulation of the growth of a tumor in vitro, Computer Programs in Biomedicine, 7 (1977), pp. 203–210.

[MI207] H.M. Byrne, The effect of time delays on the dynamics of avascular tumour growth, Math. Biosci., 144 (1997), pp. 83–117.

[MI208] H.M. Byrne and M.A.J. Chaplain, Modelling the role of cell-cell adhesion in the growth and development of carcinomas, Math. Comput. Modelling, 24 (1996), pp. 1–17.

[MI209] T. Roose, P.A. Netti, L.L. Munn, Y. Boucher, and R.K. Jain, Solid stress generated by spheroid growth estimated using a linear poroelasticity model, Microvascular Res., 66 (2003), pp. 204–212.

[MI210] D. Ambrosi and F. Mollica, The role of stress in the growth of a multicell spheroid, J. Math. Biol., 48 (2003), pp. 477–499.

[MI211] C.Y. Chen, H.M. Byrne, and J.R. King, The influence of growth-induced stress from the surrounding medium on the development of multicell spheroids, J. Math. Biol., 43(2001),

[MI212] G. Helmlinger, P.A. Netti, H.C. Lichtenbeld, R.J. Melder, and R.K. Jain, Solid stress inhibits the growth of multicellular tumor spheroids, Nature Biotechnology, 15 (1997), pp. 778–783.

[MI213] P. Canadas, V.M. Laurent, C. Oddou, D. Isabey, and S. Wendling, A cellular tensegrity model to analyse the structural viscoelasticity of the cytoskeleton, J. Theoret. Biol., 218 (2002), pp. 155–173.

[MI214] D.E. Ingber, Tensegrity I. Cell structure and hierarchical systems biology, J. Cell Sci., 116 (2003), pp. 1157–1173.

[MI215] G.Stamatakos, N.Uzunoglu, K.Delibasis, M.Makropoulou, N.Mouravliansky, A.Marsh, "A simplified simulation model and virtual reality visualization of tumor growth in vitro," Future Generation Computer Systems, vol. 14, pp.79-89, 1998.

[MI216] G.S.Stamatakos, D.D.Dionysiou, E.I.Zacharaki, N.A.Mouravliansky, K.Nikita, N.Uzunoglu, "In silico radiation oncology: combining novel simulation algorithms with current visualization techniques", Proceedings of the IEEE, vol. 90, No 11, pp.1764-1777, Nov. 2002.

[MI217] . Stamatakos, G. S., P.Antipas, V., Uzunoglu, N. K., A spatiotemporal, patient individualized simulation model of solid tumor response to chemotherapy in vivo: the paradigm of glioblastoma multiforme treated by temozolomide. IEEE Trans Biomed. Engineering 53, No 8, (2006), 1467-1477

[MI218] D. D. Dionysiou, G. S. Stamatakos, N.K. Uzunoglu, K. S. Nikita, A. Marioli, "A four-dimensional simulation model of tumour response to radiotherapy in vivo: parametric validation considering radiosensitivity, genetic profile and fractionation," Journal of Theoretical Biology 230 (2004) 1–20

[MI219] G. S. Stamatakos, V.P. Antipas, N. K. Uzunoglu, R. G. Dale, "A four dimensional computer simulation model of the in vivo response to radiotherapy of glioblastoma multiforme: studies on the effect of clonogenic cell density." British Journal of Radiology, 2006, vol. 79, 389-400

[MI220] V. P Antipas, G. S Stamatakos, N. K Uzunoglu, D. D Dionysiou, R. G Dale, " A spatio-temporal simulation model of the response of solid tumours to radiotherapy in vivo: parametric validation concerning oxygen enhancement ratio and cell cycle duration," Phys. Med. Biol. 49 (2004) 1485–1504

[MI221] G.S.Stamatakos, V.P. Antipas, N.K. Uzunoglu, "Simulating chemotherapeutic schemes in the individualized treatment context: The paradigm of glioblastoma multiforme treated by temozolomide in vivo." Comput Biol Med. Comput Biol Med. 36, 1216–1234, 2006.

[MI222] G. Stamatakos, " Spotlight on Cancer Informatics," Cancer Informatics No 2, pp.99-102, 2006.

[MI223] D. Dionysiou, G. Stamatakos and K. Marias, "Simulating cancer radiotherapy on a multi-level basis: biology, oncology and image processing," Lecture Notes in Computer Science, Special Issue on Digital Human Modeling, Vol. 4561, pp.569-575, 2007.

[MI224] Antipas, V.P., Stamatakos, G.S., Uzunoglu, N.K., 2007. A patient-specific in vivo tumor and normal tissue model for prediction of the response to radiotherapy: a computer simulation approach. Methods Inf. Med. 46, 367-375.

[MI225] Dionysiou,D.D., Stamatakos, G.S., Uzunoglu,N.K., Nikita,K.S, 2006. A computer simulation of in vivo tumour growth and response to radiotherapy: New algorithms and parametric results. Computers in Biology and Medicine 36 448–464

[MI226] Stamatakos, G., Dionysiou, D., Nikita, K., Zamboglou, N., Baltas, D., Pissakas, G., et al., 2001. In vivo tumour growth and response to radiation therapy: a novel algorithmic description. Int. J. Radiat. Oncol. Biol. Phys.,51 Suppl. 1, 240.

[MI227] Stamatakos, G.S., 2006d. Towards a collaborative formulation of the Mathematical Principles of Natural Philosophy: Living Matter. The paradigm of In Silico Oncology. DIMACS Workshop on Computational Tumor Modeling, DIMACS Center, Rutgers University, Piscataway, NJ, USA. http://dimacs.rutgers.edu/Workshops/TumorModeling/abstracts.html

[MI228] Stamatakos, G. S. and Uzunoglu, N., 2006. Computer Simulation of Tumour Response to Therapy. Cancer Bioinformatics: from therapy design to treatment. Edited by Sylvia Nagl. John Wiley & Sons, Ltd., Chichester,UK.

[MI229] Dionysiou, D.D. and Stamatakos, G.S., 2006. Applying a 4D multiscale in vivo tumor growth model to the exploration of radiotherapy scheduling: the effects of weekend treatment gaps and p53 gene status on the response of fast growing solid tumors. Cancer Informatics 2, 113-121.

[MI230] Stamatakos GS, Dionysiou DD, Graf N, et al. "The "Oncosimulator": a multilevel, clinically oriented simulation system of tumor growth and response to therapeutic schemes. [231] Towards clinical evaluation of in

silico oncology." 29th Annual International Conference of the IEEE Engineering in Medicine and Biology Society in conjunction with the biennial Conference of the French Society of Biological and Medical Engineering (SFGBM), August 23-26, 2007, Conf Proc IEEE Eng Med Biol Soc

[MI232] E. A. Kolokotroni, G. S. Stamatakos, D. D. Dionysiou, E. Ch. Georgiadi, Ch. Desmedt, N. M. Graf, "Translating Multiscale Cancer Models into Clinical Trials: Simulating Breast Cancer Tumor Dynamics within the Framework of the "Trial of Principle" Clinical Trial and the ACGT Project.," Proc. 8th IEEE International Conference on Bioinformatics and Bioengineering (BIBE 2008), Athens, Greece, 8-10 Oct. 2008. IEEE Catalog Number: CFP08266, ISBN: 978-1-4244-2845-8, Library of Congress: 2008907441, Paper No. BE-2.1.1, length: 8 pages (in electronic format). In press

[MI233] E. Ch. Georgiadi, G. S. Stamatakos, N. M. Graf, E. A. Kolokotroni, D. D. Dionysiou, A. Hoppe, N. K. Uzunoglu, "Multilevel Cancer Modeling in the Clinical Environment: Simulating the Behavior of Wilms Tumor in the Context of the SIOP 2001/GPOH Clinical Trial and the ACGT Project," Proc. 8th IEEE International Conference on Bioinformatics and Bioengineering (BIBE 2008), Athens, Greece, 8-10 Oct. 2008. IEEE Catalog Number: CFP08266, ISBN: 978-1-4244-2845-8, Library of Congress: 2008907441, Paper No. BE-2.1.2, length: 8 pages (in electronic format). In press

5. Medical Data to be Used for the Adaptation, Optimization and Validation of the Models of Clinical Tumour Growth and Response to Treatment [Code: DA]

This chapter lists the various types of (pseudo)anonymized multiscale medical data to be provided by the participating clinical partners and used for the adaptation, optimization and validation of the imageable tumour models which are described mainly in Chapters 6 and 7.

5.1 Glioma (glioblastoma) cases

A1. TREATMENT DATA

Detailed description of the treatment (chemotherapy and/or radiotherapy) scheme including

1. Drug(s) names and/or type of ionizing radiation
2. Actual treatment session dates
3. Actual dose(s) for each treatment session
4. Any other relevant data (eg. individualized pharmacokinetic data if available)

A2. NORMAL TISSUE COMPLICATION DATA

1. Side effects that will be measured are in case of patients with gliomas mainly due to irradiation. To describe these side effects the Common Terminology Criteria for Adverse Events (CTCAE) v3.0 will be used [DA1].
2. Most important are skin reactions and neurological side effects
3. Haematological toxicity will only be analysed in patients who have received chemotherapy.
4. Especially in patients with gliomas who develop new neurological symptoms it is sometime impossible to distinguish between tumour progression and side effects of treatment. In this respect the simulation of normal tissue reactions has limited potential.

A3. CLINICAL DATA

1. Age
2. Sex
3. Description of eventual previous treatments
4. Any other pertinent clinical data

A4. IMAGING DATA

In the case of glioma the following imaging data will be made available:

1. T1 Gadolinium-enhanced MRI (dense coverage of the region of interest)
2. T2 MRI (dense coverage of the region of interest)
3. Additional imaging data are desirable and will be used in the project if they are available for a patient. These imaging data are:
    i. Diffusion anisotropy MRI
    ii. PET
    iii. SPECT
    iv. fMRI

All imaging data sets correspond to a known time point before treatment initiation, eventually several time points during treatment (if this is possible) and at least one known time point after completion of treatment.

A5. SEGMENTATION DATA

1. External “conventional”boundaries of the tumour based on T2 MRI
2. External “conventional” boundaries of the tumour based on T1-gadolinium-enhanced MRI
3. Boundaries of the necrotic (“dark appearing”) region based on T1-gadolinium-enhanced MRI
4. Boundaries of any additional tumour structures lying within the previously mentioned “conventional” boundaries of the tumour (including their macroscopic characterization)
5. Desirably: boundaries of adjacent normal tissue structures with annotation.
6. Estimate of tumour volume (including calculation method)

A6. HISTOPATHOLOGICAL DATA

In the case of glioma the following histological data will be made available:

1. Detailed description of the tumour subtype including grade and stage
2. Microphotographs of indicative histopathology slices. However, due to the surgical procedure in most cases it is impossible to correlate the histology to the region of the tumour from which the bioptic material has been extracted.
3. Estimates of the amount of dead cells (necrotic, apoptotic)
4. Estimates of the spatial tumour cell density for proliferative cells (Ki67 staining)
5. The degree of neovascularization for selected cases.

The microscopic imaging data are processed in such a way that the density of tumour cells as well as the percentages of proliferative cells (Ki67) and dead cells are calculated. In few cases, in which such data are available, a mapping of the bioptic areas and the imaging will be done. This will lead to a relatively refined consideration of the tumour spatial inhomogeneities in different areas of the tumour. In all other cases where such information is not possible to get the information from the biopsy will be extrapolated to the whole tumour, knowing that this is only a rough approximation.

A7. MOLECULAR DATA

In the case of glioma the following data will be made available:

1. An extended number of novel glioma expressed antigens reactive with patients' auto-antibodies will be identified.
2. The seroreactivity of antigens will be measured using a novel automated image analysis system.
3. Information of the reactivity of the immunogenic antigens against sera of healthy controls will be provided.
4. Each glioma antigen will be classified according to its reactivity against normal sera and sera of glioma patients. AUC values for the antigens will be determined to rank them according to their information content.
5. Cytogenetic data will be provided for those glioma that can be used for short term tissue culture.
6. cDNA expression data will be provided for those glioma that are available as frozen tissues.

v. Lung cancer cases

B1. TREATMENT DATA

Detailed description of the treatment (chemotherapy and/or radiotherapy) scheme including

1. Drug(s) names and/or type of ionizing radiation
2. Actual treatment session dates
3. Actual dose(s) for each treatment session
4. Any other relevant data (eg. individualized pharmacokinetic data if available)

B2. NORMAL TISSUE COMPLICATION DATA

1. Side effects that will be measured are in case of patients with lung cancer mainly due to irradiation. To describe these side effects the Common Terminology Criteria for Adverse Events (CTCAE) v3.0 [DA1] will be used.
2. Most important are skin reactions and acute pneumonitis in case of lung cancer.
3. Haematological toxicity will only be analysed in patients who have received chemotherapy.

B3. CLINICAL DATA

1. Age
2. Sex
3. Description of eventual previous treatments
4. Any other pertinent clinical data

B4. IMAGING DATA

In case of lung cancer the following imaging data will be made available:

1. CT (dense coverage of the region of interest)
2. Any modality providing metabolic information (eg. PET, SPECT, fMRI)

All imaging data sets correspond to a known time point before treatment initiation, eventually several time points during treatment (if this is possible) and to at least one known time point after completion of treatment.

B5. SEGMENTATION DATA

1. External “conventional”boundaries of the tumour based on CT
2. Boundaries of the highly metabolically active and necrotic regions based on any modality providing metabolic information
3. Boundaries of any additional tumour structures lying within the previously mentioned “conventional” boundaries of the tumour (including their macroscopic characterization)
4. Desirably: boundaries of adjacent normal tissue structures with annotation.
5. Estimate of tumour volume (including calculation method)

B6. HISTOPATHOLOGICAL DATA

In case of lung cancer the following histological data will be made available:

1. Detailed description of the tumour subtype including grade and stage.
2. Microphotographs of indicative histopathology slices from surgically resected specimens and from biopsy specimens. The former will include central and peripheral parts of the tumour, the latter will be representative for the peripheral/ endobronchial part of the tumour.
3. Estimates of the spatial tumour cell density will be given. The amount of dead (necrotic, apoptotic) cells will be estimated.
4. Estimates of the spatial tumour cell density for prolferative cells (Ki67 staining) will be given.
5. The degree of neovascularisation is given for selected cases.

The microscopic imaging data are processed in such a way that the density of tumour cells as well as the percentages of proliferative cells (Ki67) and dead cells are calculated. In few cases, in which such data are available, a mapping of the bioptic areas and the imaging will be done. This will lead to a relatively refined consideration of the tumour spatial inhomogeneities in different areas of the tumour. In all other cases where such information is not possible to get, the information from the biopsy will be extrapolated to the whole tumour, knowing that this is only a rough approximation.

B7. MOLECULAR DATA

In the case of lung cancer the following data will be made available:

1. The mutational status of EGFR known to play a critical role in the response to targeted therapeutics will be provided. No other mutational analysis will be done.
2. Autologous antibodies against tumour specific antigens will be measured in all cases using a modified SEREX method.

References

DA1. https://webapps.ctep.nci.nih.gov/webobjs/ctc/webhelp/welcome_to_ctcae.htm

6. Modelling Clinical Tumour Growth and Response to Treatment: Continuum Based Modelling Approach [Code: CO]

6.1 Workflow of the continuum based tumour dynamics simulator

Concerning tumour simulation two major approaches have been adopted. According to the first one i.e. the continuum approach, the tumour (and in particular a glioma) is considered a spatiotemporal distribution of continuous cell density which follows the generic diffusion-reaction law. According to the second approach (see chapter 7) the tumour is considered a spatiotemporal distribution of discrete cells (and cell death products) belonging to several proliferative potential categories and cell cycling phases.

Pertinent clinical data from the list included in chapter 5 will be used in order to adapt, optimize and validate the simulators. Details regarding the types of data applicable to each particular tumour type are also provided in chapter 5.

The tumour dynamics simulator based on the continuum assumption will function as desribed below (Figure CO1).

i. The **macroscopic imaging data** of the patient (e.g. contrast enhanced MRI, CT, PET etc) are collected at baseline

ii. The macroscopic imaging data are segmented by the clinician (delineation of tumour boundaries, necrotic areas etc.), interpolated, three dimensionally reconstructed and eventually fused if more than one modalities are to be used. Both anatomy and spatial metabolic activity are the features to be provided by the processed imaging data.

iii. **NOTE** Macroscopic imaging data are used as input for the simulation and the patient specific adaptation of the model. With the help of imaging it is possible to construct input data of a patient specific model by measuring spatially resolved anatomical and physiological parameters. Macroscopic imaging data of a patient as defined above is collected at several points in time before, during, and after therapy. Furthermore, images of different imaging modalities (CT, MRI, PET, etc.), allow to measure different parameters of the patient's tissue and physiology. Therefore, in order to spatially align the information from different image modalities a registration and fusion step is necessary. The tools provided by WP7 in conjunction with the infrastructure of provided by WP3 will allow to perform this registration step. The registration results will be written together with the patient's images to the ContraCancrum database.After aligning the patient's images to fuse the information, a segmentation step is required. In this step different tissues or different physiological regions of the tumour are segmented in order to simplify modelling. A necrotic area within the tumour as well as proliferating areas will be identified. WP7 and WP3 will provide the basis for sharing segmentation results with WP4. A viewing tool to compare the segmentation results with the original images is provided as well by WP7.

iv. The **microscopic imaging data** of the tumour (photographs of histopathological sections of bioptic material etc.) are provided.

v. The microscopic imaging data are processed in such a way that the density of tumour cells as well as the percentages of the populations of the various proliferative potential categories and cell cycling phases can be estimated. Mapping of the areas from which the biopsies stem onto the imaging data (if and when feasile) could lead to a refined cosideration of the tumour spatial inhomogeneities.

vi. The **microscopic imaging data** of the tumour (photographs of histopathological sections of bioptic material etc.) are provided.

vii. The microscopic imaging data are processed in such a way that the density of tumour cells as well as the percentages of proliferative cells (Ki67) and dead cells are calculated. In few cases, in which such data are available, a mapping of the bioptic areas and the imaging will be done. This will lead to a relatively refined consideration of the tumour spatial inhomogeneities in different areas of the tumour. In all other cases where such information is not possible to get, the information from the biopsy will be extrapolated to the whole tumour, knowing that this is only a rough approximation.

viii. The pre-treatment spatial distribution of imageable and non imageable tumour cell density is estimated based on literature. Non imageable tumour cell distribution refers primarily to gliomas where tumour growth exhibits markedly diffusive patterns.

ix. Along with information based on histopathological slides eventual tumour cell cycling information (e.g. duration of cell cycle for the particular tumour) based on cell cultures is provided.

x. A discretization mesh is superimposed upon the three dimensionally reconstructed tumour. An initial tumour cell density and net proliferative rate is assigned to each node of the mesh.

xi. The **molecular data** (e.g. status, amplification and expressions of critical genes, which have been shown to drastically affect the response of the tumour under consideration to the treatment addressed) are provided. Estimates (even semi-qualitative) of their effect on the cell kill ratio per cell due to the treatment considered are also provided based on pertinent literature (e.g. [CO1]). The idea is to use the cell kill ratio value provided by the Food and Drug Administration (FDA) or general literature as a cell kill ratio reference value (e.g. for a given area under curve or radiation dose) and then to perturb it based on the effect of the molecular and/or histological profile of the tumour in order to achieve higher patient individualization of the simulation.

xii. The diffusion equation for the cell density including sources (cell division) and sinks (cell death due to necrosis, spontaneous apoptosis and response to treatment) is numerically solved for the initialized discretization mesh. One of the methods to numerically formulate and solve the diffusion eqation is the Crank Nicholson Method or θ-method whereas one of the methods to solve the

emerging linear system is the Conjugate Gradient Method. Annex A provides some details on a treatment approximating the solution and deriving such a linear system.

xiii. In parallel with the solution of the biological problem a mechanical refinement can take place based on the Fimite Element Method (Workpackage WP6). To this end any mechanical data available (primarily through literature) will be utilized in conjunction with the imaging data.

xiv. **NOTE** Using imaging data, a three-dimensional biomechanical model of the brain and lung will be built. Both models will aim at assessing the changes in mechanical environment around the tumour during growth as well as the deformation of the surrounding tissues. Two different scenarios will be tested; First the finite element method will be used to calculate only the mechanical environment around the tumour while diffusion of the cancerous cells in healthy tissue will be simulated using the continuous approach described above and the discrete approach described in Chaper7. Second, both cell diffusion and mechanical environment will be calculated using the finite element method. This approach will link the cellular approach described to the macroscopic level.

xv. Acceleration of the simulation code will be envisaged in order to significantly lower the computing time demands. Execution of the code on fast computing systems (eventually including clusters and/or grid) will also take place.

xvi. The outcome of the simulation will be the prediction of the distribution of tumour cell density and metabolism for both the case of free tumour growth [no treatment] and tumour response to treatment (chemotherapy / radiotherapy). Several forms of prediction visualization (graphs, 3D and 4D rendering etc.) will be offered.

xvii. The simulated outcome will be compared with the actual (primarily) imaging data following treatment and an optimization loop of the parameters estimation [and if necessary of the model algorithm] will be implemented.

xviii. Glioma free growth patterns will be compared with embryological brain development patterns in order to study any eventual similarities and underlying common mechanisms. Tumour cell growth (cell divisions and differentiation), vascularisation, and invasiveness (cell migration) are the most important steps in the development of gliomas. By also taking into account molecular and histopathological mechanisms it is hoped that a better understanding of both processes will be achieved.

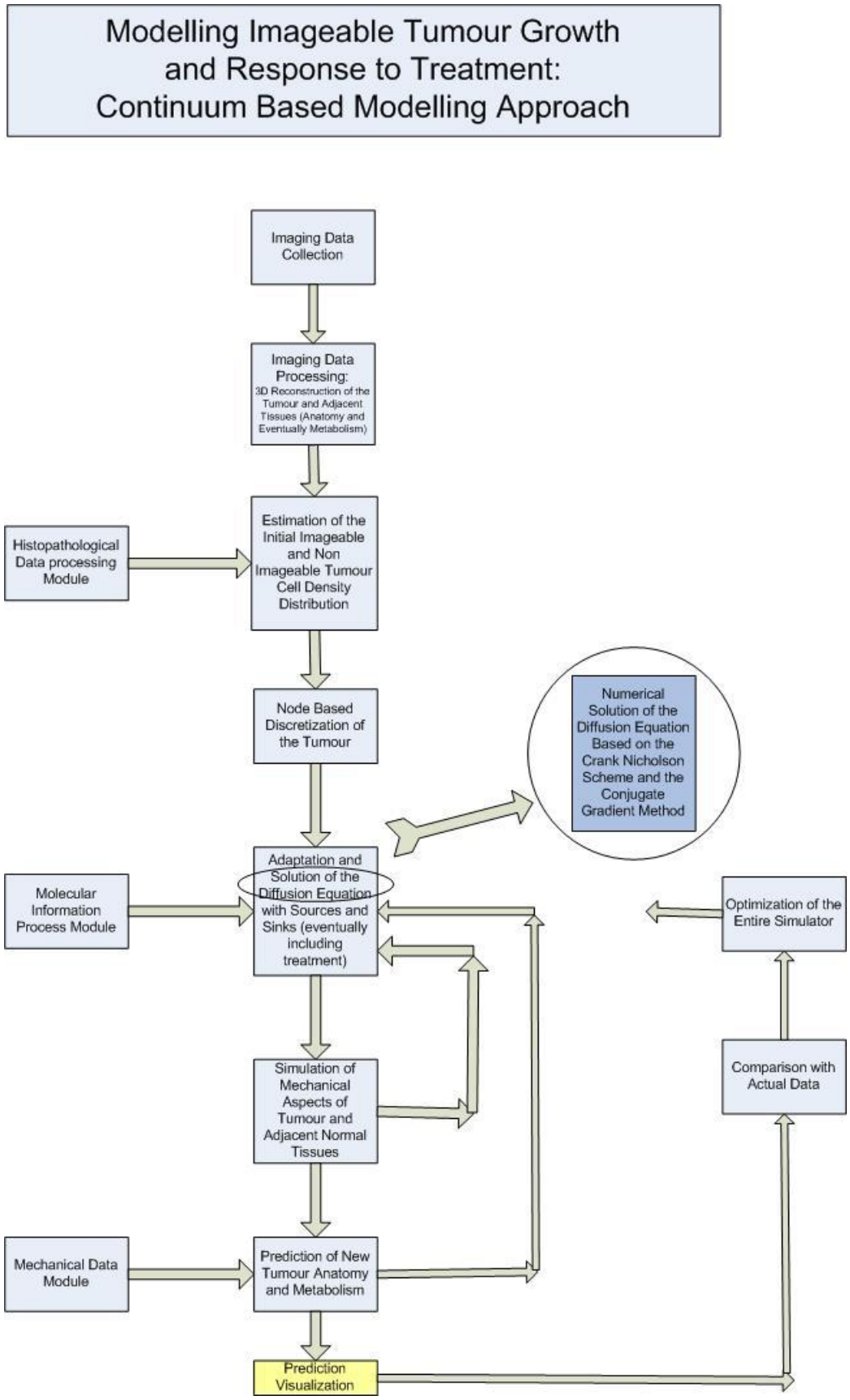

Figure CO1. Continuum based tumour and normal tissue simulator workflow

6.2 Mathematical Treatment of the Diffusion Based Simulation Module Using the Crank Nicolson in Conjunction with the Conjugate Gradient method

6.2.1 Introduction

Dynamic tumour behaviour including i.a. invasion to the surrounding normal tissues has great implications on tumour diagnosis and treatment. The boundaries between tumour and normal tissue sometimes cannot be clearly determined. This may complicate tumour detection and delineation although considerable progress in medical imaging has been achieved. Consequently, it is often difficult to determine the underlying tumour dynamics. Gliomas is a characteristic example of such a behaviour and their aggressive diffuse invasion contributes to their resistance to treatment and their practically inevitable recurrence.

Mathematical modeling of such phenomena is a plausible approach in order to describe tumour dynamics (including expansion, shrinkage due to treatment etc.). Within this context a number of multiscale clinical tumour growth models are being developed within the ContraCancrum context. The continuum based models will predict tumour growth, morphological features, invasion into the surrounding tissue as well as the response of the tumour to treatment (radiotherapy and/or chemotherapy).

By exploiting tumour imaging data the model will be able to suggest the spatial distribution of the macroscopically undetectable component of the tumour as well as its concentration distribution.

Tumour structure and morphology are affected by diffusion gradients. As a consequence the continuum based model is based on the diffusion equation and a number of pertinent alternative numerical algorithms for its solution.

6.2.2 Mathematical Basics

In an oversimplified way tumour growth and invasion can be expressed by the following statement [CO15A], [CO2]:

'Rate of Change of Tumour Cell Population= Diffusion (motility) of tumour cells + Net proliferation of tumour cells'

Mathematically, the above statement can be described by the following partial differential equation [CO15A], [CO6]:

$$\frac{\partial c}{\partial t} = \nabla (D \nabla c) + \rho c$$

c represents the cell concentration at any position and time t, D denotes the diffusion coefficient [CO5] and represents the active motility of tumour cells [CO2] and ρ is the net rate of growth of tumour cells including proliferation, loss and death.

The same equation can be written more analytically as follows [CO3, page803]:

$$\frac{\partial c}{\partial t} = \frac{\partial}{\partial x}(D\frac{\partial c}{\partial x}) + \frac{\partial}{\partial y}(D\frac{\partial c}{\partial y}) + \frac{\partial}{\partial z}(D\frac{\partial c}{\partial z}) + \rho c$$

in three spatial dimensions and more specifically on the domain [CO3, page 730]:

$$R = \{(x, y, z) \mid a < x < b, c < y < d, e < z < f\}$$

The model formulation is completed by Dirichlet boundary conditions $c(x, y, z, t) = g(x, y, z)$ along all the sides for all $(x, y, z) \in \partial R$ and initial conditions $c(x, y, z, 0) = \varphi(x, y, z)$, where $\varphi(x, y, z)$ defines the initial spatial distribution of malignant cells [CO2].

The objective is to approximate the value of the exact solution to the boundary value problem at a discrete set of points. The finite difference approximation is obtained by replacing each derivative which appears in the problem with an appropriate finite difference formula. This converts the continuous partial differential equation into a system of discrete algebraic equations. In general a continuous problem such as one formulated through differential equations has to be replaced by a discrete problem and be represented by a finite amount of data, for instance by its value at a finite number of points at its domain, even though this domain is a continuum [CO8].

The first step in the approximation process is to introduce a discretizing computational grid. In our case the computational domain is a cubic mesh that is applied on the anatomic region of interest. The domain is decomposed into a number of sub-domains. The descretization proceeds in two stages. First we descretize the space variables, then the time variable.

To achieve the spatial descretization, the intervals $[a,b],[c,d],[e,f]$ are divided into N, M, L equal sized subintervals, respectively. N, M, L are positive integers. For convenience, let

$$\Delta x = \Delta y = \Delta z = \frac{b-a}{N} = \frac{d-c}{M} = \frac{f-e}{L} = h$$

By inference, the computational grid consists of the following points (x_j, y_k, z_l),

$$x_j = a + j\Delta x,$$
$$y_k = c + k\Delta y,$$
$$z_l = e + l\Delta z$$

for $j = 0,1,2.....,N$, $k = 0,1,2.....,M$, $l = 0,1,2.....,L$. To complete the descretization of the equation the time axis is divided into uniform steps of length Δt.

Let

$$t_n = n\Delta t$$

for $n = 0,\ 1,\ 2\ldots.$ and so on. Values for the approximation solution will be obtained at these discrete time levels. At each node of the descritizing mesh a value of cell density is assigned. Time is initialized and the continuous diffusion – reaction equation is formulated, discretized and applied on the mesh nodes.

6.2.3 Numerical Procedures

Having defined the computational grid, the goal is to calculate $c(x, y, z, t)$ at each interior point for $t > 0$. In the clinical tumour growth context analytical solutions of the diffusion equation, although they may provide some high level insight, are not able to address the high spatiotemporal complexity including initial and boundary conditions of the biosystem.

Therefore, the problem has to be solved numerically. The finite difference method has proved to be a good choice in this context.

Several different numerical approaches to solve multidimensional parabolic initial / boundary value problems have been proposed. The following [CO7] three indicative methods are widelu used

1. The explicit method. It uses a forward difference at time t_n and is conditionally stable.
2. The implicit method. It uses a backward difference at time t_{n+1}.
3. The Crank-Nicolson method. Iit uses the central difference at time $t_{n+1/2}$.

Each method has its strengths and weaknesses. The analysis of numerical methods for initial value problems focuses on the discretization error and on the three important properties of consistency, convergence and stability.

In order to solve the tumour growth-invasion equation under consideration the Crank-Nicolson method has been one choice and is outlined in this section. The Crank-Nicholson method is the most accurate scheme for small time steps in contrast with the explicit method which although the easiest to implement is the least accurate and the most unstable. The implicit scheme works best for large time steps. Crank-Nicolson method is second order accurate in both time and space and unconditionally stable. Numerical stability is an important notion in numerical analysis. An algorithm is termed numerically stable if an error, whatever its cause, does not grow to become much larger during calculation [CO8].

Possesing these two characteristics the Crank-Nicolson method is considered the method of choice for many diffusion problems. For the three dimenional problem under consideration the Crank - Nicolson scheme by omitting the net proliferation term is given by [CO9]:

$$\frac{c^{t+1}_{i,j,k}-c^{t}_{i,j,k}}{\Delta t}=\frac{1}{2}D\left(\frac{c^{t+1}_{i+1,j,k}-2c^{t+1}_{i,j,k}+c^{t+1}_{i-1,j,k}}{\Delta x^2}+\frac{c^{t+1}_{i,j+1,k}-2c^{t+1}_{i,j,k}+c^{t+1}_{i,j-1,k}}{\Delta y^2}+\frac{c^{t+1}_{i,j,k+1}-2c^{t+1}_{i,j,k}+c^{t+1}_{i,j,k-1}}{\Delta z^2}\right)+$$
$$\frac{1}{2}D\left(\frac{c^{t}_{i+1,j,k}-2c^{t}_{i,j,k}+c^{t}_{i-1,j,k}}{\Delta x^2}+\frac{c^{t}_{i,j+1,k}-2c^{t}_{i,j,k}+c^{t}_{i,j-1,k}}{\Delta y^2}+\frac{c^{t}_{i,j,k+1}-2c^{t}_{i,j,k}+c^{t}_{i,j,k-1}}{\Delta z^2}\right)$$

where $c^{t}_{i,j,k}$ is the finite difference approximation of c at the grid point (i, j, k) at time t. In order to take into account the effects of source and decay terms an approach analogous to the one described in [CO3, page 874] will be implemented.

The Crank-Nicolson method can be formulated in matrix form [CO3] for one - dimensional problems as following ([CO3,page 832]):

$$(\vec{\vec{I}}+\lambda\vec{\vec{A}}+\frac{\Delta t}{2}\vec{\vec{B}}^{(n+1)})\vec{w}^{(n+1)}=(\vec{\vec{I}}-\lambda\vec{\vec{A}}-\frac{\Delta t}{2}\vec{\vec{B}}^{(n)})\vec{w}^{(n)}-\lambda(\vec{b}^{(n+1)}+\vec{b}^{(n)})$$

where $\lambda=D.\Delta t/[2(\Delta)^2]$ and $\vec{b}^{(n)}=\vec{b}(t_n)$ contating boundary conditions.

$\vec{\vec{B}}$ is the diagonal matrix

$$\vec{\vec{B}}=diag\ (\beta(x_1(t)),\beta(x_2(t)),\beta(x_3(t)),\ \ldots\ldots,\beta(x_{N-1}(t)))$$

and β is the negative value of the net rate of growth of tumor cells ρ.

NOTE: The minus sign has been used in order to be consistent with the more generic formulation of the diffusion equation as it appears in e.g. [CO3]. It is also noted that the source term can be expressed as the product of the net growth rate multiplied by the concentration of tumour cells. This implies that tumour cells themselves are the only real source of the entity undergoing diffusion.

The vector

$$\vec{w}^{(n)} = [w_1^{(n)}\ w_2^{(n)}\ w_3^{(n)}\ \ldots\ldots\ w_{N-1}^{(n)}]^T$$

is the fully discrete approximation to the solution that is $w_j^{(n)} \approx c_j(t_n)$.

Finally

$$\ddot{A} = \begin{pmatrix} 2 & -1 & 0 \\ -1 & \ddots & -1 \\ 0 & -1 & 2 \end{pmatrix}$$

The Crank-Nicolson method dictates the solution of a linear system at each time step. The resulting system of equations may be written equivalently in the form [CO11]:

$$\ddot{A}\vec{x} = \vec{b}$$

To find the structure of the coefficient matrix $\ddot{A}$ the *lexicographic ordering* common numbering scheme has been used. The number appearing next to the location of each unknown is the lexicographic number associated with that unknown. The matrix $\ddot{A}$ that is produced is a block tridiagonal matrix.

Suppose m denotes the number of nodes in the computational mesh. Then the matrix $\ddot{A} \in R^{m,m}$ is a sparse, symmetric and positive definite . $\vec{x} \in R^m$ denotes a vector that contains an approximation of the solution c at the mesh nodes at time $t = t_n$, where

$$t_n = n\Delta t, \quad \Delta t > 0$$

A major point is the achievement of convergence. The algorithm chosen should generate a sequence of approximations that converges to the desired solution as rapidly as possible. There are two principal ways of solving linear systems of equations [CO10]: Direct methods such as LU and Cholesky and iterative methods which are more efficient. In contrast to direct methods iterative methods are not expected to terminate in a number of steps. Starting from an initial guess iterative methods form successive approximations that converge to the exact solution only in the limit. A convergence criterion is specified in order to decide when a sufficiently accurate solution has (hopefully) been found. Furthermore, when using an iterative technique there is no need to store the coefficient matrix. The only piece of information that must be known is the structure of the equations. On top of that an iterative solution requires fewer total operations and is insensitive to roundoff error.

Iterative methods that are used mainly for sparse problems can be divided into stationary iterative methods such as the Gauss-Seidel method and non stationary such as the Conjugate Gradient (CG) and other Krylov type methods. Non stationary iterative methods can basically be described by a generic iterative scheme. The next iteration point is the sum of the value of the initial point plus the correction terms of all iterations. The correctors are vectors implying that they posses both magnitude and direction.

In practice numerical methods such as Jacobi (simultaneous relaxation), Gauss-Seidel (successive relaxation), SOR (successive overrelaxation) are not used due to their slow convergence which is achieved after many iterations. Instead the multigrid method and the Krylov subspace based methods, including the conjugate gradient method, are widely used for the solution of sparse linear systems.

The conjugate gradient method, which is a popular choice for the solution of large sparse systems [CO4] and a fundamental method on which many others are based, belongs to a class of techniques that is based on the equivalence between the solution of a linear system and the minimization of an associated quadratic functional [CO3]:

$$E(\vec{x}) = \frac{1}{2}\vec{x}^T \ddot{A}\, \vec{x} - \vec{b}^T \vec{x} + c$$

where $\ddot{A}$ is a matrix, $\vec{b}$ and $\vec{x}$ are vectors and c is a scalar constant. If $\ddot{A}$ is a symmetric and positive definite $E(\vec{x})$ is minimized by the solution $\ddot{A}\vec{x} = \vec{b}$.

The above mentioned technique starts with an initial guess $\vec{x}^{(0)}$ and generates the sequence $\{\vec{x}^{(m)}\}$ for the solution of the equation $\ddot{A}\vec{x} = \vec{b}$, according to the rule

$$\vec{x}^{(m+1)} = \vec{x}^{(m)} + \lambda_m \vec{d}^{(m)}$$

The vector $\vec{d}^{(m)}$ is called the search direction and the scalar λ_m is the step size.

Basically, in each iteration step the new value $\vec{x}^{(m+1)}$ equals the previous value plus λ_m times the directional factor $\vec{d}^{(m)}$ equal to the residual plus a fraction α of the previous direction factor. λ_m and α_m are determined by the orthogonal residual condition [CO10]. That is

$$\vec{d}^{(m+1)} = -\vec{r}^{(m+1)} + \alpha_m \vec{d}^{(m)}$$

where $\vec{r}^{(m)}$ is just the residual associated with the approximation $\vec{x}^{(m)}$. The scalar α_m is chosen so that the search direction $\vec{d}^{(m+1)}$ is A-conjugate to the direction $\vec{d}^{(m)}$.

By seeing conjugate gradients as an energy minimizing algorithm, CG iteration minimizes $E(\vec{x})$ on the growing Krylov subspaces. The gradient of $E(\vec{x}) = \frac{1}{2}\vec{x}^T \ddot{A}\, \vec{x} - \vec{b}^T \vec{x} + c$ is exactly $\ddot{A}\vec{x} - \vec{b}$. Every cycle of CG chooses λ_m to minimize $E(\vec{x})$ in the new search direction $\vec{x}^{(m+1)} = \vec{x}^{(m)} + \lambda_m \vec{d}^{(m)}$. The last cycle gives the overall minimizer $\vec{x}_n = \vec{x} = \ddot{A}^{-1}\vec{b}$ [CO12].

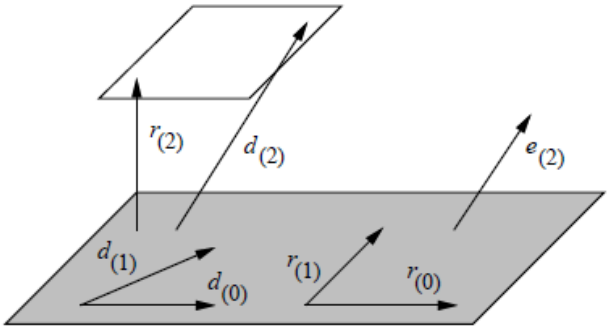

Figure CO2. Each new residual is orthogonal to all previous residuals and search directions and each new search direction is constructed (from the residual) to be A-orthogonal to all previous residuals and search directions. The error term is $e_{(2)}$.

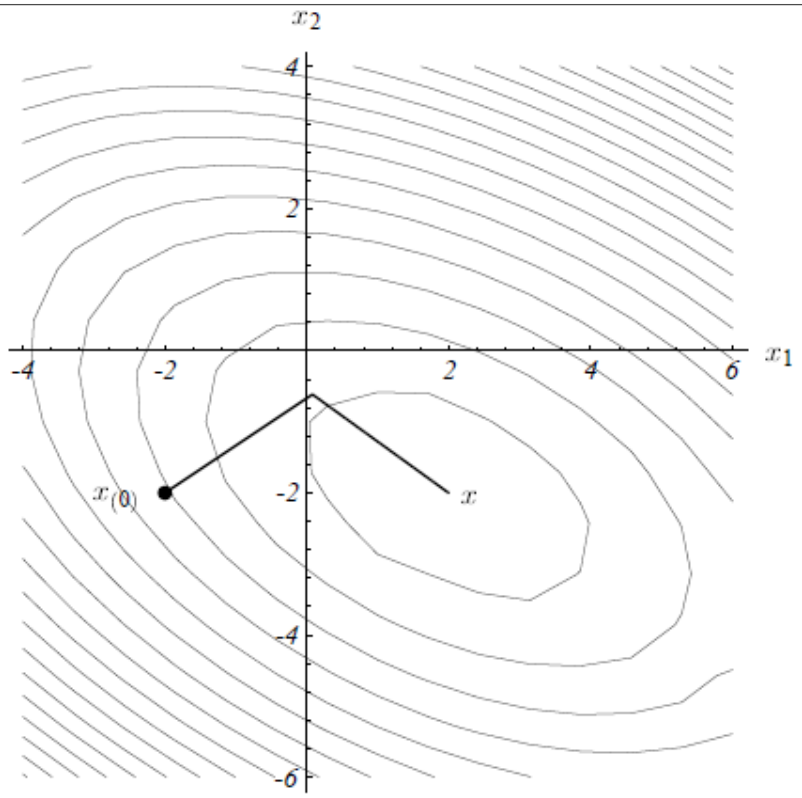

Figure CO3. The Conjugate Gradient method. Each ellipsoidal curve has a constant $E(\vec{x})$

A pseudocode implementing the Conjugate Gradient method is the following [CO3] (Figure CO2, Figure CO3):

$$\vec{r}^{(0)} = \vec{\vec{A}}\vec{x}^{(0)} - \vec{b}$$

$$\vec{d}^{(0)} = -\vec{r}^{(0)}$$

$$set\ \delta^{(0)} = \vec{r}^{(0)^{\mathrm{T}}}\vec{r}^{(0)}$$

$$for\ m = 0,1,2,...$$

$$set \quad \vec{u} = \vec{\vec{A}}\vec{d}^{(m)}$$

$$\lambda_m = \delta^{(m)} / \vec{d}^{(m)^{\mathrm{T}}}\vec{u}$$

$$\vec{x}^{(m+1)} = \vec{x}^{(m)} + \lambda_m \vec{d}^{(m)}$$

$$\vec{r}^{(m+1)} = \vec{r}^{(m)} + \lambda_m \vec{u}$$

$$set\ \delta^{(m+1)} = \vec{r}^{(m+1)^T}\vec{r}^{(m+1)}$$

$$if\ \sqrt{\delta^{(m+1)}} < TOL,\ OUTPUT\ \ \vec{x}^{(m+1)}$$

$$\alpha_m = \delta^{(m+1)} / \delta^{(m)}$$

$$\vec{d}^{(m+1)} = -\vec{r}^{(m+1)} + \alpha_m \vec{d}^{(m)}$$

The inputs to this routine are the coefficient matrix $\vec{\vec{A}}$, the right – hand side vector $\vec{b}$, the initial vector $\vec{x}^{(0)}$, which represents the initial guess, and the convergence tolerance TOL.

This method always produces the exact solution to an $n\ x\ n$ system in at most n iterations.

6.3 Mathematical Treatment of the Diffusion Based Simulation Module using the Euler (forward and backward) and the θ- Method. Treatment of Diffusion Anisotropy

6.3.1 Introduction

This section deals with a complementary mathematical treatment of tumour growth based on the diffusion equation where the Euler and the θ method. Diffusion anisotropy is also considered.

6.3.2 Diffusive Models

Cancer cells divide at varying rates among different cancers. It has been observed that metastases in lung grow according to a simple exponential law [CO14]. This has turned out to be the fire-lighter for intensive research efforts regarding quantification of tumour growth. However, this law fails when considering infiltrative cancers such as glioma because cell motility has not been included in the model. On the other hand it has been a good approximation to the microscopic behaviour of glioma. In order to take macroscopic behaviour into account diffusive models have been proposed.

The first proposer of a diffusive model for glioma growth was Murray in 1989 [CO15A]. Murray proposed the diffusion-reaction formalism as

$$\underbrace{\frac{\partial c}{\partial t}}_{\text{GBM Concentration Evolution}} \rightarrow - \underbrace{div\left(\vec{J}\right)}_{\text{Diffusion Law}} + \underbrace{S\left(c,t\right)}_{\text{Source Term}} - \underbrace{T\left(c,t\right)}_{\text{Treatment Law}} \qquad \text{(6.3.2.Eq.1)}$$

where

c denotes tumour cell concentration,

$\vec{J}$ is the diffusion flux of cells that follows Flick's law, i.e. $\vec{J} = -D\nabla c$, where ∇ is the gradient operator and D is the diffusion coefficient

$S(c,t)$ denotes the source term representing the GBM cell reproduction

$T(c,t)$ denotes the treatment representing the GBM cell loss due to treatment. This is zero when no treatment is applied.

The initial state of the model, $c\left(\vec{x},0\right) = f\left(\vec{x}\right)$, is defined as the initial distribution of cancerous cells.

This equation constitute the basis of the most of the proposed methods for glioma growth and invasion modeling. In 1995 Tracqui studied the evolution of cell concentration by using two characteristics of tumour growth i.e. proliferation and invasion [CO16]. He proposed that the cells proliferate at exponential rate, thus he modified Equation (6.3.2Eq.1) to

$$\frac{\partial c}{\partial t} = \nabla \cdot \left(D\nabla c\right) + \rho c \qquad \text{(6.3.2.Eq.2)}$$

where ρ denotes the proliferation rate of cells.

One of the key issues has been to estimate parameters D and ρ. The first estimation [CO16] made use of two groups of glioma cells: the common ones and the resistant-to-first-chemotherapy ones. Parameter D was first estimated to be $D = 10^{-2} cm^2 / day$ with the percentage of cells resistant to chemotherapy being 8% or $D = 10^{-3} cm^2 / day$ without resistant cells while ρ was estimated as $\rho = 10^{-2} / day$ [CO17]. Moreover, the derived 2-D model had the following characteristics [CO17]. First, tumour cells could not migrate either outside the skull boundaries or into the ventrical region. Secondly, brain tissue was considered homogenous and lastly the simulated tumour was a sphere having 3cm diameter at the time of diagnosis and 6cm at the time of death.

One of the next steps was to model cancer evolution after ectomy [CO16,CO18]. This was achieved by setting the concentration of the ectomized area equal to zero and then allowing the surrounding malignant cells proliferate and diffuse until the sphere reaches a diameter of 6cm.

It is noted that all these simulations studied high-grade gliomas due to their remarkably fast invasion. However, studying low-grade gliomas is important as well. Hence, Woodward suggested that the speed of growth in low-grade tumours should be 10% of the respective speed in high-grade gliomas, yielding satisfactory results [CO17].

Subsequently, Mandonnet proposed that low-grade gliomas grow slowly but linearly [CO19]. This is mathematically derivable from Equation (6.3.2Eq.2) since the expanding velocity of a population which follows only the diffusion and growth laws of Equation (6.3.2Eq.2) is

$2\sqrt{\rho D}$. Mandonnet et al used data of 27 patients to show that the average tumour velocity is 2mm per year.

Heterogeneity. Taking heterogeneity of the brain matter into account has led to the refinement of the previously mentioned models. It is known that proliferation in white brain tissue is faster than in grey tissue [CO20]. Swanson incorporated white and gray matter differentiation in the diffusion coefficient D of Equation (6.3.2Eq.2). As stated above D represets cell motility. Thus, by modifying D cell motility can be adapted to the local conditions. Equation (6.3.2Eq.2) continues to hold but D is now variable.

$$\frac{\partial c}{\partial t} = \nabla \cdot \left(D(\vec{x}) \nabla c \right) + \rho c \qquad \text{(6.3.2Eq.3)}$$

$D(\vec{x})$ varies according to position with $D(\vec{x}) = D_g$ or D_w, i.e. being constant for $\vec{x}$ within the grey and the white brain matter respectively. A brain atlas (BrainWeb database [CO21]) has been used in order to acquire information about the white and grey matter areas.

Anisotropy. Jbabdi et al. proposed to also take into account brain tissue anisotropy [CO22], dealing with the fact that glioma cell migration is facilitated in the direction of white matter fibers [CO23][CO24]. This work could also be supported by the Diffusion Tensor Magnetic Resonance imaging (DT MRI), that gives a very good 3D reconstruction of white matter fibers. Jbabdi used Equation (6.3.2Eq.3) in the following form

$$\frac{\partial c}{\partial t} = \nabla \cdot \left(\ddot{D}(\vec{x}) \nabla c \right) + \rho c \qquad \text{(6.3.2Eq.4)}$$

where $\ddot{D}$ is the diffusion tensor that describes cell diffusion i.e. a 3x3 symmetric positive definite matrix that models local anisotropy and can be expressed as

$$\ddot{D}(\vec{x}) = \begin{bmatrix} D_{11}(\vec{x}) & D_{12}(\vec{x}) & D_{13}(\vec{x}) \\ D_{12}(\vec{x}) & D_{22}(\vec{x}) & D_{23}(\vec{x}) \\ D_{13}(\vec{x}) & D_{23}(\vec{x}) & D_{33}(\vec{x}) \end{bmatrix}$$

where $D_{ij}(\vec{x})$ are the components of $\ddot{D}(\vec{x})$ at position $\vec{x}$. *1,2,3* correspond to the axes *x,y,z* respectively.

Parameters. According to [CO25] Figure CO4 can be used as an index for estimating the values of the parameters D and ρ according to glioma grade the growth velocities and the ratio D/ρ. This log-log graph includes all parameter values estimated up to Jan. 2007 for both low- and high grade gliomas. Low grade gliomas (LGG) are mapped on the bottom left rectangle (LGG) for 2mm/yr average velocities. Respectively, high grade gliomas (HCG) are mapped on the large rectangle defined by D/ρ of 2 to 20 cm^2 and average velocities from 10mm/yr to 200mm/yr.

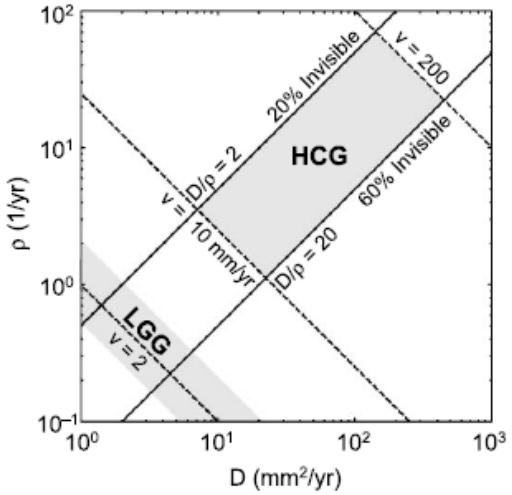

Figure CO4. Log-log graph of D vs ρ, for high- and low- grade gliomas
(from [CO25] H. L. P. Harpold, E. C. Alvord, Jr., K. R. Swanson: Visualizing Beyond the Tip of the Iceberg: The Evolution of Mathematical Modeling of Glioma Growth and Invasion. *Journal of Neuropathology and Experimental Neurology*, 66(1):1—9, (2007))

For the case of heterogenous brain matter [CO20] and for high grade gliomas a typical estimated value of ρ is ρ=0.0012 /day. A typical estimated value for low grade gliomas is ρ=0.00012 /day. Therefore, by assuming $D_w = 5D_g$, the values of $D_w = 10^{-2} mm^2 / day$ and $D_g = 2 \cdot 10^{-3} mm^2 / day$ can be used [CO22].

A list of typical parameter values used in duffusive glioma models is provided in Table CO1 [CO26]

Table CO1. The parameters of the diffusive model as proposed in the last 2 decades (from [CO26] Powathil G, Kohandel M, Oza A, and Milosevic M, Mathematical modeling of brain tumors: effects of radiotherapy and chemotherapy, Phys. Med. Biol. 52, 3291—3306 (2007))

Parameters	Value	References	
Growth rate	ρ	0.012 (1/day)	Cook *et al* (1995)
Diffusion coefficient (Gray matter)	D_G	0.0013 (cm^2 /day)	Tracqui *et al* (1995)
Diffusion coefficient (White matter)	D_W	$5D_G$ (cm^2/day)	Swanson *et al* (2000)
Initial number of tumor cells	N_0	10^5 cells	Murray (2003) and Woodward *et al* (1996)
CT threshold density		400 (cells mm^{-2})	Swanson *et al* (2000)
CT threshold radius		1.5 cm	Cook *et al* (1995) and Tracqui *et al* (1995)
Cell death rate (Chemotherapy)	k	0.0196 (1/day)	Fitting to data (Stupp *et al* (2005))
Number of fractions/day	n	1-conventional (CR) 2-hyperfractionated (HF)	Walker *et al* (1979) Werner-Wasik *et al* (1996)
Time interval	$\Delta\tau$	1 day—CR 6 h—HFR	Shibamoto *et al* (1997) Nieder *et al* (1999)

References

CO1 Sally A. Amundson, K. T. Do, L. C. Vinikoor, R. A. Lee, C. A. Koch-Paiz, J. Ahn[1], M. Reimers[3,5], Y. Chen, D. A. Scudiero, J. N. Weinstein[3], J. M. Trent, M. L. Bittner, P. S. Meltzer and A. J. Fornace, Jr., Integrating Global Gene Expression and Radiation Survival Parameters across the 60 Cell Lines of the National Cancer Institute Anticancer Drug Screen, Cancer Research 68, 415, January 15, 2008

CO2 Kristin R. Swanson, Carly Bridge, J.D. Murray, Ellsworth C. Alvord Jr. Virtual and real brain tumors: using mathematical modeling to quantify glioma growth and invasion. Journal of the Neurological Sciences 2003; 216:1-10.

CO3 Brian Bradie. A friendly Introduction to Numerical Analysis. Pearson International Edition 2006; Chapters 10 and 3.

CO4 Jonathan Richard Shewchuk. An Introduction to the Conjugate Gradient Method Without the Agonizing Pain. School of Computer Science, Carnegie Mellon University, Pittsburgh; 1994.

CO5 http://en.wikipedia.org/wiki/Diffusion_coefficient. Fick's law of diffusion 19-2-2009.

CO6 Kristin R. Swanson, Ellsworth C. Alvord Jr, J.D. Murray. Dynamics of a Model for Brain Tumors reveals a small window for therapeutic intervention. Discrete and Continuous Dynamical Systems — Series B, Volume 4, Number 1, 2004;pp289-295.

CO7 http://en.wikipedia.org/wiki/Finite_difference_method. Finite difference method. 22-2-09.

CO8 http://en.wikipedia.org/wiki/Numerical_analysis#Discretization_and_numerical_integration. Numerical analysis 22-2-2009.

CO9 Ge Baolai. Parallel Numerical Solution of PDEs with Message Passing. The University of Western Ontario. January 2008.

CO10 Fritjof Nilsson. Numerical Treatment of a Diffusion — Convection — Evaporation Model for Droplets. Master's thesis in Numerical Analysis at the school of Engineering Physics, Department of Numerical Analysis and Computer Science, Royal Institute of Technology, Stockholm, Sweden.

CO11 Xing Cai, Bjorn Fredrik Nielsen, Aslak Tveito. A note on the efficiency of the conjugate gradient method for a class of time — dependent problems. Numerical Linear Algebra with Applications 2007;14:459-467.

CO12 Gilbert Strang. Krylov Subspaces and Conjugate Gradients. 6.4, 2006

CO13 Swanson, K. R., True, L. D., Murray, J. D.: On the Use of Quantitative Modeling to Help Understand PSA Dynamics and Other Medical Problems, *American Journal of Clinical Pathology,* 119(1):14—7, (2003)

CO14 Collins V.P., Loeffer R.K, Tivey H., Observations on growth rates of human tumors, Am J Roentgenol Radium Ther Nucl Med ; 76: 988—1000, (1956)

CO15A Murray, J.D., Mathematical Biology, Springer — Verlag, Heidelberg, (1989)

CO15 Puwal, S.; Roth, B.J., Forward Euler Stability of the Bidomain Model of Cardiac Tissue, Biomedical Engineering, IEEE Transactions on Volume 54, Issue 5,Page(s):951 — 953 (2005)

CO16 Tracqui, P.: From passive diffusion to active cellular migration in mathematical models of tumor invasion, *Acta Bibliotheoretica*, 43: pp 443—464, (1995).

CO17 Woodward DE, Cook J, Tracqui P, et al. A mathematical model of glioma growth: The effect of extent of surgical resection. Cell Prolif;29:269—88 (1996)

CO18 Kreth FW, Warnke PC, Scheremet R, et al. Surgical resection and radiation therapy versus biopsy and radiation therapy in the treatment of glioblastoma multiforme. J Neurosurg ;78 :762—66 (1993)

CO19 Mandonnet E, Delattre JY, Tanguy ML, et al. Continuous growth of mean tumor diameter in a subset of grade II gliomas. Ann Neurol; 53:524—28 (2003)

CO20 Swanson, K.R, Alvord, E.C., and Murray, J.D.: A Quantitative Model for Differential Motility of Gliomas in Grey and White Matter, *Cell Proliferation* 33(5): 317—330, (2000)

CO21 Cocosco CA, Kollokian V, Evans AC, et al. Brainweb: Online interface to a 3D simulated brain database. Neuroimage;5:S425 (1997)

CO22 Jbabdi S, Mandonnet E, Duffau H, et al. Simulation of anisotropic growth of low-grade gliomas using diffusion tensor imaging. Magn Reson Med;54:616—24 (2005)

CO23 Belien AT, Paganetti PA, Schwab ME, Membrane-type 1 matrix metalloprotease (mt1-mmp) enables migration of glioma cells in central nervous system white matter, J. Cell Biol; 144:373—384(1999)

CO24 Giese A, Bjerkvig R, Berens ME, Westphal M. , Cost of migration: invasion of malignant gliomas and implications for treatment. J Clin Oncol; 21:1624—1636 (2003)

CO25 H. L. P. Harpold, E. C. Alvord, Jr., K. R. Swanson: Visualizing Beyond the Tip of the Iceberg: The Evolution of Mathematical Modeling of Glioma Growth and Invasion*. Journal of Neuropathology and Experimental Neurology*, 66(1):1—9, (2007)

CO26 Powathil G, Kohandel M, Oza A, and Milosevic M, Mathematical modeling of brain tumors: effects of radiotherapy and chemotherapy, Phys. Med. Biol. 52, 3291—3306 (2007)

7. Modelling Clinical Tumour Growth and Response to Treatment: Discrete Event/Entity Based Modelling Approach [Code: DI]

7.1 Workflow of the discrete event/entity based tumour dynamics simulator

Although a continuum based description of tumour growth using the diffusion equation is a good model for pronounced tumour invasion it does not allow for an in depth simulation of numerous biological mechanisms most of which have a discrete character (e.g. cell cycle phases, differing radiosensitivities and chemosensitivities for different cell cycle phases, stem, progenitor, differentiated cell categories etc.). Since the latter is of utmost clinical importance, in parallel with the continuum based models discrete event/entity simulation models are being developed focusing primarily on tumour response to treatment. These models incorporate numerous biological mechanisms and their interdependences and are based on the *top-down* tumour dymamics simulation approach developed by the *In Silico* Oncology Group, ICCS, National Technical University of Athens (http://www.in-silico-oncology.iccs.ntua.gr/).

Pertinent clinical data from the list included in Chapter 5 will be used in order to adapt, optimize and validate the discrete simulator. Details regarding the types of data applicable to each particular tumour type (gliomas and lung cancer) are also provided in Chapter 5.

According to the discrete event/entity based modelling approach the tumour is considered a spatiotemporal distribution of discrete cells (and cell death products) belonging to several proliferative potential categories and cell cycling phases. The discrete simulator module will function as follows (Figure DI1)

i. The **macroscopic imaging data** of the patient (e.g. contrast enhanced MRI, CT, PET etc) are collected at baseline

ii. The macroscopic imaging data are segmented by the clinician (delineation of tumour boundaries, necrotic areas etc.), interpolated, three dimensionally reconstructed and eventually fused if more than one modalities are used. Both anatomy and spatial metabolic activity are the features to be ideally provided by the processed imaging data.

iii. The **microscopic imaging data** of the tumour (photographs of histopathological sections of bioptic material etc.) are provided.

iv. The microscopic imaging data are processed in such a way that the density of tumour cells as well as the percentages of the populations of the various cell categories and cell cycling phases are estimated. Mapping of the areas from which the biopsies stem onto the imaging data could lead to a relatively refined cosideration of the tumour spatial inhomogeneities.

v. Along with information based on histopathological slides tumour cell cycling information (e.g. duration of cell cycle for the particular tumour) is provided from literature

vi. The pre-treatment spatial distribution of imageable and non imageable tumour cell density is estimated based on both imaging data and literature. Non imageable tumour cell distribution refers primarily to gliomas where tumour growth exhibits markedly diffusive patterns.

vii. A discretization mesh is superimposed upon the three dimensionally reconstructed tumour. In contrast with the mesh nodes that are used in the continuum approach the geometrical cells formed by the discretization mesh constitute the elementary spatial units of the problem in the discrete event/entity based approach. Within each geometrical cell biological cells are clustered together based primarily on their mitotic potential, their cell proliferation phase and the treatment killing effect upon them. Based on *mitotic potential* they may be stem cells (having theoretically infinite mitotic potential), progenitor cells (having limited mitotic potential that is defined by the number of mitoses that can still undergo), differentiated cells (no mitoses possible anymore) and dead cells. Based on the *cell proliferation phase* in which they are found they may belong to the G1 or the S or the G2 or the Mitosis or the G0 or the necrosis or the apoptosis equivalence class. Based on the *treatment killing effect* they may be treatment hit or treatment non hit cells. A careful hierarchical positioning of the various equivalence classes is adopted in order to avoid ambiguities in the description of a biological cell or biological cell cluster.

viii. The **molecular data** (e.g. status, amplification and expressions of critical genes, which have been shown to drastically affect the response of the tumour under consideration to the treatment addressed) are provided. Details concerning the two tumour types considered (gliomas and lung cancer) are provided in Chapter 5. Estimates (even semi-qualitative) of their effect on the cell kill ratio per cell due to the treatment considered are also provided based on pertinent literature [e.g. DI1]. The idea is to use the cell kill ratio value provided by the Food and Drug Administration (FDA) or general literature as a cell kill ratio reference value (e.g. for a given area under curve or radiation dose) and then perturb it based on the effect of the molecular and/or histological profile of the tumour in order to achieve higher patient individualization of the simulation.

ix. The model parameters are estimated based on the previously mentioned data as well as literature based information.

x. The discretization mesh is scanned every time unit and on each geometrical cell metabolic, cell cycling, survival following treatment and simple mechanical laws are applied. The outcome is an update of the spatiotemporal distribution of the various tumour cell categories and cell cycling phases over the entire tumour.

xi. In parallel with the solution of the biological problem a mechanical refinement can take place based on the Fimite Element Method (Workpackage WP6). To

this end any mechanical data available (primarily through literature) will be utilized in conjunction with the imaging data.

xii. **NOTE** Acceleration of the simulation code will be envisaged in order to significantly lower the computing time demands. Execution of the code on fast computing systems (eventually including clusters and/or grid) will also take place. Tumour growth simulators can estimate the evolution of tumour volume and the various cell category populations in function of the time (see Section 7.2), however, the execution time of each simulation instance of e.g. the ACGT Oncosimulator (a precursor of the ContraCancrum integrated simulator) currently takes several minutes, which makes it far from an interactive tool. Modern graphics processing units (GPUs) provide not only a powerful graphics engine but also a highly parallel programmable processor featuring peak arithmetic and memory bandwidth that substantially outpaces its CPU counterpart. A state-of-the-art GPU can perform over 500 billion arithmetic operations per second, and this represents a tremendous computational resource that can now be utilised for general purpose computing as a result of recent advances in GPU hardware and software architecture. By programming an NVIDIA GPU device with the CUDA (Compute Unified Device Architecture) extension of the C language, we shall design parallel algorithms to parallelise the whole time-consuming process of tumour simulation on the GPU.Tumour evolution is computed by hourly scanning in order to allow the local application of basic biological rules; this leads to the spatiotemporal simulation of the tumour system. At each iteration, we shall assign one thread to each GC (geometrical cell) and execute the following 3 scanning steps via parallel GPU kernels:1)Cell growing. Each parallel computing thread computes all the cell cycle phase transitions and any cell that has died due to chemotherapy or radiotherapy within the GC.2) Cell transfer in the GC neighbourhood – unloading the remaining or excess cells into the surrounding 26 GCs of the current GC. This can be implemented on GPU by 27 subpasses by interleaving the 27 neighbouring GCs at each subpass. This GPU implementation takes advantage of all of the GPU resources made available under the CUDA programming model. All the cell transferences between 27 local neighbouring GCs (a box) are evaluated in a single thread, with each thread block responsible for a row of boxes. All threads in a block simultaneously iterate through the neighbouring GCs in shared memory, computing the transfers on the boxes in their individual registers. Since all threads in a block access the same shared memory location, data are broadcast to all threads by the hardware, and no bank conflict penalty is incurred. 3) Differential tumour shrinkage. This frees the GCs that contain too few cells or creates new GCs for differential tumour expansion. It also deals with the restoration of tumour contiguity in cases where tumour fragmentation has occurred.

xiii. A prediction of the spatiotemporal distribution of the tumour cell categories and the cell cycling phases for free tumour growth [no treatment] and/or tumour response to treatment (chemotherapy / radiotherapy) is obtained. Several forms of prediction visualization (graphs, 3D and 4D rendering etc.) are offered.

xiv. The simulated outcome is compared with the actual (primarily) imaging data following treatment and an optimization loop of the parameters estimation [and if necessary of the model algorithm iself] is initiated.

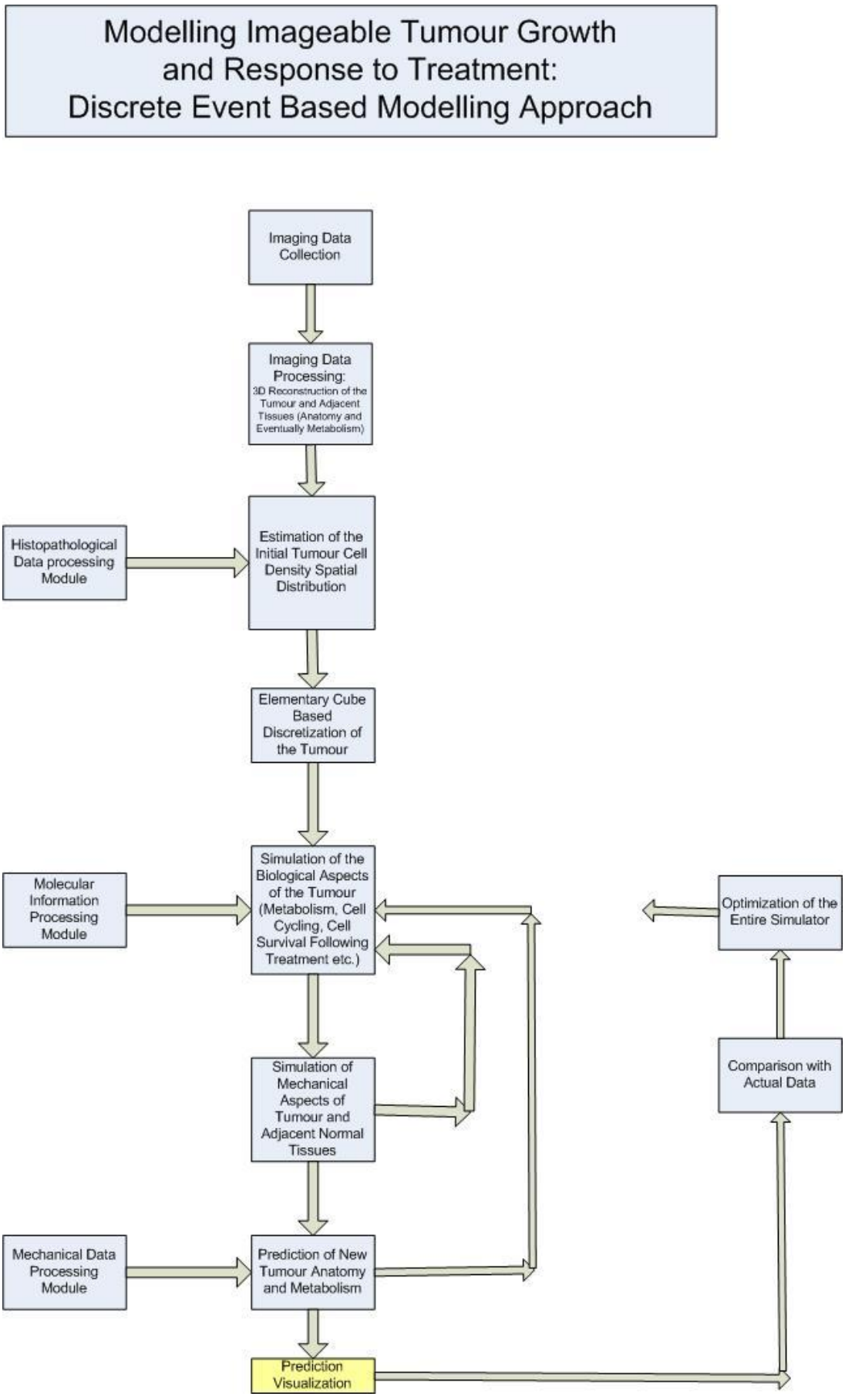

Figure DI1. Discrete event based tumour and normal tissue simulator workflow

7.2 A Brief Outline of the Fundamentals of Discrete Event Based Simulation Modelling

Although considerable extensions and improvements of discrete event simulators will take place during the ContraCancrum lifetime a detailed presentation of their theoretical, mathematical and computational fundamentals can be found in publications [DI2-DI18]. In the following only a high level brief outline of the basics is presented.

The tree dimensionally reconstructed tumour (based on the segmentation of the imaging data) is discretized using a cubic mesh. Discrimination between the well and poorly vascularized regions of the tumour - when possible - can be exploited by the model. Each elementary cube of the mesh is called a geometrical cell (GC) and is used as the unit for the description of the biological activity of an imageable tumour. Each GC of volume $1mm^3$ is assumed to contain 10^6 biological cells according to the classical radiobiological assumption. The following categories of tumour cells are considered:

- Stem cells
- Limited mitotic potential or progenitor cells (LIMP cells)
- Differentiated cells
- Dead cells

Proliferating stem cells as well as proliferating LIMP cells are further discriminated according to their cell cycle phase. Dead cells are divided into necrotic and apoptotic. Within each GC, cells are clustered into equivalence classes based primarily on their proliferative potential (e.g. stem, progenitor, differentiated, dead cell categories) and on the cell cycling phases (e.g. G1, S, G2, Mitosis phases) in which they (temporarily) belong. Distribution of the cells into the various equivalence classes is dictated by the metabolic activity of their neighbourhood as estimated from the imaging data. In order to simulate the statistical character of reality *local perturbations* of the populations of each equivalence class are achieved through the use of pseudo-random numbers (generic Monte Carlo technique).

The discretization mesh is scanned every time unit (e.g. hour) and the fundamental rules of metabolism, cell cycling (Figure DI2), mechanics and cell survival following treatment (chemotherapy and/or radiotherapy) are applied. This may lead to cell category and cell phase transitions. Cell kill probabilities per cell, per treatment session and for a given treatment dose are calculated based on pharmacokinetics-pharmacodynamics and/or radiobiology principles and data.

In order to effectively simulate tumour expansion or shrinkage a provisionally acceptable upper limit (NBC_{upper}) and a provisionally acceptable lower limit (NBC_{lower}) of the number of cells that can be contained within each GC are defined. If the number of tumour cells within a given GC becomes less than NBC_{lower} during the simulation process, a procedure that attempts to “unload” the remaining cells in the neighbouring GCs is initiated. If the given GC becomes empty it “attracts” cells from its neighbourhood so that no artificial voids are created within the tumour (“*horror vacui*”). An appropriate shift of a chain of GCs intended to fill in the “vacuum” leads to tumour shrinkage. Similarly differential tumour expansion is achieved by an appropriate shift of a chain of GCs towards the boundaries of the tumour. In order to further refine the mechanical handling of the tumour, fusion of the simulator with the biomechanics module being developed within the framework of WP6 has been planned.

By also taking into account a number of restrictions and many other details the simulator provides at each simulated time point a spatial prediction of the tumour volume (Figure DI3) along with the spatial distribution of its cells over proliferative potential categories, cell cycling phases (e.g. G1, S, G2, Mitosis phases) etc.

The simulator predictions are visualized using several techniques (standard graphs, 2D, 3D, 4D animations, virtual cuts through the tumour etc.) . Based on pertinent clinical criteria the predicted outcome of the treatment is juged as *favourable* or *unfavourable* for the individual patient.

The cellular and higher biocomplexity levels simulator will serve as the basis for the development of the integrated ContraCancrum simulator which is envisaged to finally serve as a patient individualized treatment optimization support system.

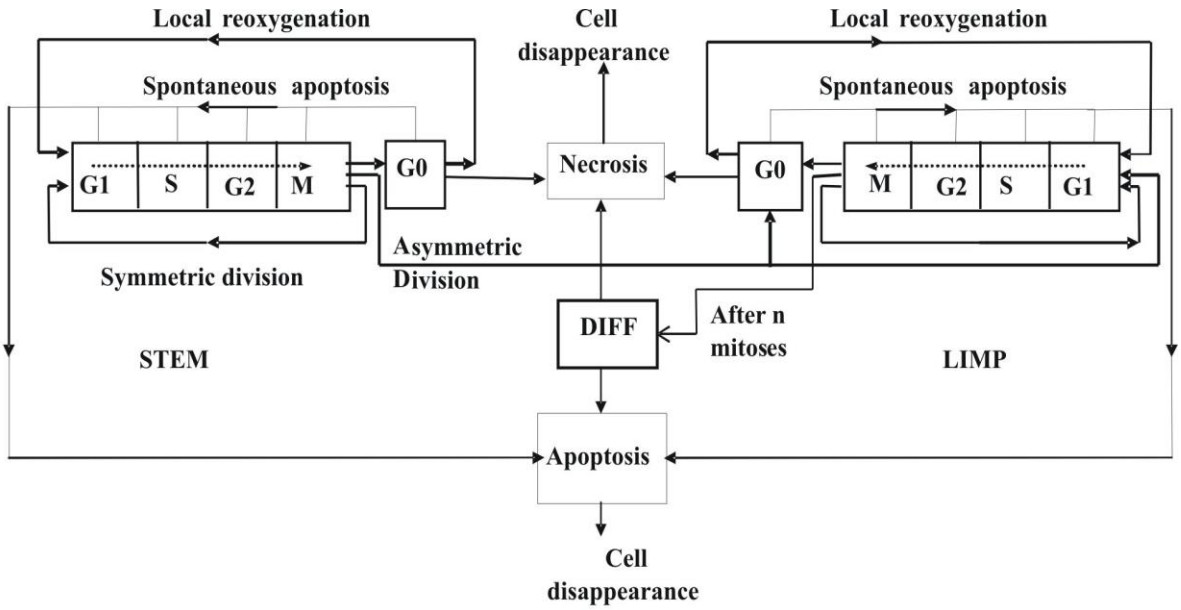

Figure DI2. A generic cytokinetic model for free tumour growth. STEM: stem cells. LIMP: Limited proliferative potential cells (progenitor cells). DIFF: terminally differentiated cells. An extension of the diagram includes also the effect of treatment on the cell [DI17,DI18]

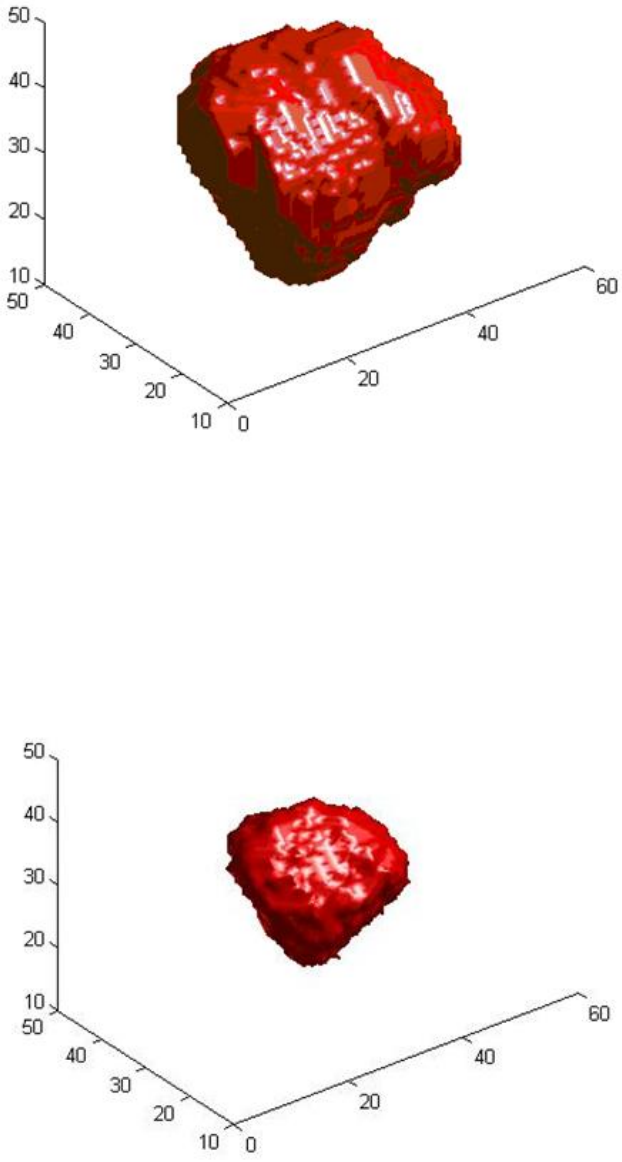

Figure DI3 : A typical 3D tumour visualization of the response of an actual large clinical tumour treated with chemotherapy (from the ACGT project). Upper panel: tumour four days before treatment initiation, lower panel: predicted tumour three days after completion of the treatment course.

References

DI1 Sally A. Amundson, K. T. Do, L. C. Vinikoor, R. A. Lee, C. A. Koch-Paiz, J. Ahn[1], M. Reimers[3,5], Y. Chen, D. A. Scudiero, J. N. Weinstein[3], J. M. Trent, M. L. Bittner, P. S. Meltzer and A. J. Fornace, Jr., Integrating Global Gene Expression and Radiation Survival Parameters across the 60 Cell Lines of the National Cancer Institute Anticancer Drug Screen, Cancer Research 68, 415, January 15, 2008

DI2. G.S.Stamatakos, D.D.Dionysiou, E.I.Zacharaki, N.A.Mouravliansky, K.Nikita, N.Uzunoglu, "In silico radiation oncology: combining novel simulation algorithms with current visualization techniques", Proceedings of the IEEE, vol. 90, No 11, pp.1764-1777, Nov. 2002.

DI3. Stamatakos, G. S., P.Antipas, V., Uzunoglu, N. K., A spatiotemporal, patient individualized simulation model of solid tumor response to chemotherapy in vivo: the paradigm of glioblastoma multiforme treated by temozolomide. IEEE Trans Biomed. Engineering 53, No 8, (2006), 1467-1477

DI4. D. D. Dionysiou, G. S. Stamatakos, N.K. Uzunoglu, K. S. Nikita, A. Marioli, "A four-dimensional simulation model of tumour response to radiotherapy in vivo: parametric validation considering radiosensitivity, genetic profile and fractionation," Journal of Theoretical Biology 230 (2004) 1–20

DI5. G. S. Stamatakos, V.P. Antipas, N. K. Uzunoglu, R. G. Dale, "A four dimensional computer simulation model of the in vivo response to radiotherapy of glioblastoma multiforme: studies on the effect of clonogenic cell density." British Journal of Radiology, 2006, vol. 79, 389-400

DI6. V. P Antipas, G. S Stamatakos, N. K Uzunoglu, D. D Dionysiou, R. G Dale, " A spatio-temporal simulation model of the response of solid tumours to radiotherapy in vivo: parametric validation concerning oxygen enhancement ratio and cell cycle duration," Phys. Med. Biol. 49 (2004) 1485–1504

DI7. G.S.Stamatakos, V.P. Antipas, N.K. Uzunoglu, "Simulating chemotherapeutic schemes in the individualized treatment context: The paradigm of glioblastoma multiforme treated by temozolomide in vivo." Comput Biol Med. Comput Biol Med. 36, 1216–1234, 2006.

DI8. G. Stamatakos, " Spotlight on Cancer Informatics," Cancer Informatics No 2, pp.99-102, 2006.

DI9. D. Dionysiou, G. Stamatakos and K. Marias, "Simulating cancer radiotherapy on a multi-level basis: biology, oncology and image processing," Lecture Notes in Computer Science, Special Issue on Digital Human Modeling, Vol. 4561, pp.569-575, 2007.

DI10. Antipas, V.P., Stamatakos, G.S., Uzunoglu, N.K., 2007. A patient-specific in vivo tumor and normal tissue model for prediction of the response to radiotherapy: a computer simulation approach. Methods Inf. Med. 46, 367-375.

DI11. Dionysiou,D.D., Stamatakos, G.S., Uzunoglu,N.K., Nikita,K.S, 2006. A computer simulation of in vivo tumour growth and response to radiotherapy: New algorithms and parametric results. Computers in Biology and Medicine 36 448–464

DI12. Stamatakos, G., Dionysiou, D., Nikita, K., Zamboglou, N., Baltas, D., Pissakas, G., et al., 2001. In vivo tumour growth and response to radiation therapy: a novel algorithmic description. Int. J. Radiat. Oncol. Biol. Phys.,51 Suppl. 1, 240.

DI13. Stamatakos, G.S., 2006d. Towards a collaborative formulation of the Mathematical Principles of Natural Philosophy: Living Matter. The paradigm of In Silico Oncology. DIMACS Workshop on Computational Tumor Modeling, DIMACS Center, Rutgers University, Piscataway, NJ, USA. http://dimacs.rutgers.edu/Workshops/TumorModeling/abstracts.html

DI14. Stamatakos, G. S. and Uzunoglu, N., 2006. Computer Simulation of Tumour Response to Therapy. Cancer Bioinformatics: from therapy design to treatment. Edited by Sylvia Nagl. John Wiley & Sons, Ltd., Chichester,UK.

DI15. Dionysiou, D.D. and Stamatakos, G.S., 2006. Applying a 4D multiscale in vivo tumor growth model to the exploration of radiotherapy scheduling: the effects of weekend treatment gaps and p53 gene status on the response of fast growing solid tumors. Cancer Informatics 2, 113-121.

DI16. Stamatakos GS, Dionysiou DD, Graf N, et al. “The “Oncosimulator”: a multilevel, clinically oriented simulation system of tumor growth and response to therapeutic schemes. [231] Towards clinical evaluation of in silico oncology.” 29th Annual International Conference of the IEEE Engineering in Medicine and Biology Society in conjunction with the biennial Conference of the French Society of Biological and Medical Engineering (SFGBM), August 23-26, 2007, Conf Proc IEEE Eng Med Biol Soc

DI17. E. A. Kolokotroni, G. S. Stamatakos, D. D. Dionysiou, E. Ch. Georgiadi, Ch. Desmedt, N. M. Graf, “Translating Multiscale Cancer Models into Clinical Trials: Simulating Breast Cancer Tumor Dynamics within the Framework of the “Trial of Principle” Clinical Trial and the ACGT Project.,” Proc. 8th IEEE International Conference on Bioinformatics and Bioengineering (BIBE 2008), Athens, Greece, 8-10 Oct. 2008. IEEE Catalog Number: CFP08266, ISBN: 978-1-4244-2845-8, Library of Congress: 2008907441, Paper No. BE-2.1.1, length: 8 pages (in electronic format). In press

DI18. E. Ch. Georgiadi, G. S. Stamatakos, N. M. Graf, E. A. Kolokotroni, D. D. Dionysiou, A. Hoppe, N. K. Uzunoglu, “Multilevel Cancer Modeling in the Clinical Environment: Simulating the Behavior of Wilms Tumor in the Context of the SIOP 2001/GPOH Clinical Trial and the ACGT Project,” Proc. 8th IEEE International Conference on Bioinformatics and Bioengineering (BIBE 2008), Athens, Greece, 8-10 Oct. 2008. IEEE Catalog Number: CFP08266, ISBN: 978-1-4244-2845-8, Library of Congress: 2008907441, Paper No. BE-2.1.2, length: 8 pages (in electronic format). In press

8. Modelling Normal Tissue Response to Treatment [Code: NO]

The limitations imposed by the adverse effects of treatment (chemotherpy / radiotherapy) on normal tissues will be addressed by either or both of the following approaches (Figure NO1) :

8.1 First Approach

Based on toxicological (preclinical and clinical) data, upper clinically acceptable limits for the treatment dose are available for a number of treatment modalities. In case that a candidate treatment scheme leads to unacceptable side effects based on the above limits no consideration for actual treatment [i.e. candidate scheme simulation] based on this scheme is allowed.

8.2 Second Approach

Simple simulation models based on cell cycling and homeostasis for flexible (e.g. brain) [NO1] and/or hierarchical (e.g. blood) normal tissues are developed. The outcome of the simulation of the response of normal tissues to the candidate tumour treatment is visualized through several techniques. The prediction *in conjunction with* any limits based on toxicological studies may be used in order to allow or not further consideration of the treatment scheme. The simulation outcome is compared with any known actual side effects, thus leading to the optimization of the normal tissue simulation module.

Details regarding the complication data to be provided by the clinical partners in order to adapt, optimize and validate the models are included in Chapter 5.

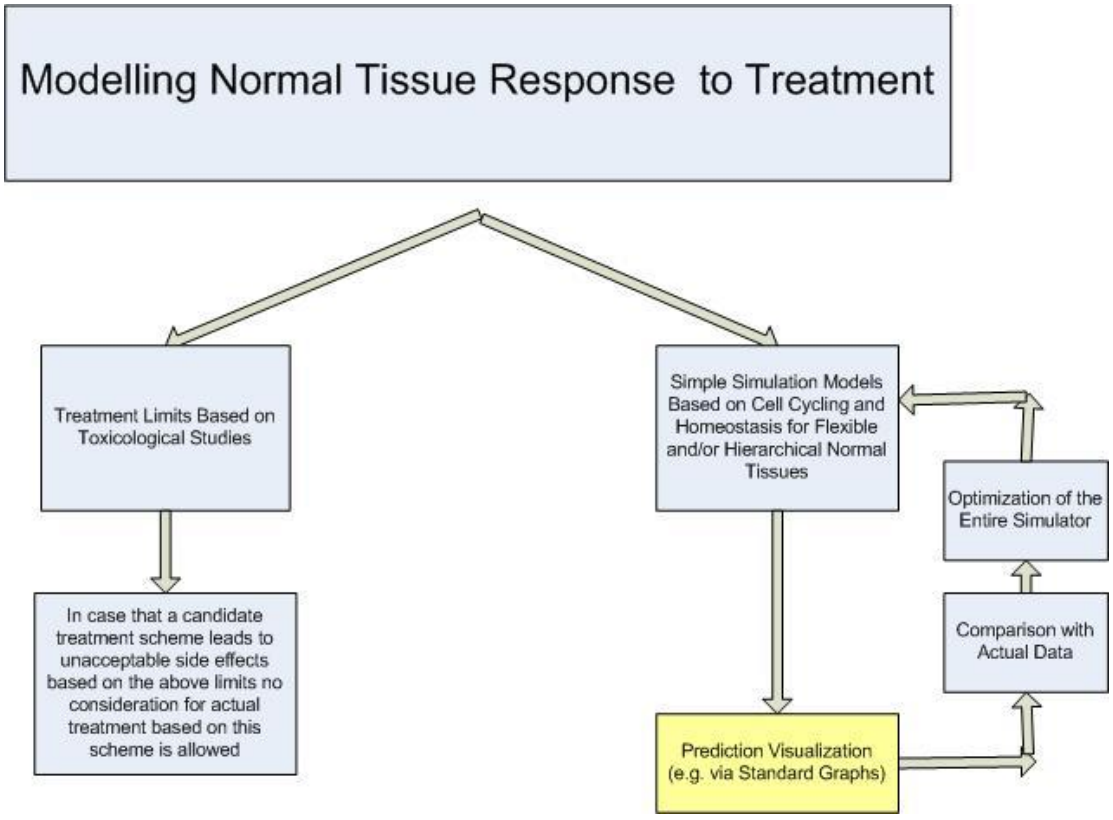

Figure NO1. Two alternatives to take into account the response of normal tissues to treatment

References

NO1. Antipas, V.P., Stamatakos, G.S., Uzunoglu, N.K., 2007. A patient-specific in vivo tumor and normal tissue model for prediction of the response to radiotherapy: a computer simulation approach. Methods Inf. Med. 46, 367-375.

9. Conclusions [Code: CC]

A high level outline of the various simulation modules that constitute the cell and higher biocomplexity level tumour dynamics simulator of the ContraCancrum project has been provided. An introduction to the emerging field of *in silico* oncology in conjunction with a brief literature review have preceded the basics of the models. The latter refer to several fundamental microscopic mechanisms of tumour growth and response to treatment (including i.a. prevascular tumour growth, prevascular tumour response to treatment i.e. chemotherapy and/or radiotherapy, angiogenesis, invasion, metastasis etc.) as well as to the dynamics (growth and treatment response) of (imageable) clinical tumours. In order to address large tumours two mutually complementary approaches have been adopted. The first one is based on a continuum treatment of the tumour via the diffusion equation whereas the second one is based on discrete event/entity simulation techniques that make use of cellular automata, the Monte Carlo method, cell clustering into equivalence classes as well as numerous dedicated algorithms. In this way both diffusion phenomena and complex multiscale biological mechanisms of a predominantly discrete character have been addressed. Alternative ways to consider the treatment side effects have been delineated. Since gliomas and lung cancer constitute the ContraCancrum modeling paradigms, a description of the multiscale data to be provided by the clinical partners in order to drive, adapt, optimize and validate the imageable tumour models has also been presented..

ANNEX A
Numerical Solution of the Diffusion Equation in Three Dimensional Heterogenous and Anisotropic Brain

I. 3D expansion

The diffusion equation

$$\frac{\partial c}{\partial t} = \nabla \cdot \left(\vec{\vec{D}}(\vec{x}) \nabla c \right) + \rho c$$

where

$$\vec{\vec{D}}(\vec{x}) = \begin{bmatrix} D_{11}(\vec{x}) & D_{12}(\vec{x}) & D_{13}(\vec{x}) \\ D_{12}(\vec{x}) & D_{22}(\vec{x}) & D_{23}(\vec{x}) \\ D_{13}(\vec{x}) & D_{23}(\vec{x}) & D_{33}(\vec{x}) \end{bmatrix}$$

is expanded in 3 dimensions so that it can be solved numerically

$$\frac{\partial c}{\partial t} = \nabla \cdot \left(\vec{\vec{D}}(\vec{x}) \nabla c \right) + \rho c \overset{\nabla = \frac{\partial}{\partial x_1}\vec{e}_1 + \frac{\partial}{\partial x_2}\vec{e}_2 + \frac{\partial}{\partial x_3}\vec{e}_3}{\Leftrightarrow}$$

$$\frac{\partial c}{\partial t} = \nabla \cdot \left(\vec{\vec{D}}(\vec{x}) \left(\frac{\partial c}{\partial x_1}\vec{e}_1 + \frac{\partial c}{\partial x_2}\vec{e}_2 + \frac{\partial c}{\partial x_3}\vec{e}_3 \right) \right) + \rho c \Leftrightarrow$$

$$\frac{\partial c}{\partial t} = \nabla \cdot \left(\frac{\partial c}{\partial x_1}\vec{\vec{D}}(\vec{x})\vec{e}_1 + \frac{\partial c}{\partial x_2}\vec{\vec{D}}(\vec{x})\vec{e}_2 + \frac{\partial c}{\partial x_3}\vec{\vec{D}}(\vec{x})\vec{e}_3 \right) + \rho c$$

The product of the diffusion tensor $\vec{\vec{D}}(\vec{x})$ multiplied by the standard base vectors $\vec{e}_1, \vec{e}_2, \vec{e}_3$ yields

$$\vec{\vec{D}}(\vec{x})\vec{e}_1 = \begin{bmatrix} D_{11} & D_{12} & D_{13} \\ D_{21} & D_{22} & D_{23} \\ D_{31} & D_{32} & D_{33} \end{bmatrix} \begin{bmatrix} 1 \\ 0 \\ 0 \end{bmatrix} = \begin{bmatrix} D_{11} & D_{21} & D_{31} \end{bmatrix}^T,$$

$$\vec{\vec{D}}(\vec{x})\vec{e}_2 = \begin{bmatrix} D_{11} & D_{12} & D_{13} \\ D_{21} & D_{22} & D_{23} \\ D_{31} & D_{32} & D_{33} \end{bmatrix} \begin{bmatrix} 0 \\ 1 \\ 0 \end{bmatrix} = \begin{bmatrix} D_{12} & D_{22} & D_{32} \end{bmatrix}^T,$$

$$\vec{\vec{D}}(\vec{x})\vec{e}_3 = \begin{bmatrix} D_{11} & D_{12} & D_{13} \\ D_{21} & D_{22} & D_{23} \\ D_{31} & D_{32} & D_{33} \end{bmatrix} \begin{bmatrix} 0 \\ 0 \\ 1 \end{bmatrix} = \begin{bmatrix} D_{13} & D_{23} & D_{33} \end{bmatrix}^T$$

Direct substitution into the diffusion equation yields after some straightforward algebraic manipulations

$$\frac{\partial c}{\partial t}=\frac{\partial}{\partial x_1}\left(\frac{\partial c}{\partial x_1}D_{11}\right)+\frac{\partial}{\partial x_1}\left(\frac{\partial c}{\partial x_2}D_{12}\right)+\frac{\partial}{\partial x_1}\left(\frac{\partial c}{\partial x_3}D_{13}\right)+$$
$$+\frac{\partial}{\partial x_2}\left(\frac{\partial c}{\partial x_1}D_{21}\right)+\frac{\partial}{\partial x_2}\left(\frac{\partial c}{\partial x_2}D_{22}\right)+\frac{\partial}{\partial x_2}\left(\frac{\partial c}{\partial x_3}D_{23}\right)+$$
$$+\frac{\partial}{\partial x_3}\left(\frac{\partial c}{\partial x_1}D_{31}\right)+\frac{\partial}{\partial x_3}\left(\frac{\partial c}{\partial x_2}D_{32}\right)+\frac{\partial}{\partial x_3}\left(\frac{\partial c}{\partial x_3}D_{33}\right)+$$
$$+\rho c \Leftrightarrow$$
$$\frac{\partial c}{\partial t}=\frac{\partial^2 c}{\partial x_1^2}D_{11}+\frac{\partial D_{11}}{\partial x_1}\frac{\partial c}{\partial x_1}+\frac{\partial^2 c}{\partial x_1\partial x_2}D_{12}+\frac{\partial D_{12}}{\partial x_1}\frac{\partial c}{\partial x_2}+\frac{\partial^2 c}{\partial x_1\partial x_3}D_{13}+\frac{\partial D_{13}}{\partial x_1}\frac{\partial c}{\partial x_3}+$$
$$+\frac{\partial^2 c}{\partial x_2\partial x_1}D_{21}+\frac{\partial D_{21}}{\partial x_2}\frac{\partial c}{\partial x_1}+\frac{\partial^2 c}{\partial x_2^2}D_{22}+\frac{\partial D_{22}}{\partial x_2}\frac{\partial c}{\partial x_2}+\frac{\partial^2 c}{\partial x_2\partial x_3}D_{23}+\frac{\partial D_{23}}{\partial x_2}\frac{\partial c}{\partial x_3}+$$
$$+\frac{\partial^2 c}{\partial x_3\partial x_1}D_{31}+\frac{\partial D_{31}}{\partial x_3}\frac{\partial c}{\partial x_1}+\frac{\partial^2 c}{\partial x_3\partial x_2}D_{32}+\frac{\partial D_{32}}{\partial x_3}\frac{\partial c}{\partial x_2}+\frac{\partial^2 c}{\partial x_3^2}D_{33}+\frac{\partial D_{33}}{\partial x_3}\frac{\partial c}{\partial x_3}+$$
$$+\rho c$$

Term grouping

$$\frac{\partial c}{\partial t}=\frac{\partial^2 c}{\partial x_1^2}D_{11}+\frac{\partial^2 c}{\partial x_1\partial x_2}D_{12}+\frac{\partial^2 c}{\partial x_1\partial x_3}D_{13}+\frac{\partial^2 c}{\partial x_2\partial x_1}D_{21}+\frac{\partial^2 c}{\partial x_2^2}D_{22}+\frac{\partial^2 c}{\partial x_2\partial x_3}D_{23}+\frac{\partial^2 c}{\partial x_3\partial x_1}D_{31}+\frac{\partial^2 c}{\partial x_3\partial x_2}D_{32}+\frac{\partial^2 c}{\partial x_3^2}D_{33}+$$
$$+\frac{\partial D_{11}}{\partial x_1}\frac{\partial c}{\partial x_1}+\frac{\partial D_{12}}{\partial x_1}\frac{\partial c}{\partial x_2}+\frac{\partial D_{13}}{\partial x_1}\frac{\partial c}{\partial x_3}+\frac{\partial D_{21}}{\partial x_2}\frac{\partial c}{\partial x_1}+\frac{\partial D_{22}}{\partial x_2}\frac{\partial c}{\partial x_2}+\frac{\partial D_{23}}{\partial x_2}\frac{\partial c}{\partial x_3}+\frac{\partial D_{31}}{\partial x_3}\frac{\partial c}{\partial x_1}+\frac{\partial D_{32}}{\partial x_3}\frac{\partial c}{\partial x_2}+\frac{\partial D_{33}}{\partial x_3}\frac{\partial c}{\partial x_3}+$$
$$+\rho c$$

leads to the expression

$$\frac{\partial c}{\partial t}=\sum_{i=1}^{3}\sum_{j=1}^{3}\frac{\partial^2 c}{\partial x_i\partial x_j}D_{ij}+\sum_{j=1}^{3}\frac{\partial c}{\partial x_j}\left(\sum_{i=1}^{3}\frac{\partial D_{ij}}{\partial x_i}\right)+\rho c \qquad \text{(A1)}$$

II. Finite Differences.

A detailed procedure on how to derive a linear system that expresses the diffusion – reaction equation is presented. The forward Euler method is studied first, then the backward Euler method and last the θ- method. The Crank-Nicolson method is a subcase of the θ-method approach.

III. Forward Euler

The Forward Euler method is applied in order to approximate the local derivatives in (A1).

If $c\left(n\Delta T, i\Delta X, j\Delta Y, k\Delta Z\right)\equiv C_{i,j,k}^{n}$, $i=0,...,N_X-1, y=0,...,N_Y-1, k=0,...,N_Z-1$then the partial derivatives of (A1) at the point $\left(i\Delta X, j\Delta Y, k\Delta Z\right)$ can be approximated as

$$\frac{\partial c}{\partial t} \to \frac{C_{i,j,k}^{n+1} - C_{i,j,k}^{n}}{\Delta T}$$
$$\frac{\partial c}{\partial x} \to \frac{C_{i+1,j,k}^{n} - C_{i-1,j,k}^{n}}{2\Delta X}$$
$$\frac{\partial c}{\partial y} \to \frac{C_{i,j+1,k}^{n} - C_{i,j-1,k}^{n}}{2\Delta Y}$$
$$\frac{\partial c}{\partial z} \to \frac{C_{i,j,k+1}^{n} - C_{i,j,k-1}^{n}}{2\Delta Z} \qquad \text{(A2)}$$
$$\frac{\partial^2 c}{\partial x^2} \to \frac{C_{i+1,j,k}^{n} - 2C_{i,j,k}^{n} + C_{i-1,j,k}^{n}}{\Delta X^2}$$
$$\frac{\partial^2 c}{\partial y^2} \to \frac{C_{i,j+1,k}^{n} - 2C_{i,j,k}^{n} + C_{i,j-1,k}^{n}}{\Delta Y^2}$$
$$\frac{\partial^2 c}{\partial z^2} \to \frac{C_{i,j,k+1}^{n} - 2C_{i,j,k}^{n} + C_{i,j,k-1}^{n}}{\Delta Z^2}$$
$$\frac{\partial^2 c}{\partial x \partial y} = \frac{\partial^2 c}{\partial y \partial x} \to \frac{C_{i+1,j+1,k}^{n} + C_{i-1,j-1,k}^{n} - C_{i+1,j-1,k}^{n} - C_{i-1,j+1,k}^{n}}{4\Delta X \Delta Y}$$
$$\frac{\partial^2 c}{\partial x \partial z} = \frac{\partial^2 c}{\partial z \partial x} \to \frac{C_{i+1,j,k+1}^{n} + C_{i-1,j,k-1}^{n} - C_{i+1,j,k-1}^{n} - C_{i-1,j,k+1}^{n}}{4\Delta X \Delta Z}$$

$$\frac{\partial^2 c}{\partial z \partial y} = \frac{\partial^2 c}{\partial y \partial z} \to \frac{C_{i,j+1,k+1}^{n} + C_{i,j-1,k-1}^{n} - C_{i,j+1,k-1}^{n} - C_{i,j-1,k+1}^{n}}{4\Delta Z \Delta Y}$$
$$\frac{\partial D_{kl}}{\partial x} \to \frac{D_{kl,i+1,j,k}^{\ n} - D_{kl,i-1,j,k}^{\ n}}{2\Delta X}$$

Substituting the (A2) approximations into leads to the following expression

$$
\begin{aligned}
\frac{C_{i,j,k}^{n+1}-C_{i,j,k}^{n}}{\Delta T} &= \left(-2\frac{D_{11}}{\Delta X^2}-2\frac{D_{22}}{\Delta Y^2}-2\frac{D_{33}}{\Delta Z^2}\right)C_{i,j,k}^{n}+\rho c+\\
&+\left(\frac{D_{11}}{\Delta X^2}+\frac{D_{11,i+1,j,k}-D_{11,i-1,j,k}}{4\Delta X^2}+\frac{D_{21,i,j+1,k}-D_{21,i,j-1,k}}{4\Delta Y\Delta X}+\frac{D_{31,i,j,k+1}-D_{31,i,j,k-1}}{4\Delta Z\Delta X}\right)C_{i+1,j,k}^{n}\\
&+\left(\frac{D_{11}}{\Delta X^2}-\frac{D_{11,i+1,j,k}-D_{11,i-1,j,k}}{4\Delta X^2}-\frac{D_{21,i,j+1,k}-D_{21,i,j-1,k}}{4\Delta Y\Delta X}-\frac{D_{31,i,j,k+1}-D_{31,i,j,k-1}}{4\Delta Z\Delta X}\right)C_{i-1,j,k}^{n}\\
&+\left(\frac{D_{22}}{\Delta Y^2}+\frac{D_{12,i+1,j,k}-D_{12,i-1,j,k}}{4\Delta X\Delta Y}+\frac{D_{22,i,j+1,k}-D_{22,i,j-1,k}}{4\Delta Y^2}+\frac{D_{32,i,j,k+1}-D_{32,i,j,k-1}}{4\Delta Z\Delta Y}\right)C_{i,j+1,k}^{n}\\
&+\left(\frac{D_{22}}{\Delta Y^2}-\frac{D_{12,i+1,j,k}-D_{12,i-1,j,k}}{4\Delta X\Delta Y}-\frac{D_{22,i,j+1,k}-D_{22,i,j-1,k}}{4\Delta Y^2}-\frac{D_{32,i,j,k+1}-D_{32,i,j,k-1}}{4\Delta Z\Delta Y}\right)C_{i,j-1,k}^{n}\\
&+\left(\frac{D_{33}}{\Delta Z^2}+\frac{D_{13,i+1,j,k}-D_{13,i-1,j,k}}{4\Delta X\Delta Z}+\frac{D_{23,i,j+1,k}-D_{23,i,j-1,k}}{4\Delta Y\Delta Z}+\frac{D_{33,i,j,k+1}-D_{33,i,j,k-1}}{4\Delta Z^2}\right)C_{i,j,k+1}^{n}\\
&+\left(\frac{D_{33}}{\Delta Z^2}-\frac{D_{13,i+1,j,k}-D_{13,i-1,j,k}}{4\Delta X\Delta Z}-\frac{D_{23,i,j+1,k}-D_{23,i,j-1,k}}{4\Delta Y\Delta Z}-\frac{D_{33,i,j,k+1}-D_{33,i,j,k-1}}{4\Delta Z^2}\right)C_{i,j,k-1}^{n}\\
&+\left(\frac{D_{12}}{2\Delta X\Delta Y}\right)C_{i+1,j+1,k}^{n}+\left(\frac{D_{12}}{2\Delta X\Delta Y}\right)C_{i-1,j-1,k}^{n}+\left(-\frac{D_{12}}{2\Delta X\Delta Y}\right)C_{i+1,j-1,k}^{n}+\left(-\frac{D_{12}}{2\Delta X\Delta Y}\right)C_{i-1,j+1,k}^{n}+\\
&+\left(\frac{D_{13}}{2\Delta X\Delta Z}\right)C_{i+1,j,k+1}^{n}+\left(\frac{D_{13}}{2\Delta X\Delta Z}\right)C_{i-1,j,k-1}^{n}+\left(-\frac{D_{13}}{2\Delta X\Delta Z}\right)C_{i+1,j,k-1}^{n}+\left(-\frac{D_{13}}{2\Delta X\Delta Z}\right)C_{i-1,j,k+1}^{n}+\\
&+\left(\frac{D_{23}}{2\Delta Z\Delta Y}\right)C_{i,j+1,k+1}^{n}+\left(\frac{D_{23}}{2\Delta Z\Delta Y}\right)C_{i,j-1,k-1}^{n}+\left(-\frac{D_{23}}{2\Delta Z\Delta Y}\right)C_{i,j+1,k-1}^{n}+\left(-\frac{D_{23}}{2\Delta Z\Delta Y}\right)C_{i,j-1,k+1}^{n}
\end{aligned}
\tag{A3}
$$

Introducing for each point $P(i,j,k)$ the constants below

$$
\begin{aligned}
A(i,j,k)_0 &= \rho-2\frac{D_{11,i,j,k}}{\Delta X^2}-2\frac{D_{22}}{\Delta Y^2}-2\frac{D_{33}}{\Delta Z^2}\\
A(i,j,k)_1 &= \frac{D_{11}}{\Delta X^2}+\frac{D_{11,i+1,j,k}-D_{11,i-1,j,k}}{4\Delta X^2}+\frac{D_{21,i,j+1,k}-D_{21,i,j-1,k}}{4\Delta Y\Delta X}+\frac{D_{31,i,j,k+1}-D_{31,i,j,k-1}}{4\Delta Z\Delta X}\\
A(i,j,k)_2 &= \frac{D_{11}}{\Delta X^2}-\frac{D_{11,i+1,j,k}-D_{11,i-1,j,k}}{4\Delta X^2}-\frac{D_{21,i,j+1,k}-D_{21,i,j-1,k}}{4\Delta Y\Delta X}-\frac{D_{31,i,j,k+1}-D_{31,i,j,k-1}}{4\Delta Z\Delta X}\\
A(i,j,k)_3 &= \frac{D_{22}}{\Delta Y^2}+\frac{D_{12,i+1,j,k}-D_{12,i-1,j,k}}{4\Delta X\Delta Y}+\frac{D_{22,i,j+1,k}-D_{22,i,j-1,k}}{4\Delta Y^2}+\frac{D_{32,i,j,k+1}-D_{32,i,j,k-1}}{4\Delta Z\Delta Y}\\
A(i,j,k)_4 &= \frac{D_{22}}{\Delta Y^2}-\frac{D_{12,i+1,j,k}-D_{12,i-1,j,k}}{4\Delta X\Delta Y}-\frac{D_{22,i,j+1,k}-D_{22,i,j-1,k}}{4\Delta Y^2}-\frac{D_{32,i,j,k+1}-D_{32,i,j,k-1}}{4\Delta Z\Delta Y}\\
A(i,j,k)_5 &= \frac{D_{33}}{\Delta Z^2}+\frac{D_{13,i+1,j,k}-D_{13,i-1,j,k}}{4\Delta X\Delta Z}+\frac{D_{23,i,j+1,k}-D_{23,i,j-1,k}}{4\Delta Y\Delta Z}+\frac{D_{33,i,j,k+1}-D_{33,i,j,k-1}}{4\Delta Z^2}\\
A(i,j,k)_6 &= \frac{D_{33}}{\Delta Z^2}-\frac{D_{13,i+1,j,k}-D_{13,i-1,j,k}}{4\Delta X\Delta Z}-\frac{D_{23,i,j+1,k}-D_{23,i,j-1,k}}{4\Delta Y\Delta Z}-\frac{D_{33,i,j,k+1}-D_{33,i,j,k-1}}{4\Delta Z^2}
\end{aligned}
\tag{A4}
$$

$$A(i,j,k)_7 = A_8 = -A_9 = -A_{10} = \frac{D_{12}}{2\Delta X \Delta Y}$$

$$A(i,j,k)_{11} = A_{12} = -A_{13} = -A_{14} = \frac{D_{13}}{2\Delta X \Delta Z}$$

$$A(i,j,k)_{15} = A_{16} = -A_{17} = -A_{18} = \frac{D_{23}}{2\Delta Z \Delta Y}$$

yields

$$\frac{C_{i,j,k}^{n+1} - C_{i,j,k}^{n}}{\Delta T} = \begin{bmatrix} A(i,j,k)_0 & A(i,j,k)_1 & A(i,j,k)_2 & A(i,j,k)_3 & .... & A(i,j,k)_{16} & A(i,j,k)_{17} & A(i,j,k)_{18} \end{bmatrix} \begin{bmatrix} C_{i,j,k}^{n} \\ C_{i+1,j,k}^{n} \\ C_{i-1,j,k}^{n} \\ C_{i,j+1,k}^{n} \\ .... \\ C_{i,j-1,k-1}^{n} \\ C_{i,j+1,k-1}^{n} \\ C_{i,j-1,k+1}^{n} \end{bmatrix} \quad \text{(A5)}$$

Using the vector form of $C_{i,j,k}^{n}$

$$\vec{C}^{m} \equiv \left[\underbrace{C_{0,0,0}^{m} \quad C_{0,0,1}^{m} \quad ... \quad C_{0,0,N_Z-1}^{m} \quad C_{0,1,0}^{m} \quad ... \quad C_{0,N_Y-2,N_Z-1}^{m} \quad C_{0,N_Y-1,0}^{m} \quad ... \quad C_{0,N_Y-1,N_Z-1}^{m} \quad C_{1,0,0}^{m} \quad ... \quad C_{N_X-1,N_Y-1,N_Z-1}^{m}}_{N_X N_Y N_Z} \right]^{T} \quad \text{(A6)}$$

the overall solution of the equation at the time point *n+1* can be found by solving

$$\frac{\vec{C}^{n+1} - \vec{C}^{n}}{\Delta T} = \vec{\vec{A}} \vec{C}^{n}$$

where $\vec{\vec{A}}$ is a $N_X N_Y N_Z \times N_X N_Y N_Z$ matrix with its elements defined as

$$\vec{\vec{A}}_{mn} = \begin{cases} A(i,j,k)_0 & ,n = m \\ A(i,j,k)_1 & ,n = m + N_Y N_Z \\ A(i,j,k)_2 & ,n = m - N_Y N_Z \\ A(i,j,k)_3 & ,n = m + N_Z \\ A(i,j,k)_4 & ,n = m - N_Z \\ A(i,j,k)_5 & ,n = m + 1 \\ A(i,j,k)_6 & ,n = m - 1 \\ A(i,j,k)_7 & ,n = m + N_Y N_Z + N_Z \\ A(i,j,k)_8 & ,n = m - N_Y N_Z - N_Z \\ A(i,j,k)_9 & ,n = m + N_Y N_Z - N_Z \\ A(i,j,k)_{10} & ,n = m - N_Y N_Z + N_Z \\ A(i,j,k)_{11} & ,n = m + N_Y N_Z + 1 \\ A(i,j,k)_{12} & ,n = m - N_Y N_Z - 1 \\ A(i,j,k)_{13} & ,n = m + N_Y N_Z - 1 \\ A(i,j,k)_{14} & ,n = m - N_Y N_Z + 1 \\ A(i,j,k)_{15} & ,n = m + N_Z + 1 \\ A(i,j,k)_{16} & ,n = m - N_Z - 1 \\ A(i,j,k)_{17} & ,n = m + N_Z - 1 \\ A(i,j,k)_{18} & ,n = m - N_Z + 1 \\ 0 & ,otherwise \end{cases} , m = iN_Y N_Z + jN_Z + k \tag{A7}$$

This is a $N_X N_Y N_Z \times N_X N_Y N_Z$ sparse matrix with 19 diagonals, as shown in Figure A1. In Figure A.1 the light areas correspond to zero values whereas the black lines correspond to the non-zero diagonals. Note that the thicker lines represent 3 consecutive diagonals while the thin ones represent isolated diagonals.

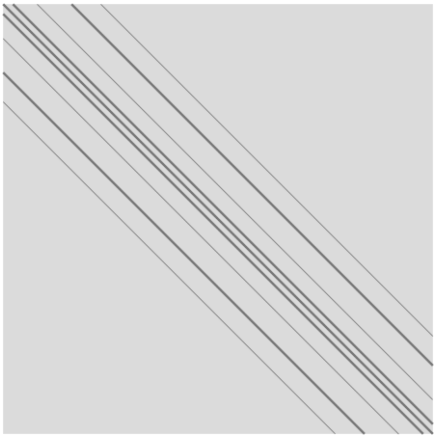

Figure A1. The sparse matrix A

Matrix A is tridiagonal with fringes. It posseses one central and four additional tridiagonal areas as well as four single diagonal areas. Having acquired the $\vec{\vec{A}}$ matrix a direct solution can be found simply by calculating

$$\boxed{\vec{C}^{n+1} = \left(\vec{\vec{I}} + \Delta T\, \vec{\vec{A}}\right)\vec{C}^{n}} \tag{A8}$$

This is a very easy to implement solution since there is no need to solve a linear system of equations but just to perform direct substitution. However, numerical stability is the main issue. As proven in [CO15] the method is stable and thus provides reliable results if

$$\Delta T \leq \min_{(x,y,z)} \left(\frac{1}{2} \frac{1}{\dfrac{D_{11}(x,y,z)}{\Delta X^{2}} + \dfrac{D_{22}(x,y,z)}{\Delta Y^{2}} + \dfrac{D_{33}(x,y,z)}{\Delta Z^{2}}} \right) \tag{A9}$$

IV. Backward Euler

Now the Backward Euler method is addressed. The approximate expressions for the local derivatives (Equation A1) at the internal points of the mesh are given below. A solution achieved using the Backward Euler is preferrable to its Forward Euler counterpart since there are no constraints regarding numerical stability. According to the Backward Euler method the local derivatives can be approximated as

$$\frac{\partial c}{\partial t} \to \frac{C_{i,j,k}^{n+1} - C_{i,j,k}^{n}}{\Delta T}$$

$$\frac{\partial c}{\partial x} \to \frac{C_{i+1,j,k}^{n+1} - C_{i-1,j,k}^{n+1}}{2\Delta X}$$

$$\frac{\partial c}{\partial y} \to \frac{C_{i,j+1,k}^{n+1} - C_{i,j-1,k}^{n+1}}{2\Delta Y}$$

$$\frac{\partial c}{\partial z} \to \frac{C_{i,j,k+1}^{n+1} - C_{i,j,k-1}^{n+1}}{2\Delta Z}$$

$$\frac{\partial^2 c}{\partial x^2} \to \frac{C_{i+1,j,k}^{n+1} - 2C_{i,j,k}^{n+1} + C_{i-1,j,k}^{n+1}}{\Delta X^2}$$

$$\frac{\partial^2 c}{\partial y^2} \to \frac{C_{i,j+1,k}^{n+1} - 2C_{i,j,k}^{n+1} + C_{i,j-1,k}^{n+1}}{\Delta Y^2}$$

$$\frac{\partial^2 c}{\partial z^2} \to \frac{C_{i,j,k+1}^{n+1} - 2C_{i,j,k}^{n+1} + C_{i,j,k-1}^{n+1}}{\Delta Z^2}$$

$$\frac{\partial^2 c}{\partial x \partial y} = \frac{\partial^2 c}{\partial y \partial x} \to \frac{C_{i+1,j+1,k}^{n+1} + C_{i-1,j-1,k}^{n+1} - C_{i+1,j-1,k}^{n+1} - C_{i-1,j+1,k}^{n+1}}{4\Delta X \Delta Y}$$

$$\frac{\partial^2 c}{\partial x \partial z} = \frac{\partial^2 c}{\partial z \partial x} \to \frac{C_{i+1,j,k+1}^{n+1} + C_{i-1,j,k-1}^{n+1} - C_{i+1,j,k-1}^{n+1} - C_{i-1,j,k+1}^{n+1}}{4\Delta X \Delta Z}$$

$$\frac{\partial^2 c}{\partial z \partial y} = \frac{\partial^2 c}{\partial y \partial z} \to \frac{C_{i,j+1,k+1}^{n+1} + C_{i,j-1,k-1}^{n+1} - C_{i,j+1,k-1}^{n+1} - C_{i,j-1,k+1}^{n+1}}{4\Delta Z \Delta Y}$$

$$\frac{\partial D_{kl}}{\partial x} \to \frac{D_{kl,i+1,j,k}^{n+1} - D_{kl,i-1,j,k}^{n+1}}{2\Delta X}$$

In a way similar to the one followed by the Forward Euler method the following equation is derived

$$\frac{\vec{C}^{n+1} - \vec{C}^{n}}{\Delta T} = \ddot{A}\vec{C}^{n+1}$$

where $\ddot{A}$ is exactly the same sparse matrix that was derived using the Forward Euler method. Therefore, finding a solution to the equation $\frac{\vec{C}^{n+1} - \vec{C}^{n}}{\Delta T} = \ddot{A}\vec{C}^{n+1}$ is equivalent to finding a solution to the linear system

$$\boxed{\left(\ddot{I} - \Delta T\, \ddot{A}\right)\vec{C}^{n+1} = \vec{C}^{n}} \qquad \text{(A10)}$$

where $\ddot{I}$ is the $N_X N_Y N_Z \times N_X N_Y N_Z$ identity matrix. One of the methods that can be used to solve this linear system is the Conjugate Gradient Method (see Section 6.2.3)

Stability and accuracy are the main advantages of the Backward Euler method (in relation to the Forward Euler method) at the expense of increased computational and storage demands.

V. The *θ*-method

The θ-method when applied to approximate the local derivatives leads to the equation

$$\frac{\vec{C}^{n+1} - \vec{C}^{n}}{\Delta T} = \theta\, \ddot{A}\vec{C}^{n+1} + (1-\theta)\, \ddot{A}\vec{C}^{n}$$

or equivalently

$$\left(\ddot{I} - \theta \Delta T\, \ddot{A}\right)\vec{C}^{n+1} = \left((1-\theta)\Delta T\, \ddot{A} + \ddot{I}\right)\vec{C}^{n}$$

where $\ddot{A}$ is exactly the same sparse matrix as the one derived by the Forward Euler method. As stated in [CO22] θ is optimally chosen if $\theta = \dfrac{1}{e^{\rho \Delta T} - 1}$. Moreover, selection of θ=1/2 produces the Crank-Nicolson method. Here again an iterative numerical method to solve the linear system (A11) is to be applied.

$$\boxed{\left(\ddot{I} - \theta \Delta T\, \ddot{A}\right)\vec{C}^{n+1} = \left((1-\theta)\Delta T\, \ddot{A} + \ddot{I}\right)\vec{C}^{n}} \qquad \text{(A11)}$$

Both the θ- and the Crank Nicolson methods are stable and more accurate than the Backward Euler [CO22] but their computational and storage requirements are higher.

List of Abbreviations

ACGT	Advancing ClinicoGenomic Trials on Cancer
AUC	Area Under Curve
BED	University of Bedfordshire
CG	Conjugate Gradient
CT	Computerized Tomography
DBC	Digital Biological Cell
EC	European Commission
EC	Endothelial Cell
ECM	Extracellular Matrix
FN	Fibronectin
FORTH-ICS	Foundation for Research and Technology – Hellas, Institute of Computer Science
GC	Geometrical Cell
GBM	Glioblastoma Multiforme
HGG	High Grade Glioma
ICCS-NTUA	Institute of Communication and Computer Systems – National Technical University of Athens
LGG	Low Grade Glioma
MCS	Monte Carlo Steps

MDE	Matrix Degrading Enzyme
MFF CUNI	Charles University in Prague Faculty of Mathematics and Physics
MRI	Magnetic Resonance Imaging
ODE	Ordinary Differential Equation
PDE	Partial Differential Equation
PFL-H	Philips Technologie GmbH Forschungslaboratorien
TAF	Tumour Angiogenesis Factor
UBERN	Universität Bern
USAAR	Universität des Saarlandes
WP	Workpackage